THE PROCESSING, MICROSTRUCTURAL EVALUATION AND MECHANICAL PROPERTIES OF SiC DISPERSOID REINFORCED Si_3N_4 COMPOSITES.

A thesis submitted for the degree of
DOCTOR OF PHILOSOPHY
of the University of Warwick
by

STEPHEN MARTIN KETCHION

January 1992

Department of Physics
University of Warwick
Coventry, CV4 7AL.

ABSTRACT

A range of composites have been prepared by dispersing various sources of SiC whiskers and platelets into a Si_3N_4 based matrix intended for high temperature applications. The main objective was to improve the fracture toughness of the Si_3N_4 monolith without any detrimental effect on other properties such as the excellent high temperature deformation behaviour. The matrix composition was tailored so that the intergranular phase formed desirable crystallisation products within the Si_3N_4 - Si_2N_2O - $Y_2Si_2O_7$ phase system. A slip casting technique was used to prepare the composites, in order to preferentially align the dispersoids, and conventional powder pressing methods were used to achieve a random distribution of dispersoids.

Composites containing at least 30 weight % dispersoid content were fully densified using ABB Cerama's glass encapsulated HIP process. The resulting composites showed steadily increasing fracture toughness values with increasing SiC content, although the maximum increment was only approximately 30%. Platelet containing composites had slightly higher values than composites containing a similar volume fraction of whiskers, although there was a significantly lower fracture strength in the former. A microstructural survey of the materials indicated that the mechanical properties were influenced by the dispersoid / matrix interfacial characteristics. Fracture surfaces of the platelet containing composites showed there was significant debonding at the interface, whereas the whiskers appeared strongly bonded to the matrix.

Whisker reinforced Si_3N_4 composites showed excellent creep resistance at 1400°C, which appeared slightly better than the monolith. Both materials had a similar stress exponent value close to 1, which suggests the deformation mechanisms in both these materials are similar and follow a grain boundary diffusional flow mechanism. There appeared to be a threshold stress level of 250 MPa at 1400°C for both materials where failure did not occur after prolonged deformation. This result and the absence of cavity formation within the intergranular region suggests there is a sub-critical residual glass volume at this stress level for the nucleation of cavities and hence for slow crack growth. Both monolith and composites show good oxidation resistance at these elevated temperatures.

ACKNOWLEDGEMENTS.

I wish to thank Professor S.B.Palmer for the provision of laboratory facilities at the University, Rolls -Royce plc for financial support and Dr. A. Hepworth for access to laboratory facilities at T and N Technology Ltd, Rugby.

I am especially grateful to Professor M.H.Lewis for guidance and advice throughout this research programme. I am also grateful for the technical advice of Dr. G. Leng-Ward and the helpful discussions with my former research colleagues, Markys Cain, John Fernie, John Lumby, Dr. V.S.R. Murty, Mark Pharaoh, Kevin Plucknett and Olwen Pullum.

I would like to thank the departmental technical staff, especially Gerry Smith and Steve York for their expertise and tuition in electron microscopy, and Dan Lee, Pat Beecroft and Dave Hammond for assistance in the mechanical workshops.

My special thanks go to my wife Angela for her patience, understanding and support over the last few years. I would also like to take this opportunity to thank both my parents and Angela's parents for their encouragement and help.

CONTENTS

CHAPTER ONE.

INTRODUCTION.

1.1. ENGINEERING CERAMICS.

Improvements in the performance and efficiency of engineering devices often requires the introduction of new and revolutionary materials. One such field is in gas turbine engines where the current nickel based superalloys are approaching the limits of their operational capabilities. Any further efficiency improvement to the levels now sought, is limited by the small potential rise of operating temperature with continuous development of already complex and expensive metals. Elaborate cooling systems have been developed but this adversely affects the pressure ratio and thus reduces the efficiency of the engine. At high temperatures (> 1000°C) the metals plastically deform and are chemically attacked by the atmosphere and corrosive fuel elements. This has stimulated the development of high purity synthetic ceramics which have the potential to replace these metallic components in a number of areas because of an excellent combination of properties, Table1.1. The main advantages offered by these engineering ceramics are :

1) increased operating temperature from around 1000°C to the region of 1400°C, which result in improved thermodynamic efficiency and consequently reduced fuel consumption [1,2];

2) lower density components which will increase thrust to weight ratios and lower centrifugal forces on rotating parts [3];

3) they consist of relatively abundant and non-strategic materials.

Material	Density g/cm^3	Melting Point °C	Yng. Mod. GN m^{-2}	K_c MN m$^{-3/2}$	Therm. Cond. Wm^{-1}K^{-1}	Expansion coeff. 10^6 K^{-1}
Al_2O_3	3.9 - 4.0	2040	360	3 - 4	7	6.9 - 8.6
ZrO_2	5.7 - 6	2680		8 - 12	2	10
Si_3N_4	3.2 - 3.3	1900 (D)	310	4 - 6	16	3
SiC	3.2 - 3.3	2723 (D)	420	3 - 4	60	4.5 - 5.0
Nimonic alloys	8	1320	200	100	12	12.5

Thermal Conductivity at approx. 1000°C. Thermal Expansion coeff. (20 - 1000° C)
(D) = Decomposition temperature.

Table. 1.1. Selected Properties of Engineering Materials [4].

Al_2O_3 has found wide application in industry for machining purposes, but poor thermal shock resistance and low toughness has restricted its use.

ZrO_2 based ceramics, e.g. PSZ (partially stabilised zirconia), show enhanced fracture toughness values at low and intermediate temperatures. This is due to the transformation of the metastable tetragonal precipitates to the monoclinic form in the stress field of a propagating crack, and results in a volume expansion [5,6]. Other mechanisms such as crack deflection and microcracking result in a higher stress for fracture. Also, ZrO_2 based ceramics have low thermal conductivity and thermal expansion compatibility with metallic alloys, which could make them valuable as coatings on cylinder walls and exhaust manifolds in adiabatic diesel engines [7]. However, their mechanical properties are not maintained above 700 - 800°C because the transformation toughening decreases as the tetragonal to monoclinic transformation " driving - force " is reduced. Thus ZrO_2 based ceramics alone will find little application as gas turbine components. The main candidates for the high

temperature applications are Si_3N_4 and SiC based ceramics. They offer desirable properties such as high specific strength, high elastic modulus and hardness, which derive from their mainly covalent bonding, and also high creep resistance, low thermal expansion and good oxidation resistance [8].

The U.K. was in the forefront of engineering ceramic research in the mid -1960's, but this tailed off in the early 1970's partly because of the limitation in performance caused by inadequate quality of the ceramic products [9]. After the oil crisis of 1973, the U.S. government initiated its gas turbine program [10] and since then, research and development expenditure has increased substantially [11]. Theoretical studies showed increases in gas turbine efficiency of around 20% with the introduction of silicon nitride components [12] and significant savings in fuel, Table 1.2. As a consequence, numerous market surveys [13,14] predicted large increases in the use of ceramic components by 1990 and beyond.

Type of Engine	% Reduction in Fuel	Operating Temperature °C
Gas Turbine (Automotive) 150 hp single shaft engine	27	1370
Gas Turbine (Truck) 350 hp two shaft engine	17	1240
Gas Turbine (Industrial) 1000 hp three stage engine	10	1370
Diesel engine Truck adiabatic turbo-compound 500 hp	22	1210

Table 1.2 Projected Energy Savings Using Ceramic Technology [8].

Various national programs, such as the U.K's ACT program, have investigated potential applications such as aerofoils, shroud rings and combustor components in gas turbines [15,16], but these still remain in the research and development stage. Both Nissan [17] and Daimler Benz [18] have demonstrated the use of ceramics in automotive gas turbines. Parts fabricated include the piston cap, cylinder liner spacer and the head plate. However, there has not been the rapid progress in turbine component substitution as forseen in the early 1980's. Established applications are mainly for low risk areas such as cutting tools and wear resistant parts. In the high risk areas such as advanced gas turbine components, technical problems and cost effectiveness are significant delaying factors. The main material problems responsible are :

a) the brittle nature of the monolithic ceramics, which results in an extreme sensitivity to microflaws introduced during sintering, machine finishing or by contact stresses when in service. This results in variable and thus unreliable mechanical properties. Si_3N_4 is superior in this respect compared to SiC and thus it is given preference for some applications;

b) the presence of sintering additives, which are needed during processing to achieve full densification. These usually remain as an intergranular phase and effectively control the high temperature time-dependent behaviour;

c) difficulty in the design and manufacture of complicated shapes, arising partly from the problem of machining ceramics.

1.2. THE COMPOSITE APPROACH

Significant progress has been made towards solving some of the problems mentioned above, by optimising the microstructural features of Si_3N_4-based

monolithic ceramics. However, a different microstructural design approach is needed in order for these ceramics to be used as reliable components in mechanically demanding engineering areas. One potential method of overcoming the flaw sensitivity of Si_3N_4 based monolithic ceramics is by making a composite. The principle of adding high modulus, high strength fibres within polymer matrices is well-established, but developments using ceramic matrices have been restricted, until recently, by the availability of suitable reinforcing materials. There are two different approaches in forming ceramic composites. One has been to incorporate modest volumes of short discontinuous 'fibres' and produce a composite which should to a great extent, reflect the properties of the monolith, but with improved toughness. The other has been an analogy with the development of conventional fibre composites, i.e. to utilize the high strength and stiffness of the fibre, by forming a composite with a high volume fraction of continuous fibres, and the matrix is of secondary importance but it imparts its high temperature characteristics. However, developments of such Si_3N_4-based composites have only been successful in producing composites with improved properties at low temperatures [19].

Initial work on incorporating short, refractory and randomly oriented, fibres , such as W, Mo and Ta, into a Si_3N_4 matrix, were unsatisfactory [20]. This was because the matrix failed to protect the fibres from rapid degradation in oxidising environments at high temperatures. Also, the metal fibres resulted in increased density over the monolith, and stress caused by excessive thermal expansion mismatch. Coating W wires with SiC increased work of fracture but they still had poor oxidation resistance and there was a dramatic loss of strength above 800°C [21]. Work on carbon fibre reinforcement showed detrimental fibre/ matrix reactions as well as large tensile stresses along the fibre lengths caused by thermal expansion mismatch [22]. The

development of SiC fibres from polymer precursors [23] led to renewed activity, particularly when high strength and fracture toughness were obtained for silicate glass ceramics incorporating Nicalon SiC fibres [24]. The fracture toughness of a hot pressed SiC - fibre reinforced Si_3N_4 was found to be significantly higher than the monolith [25] but at high temperatures there were reductions in the strength because of degradation of the fibres. Slurry coating and filament winding techniques have been successfully applied to fabricate SiC / Si_3N_4 composites with moderate loading, uniform distribution and a dense matrix. However, high strength and fracture toughness have not as yet been achieved at high temperature [26]

Considering the difficulties encountered in the developments of fibre reinforced Si_3N_4 materials, the use of dispersoids such as particles, whiskers and platelets as toughening constituents, offers an alternative. Theoretically, fibre reinforcement shows significantly greater toughening increments over dispersoids, but these gains are obtained at considerable cost, both in terms of the use of expensive raw materials and in the difficulty of fabrication and consolidation [27]. Dispersoid reinforced composites can be processed by conventional powder processing techniques [28]. For fibre reinforced composites, techniques such as lay up of fibres impregnated by a matrix precursor, followed by pyrolysis and binder burnout, are typically used [29]. Also, whiskers derived from rice hulls are now produced in reasonable quantity and at costs well below that possible with polymer derived fibres or with CVD monofilaments [30].

Whiskers are single crystals of stoichiometric compounds, thus there is no tendency, as with polymer derived fibres, for recrystalliasation, chemical reactions or other detrimental processes. They are commonly grown in favourable crystal orientations which gives them a relatively high Young's modulus, e.g. β - SiC whiskers

have a typical Young's modulus of 580 GPa [31]. Thus, together with their intrinsic thermal and chemical stability [31b], whiskers offer a good reinforcement potential for high temperature ceramic composites.

1.3 PROGRAMME OBJECTIVES.

The broad aims of this research programme were:

1) to fabricate a range of fully dense and homogeneous SiC dispersoid reinforced Si_3N_4 composites, principally by hot isostatic pressing (HIP). Various different types and sources of dispersoid were used, particularly whiskers but also particles and platelets. These were dispersed into a tailored Si_3N_4 based matrix composition, which has been shown to have desirable high temperature properties ;

2) to study the effect of dispersoid additions on the crystallisation behaviour of the matrix intergranular phase;

3) to study the microstructure and interfacial stability of the composites using optical, electron microscopic and microanalytical techniques ;

4) to measure various mechanical properties of the composites as a function of volume, type and orientation of the dispersoids, and to relate these results to the microstructural features in order to gain an insight into the toughening mechanisms taking place in these composites;

5) to examine the high temperature deformation, stress rupture and oxidation behaviour of representative compositions.

CHAPTER TWO

A REVIEW OF THE PROCESSING, TOUGHENING MECHANISMS AND PROPERTIES OF DISPERSOID REINFORCED CERAMIC COMPOSITES.

This chapter outlines the techniques used to process and fabricate Si_3N_4 ceramics, the mechanisms involved in toughening brittle monoliths and a review of the properties of SiC dispersoid reinforced ceramic matrices.

2.1. PROCESSING OF Si_3N_4 BASED COMPOSITES.

2.1.1. Introduction.

Normal metallurgical processing practice is inappropriate for ceramics because of their high melting points or decompositional problems, and their resistance to plastic flow. This processing constraint means Si_3N_4 ceramics are usually formed by sintering, i.e. consolidation of pressed particle aggregates. Due to the very low rate of self-diffusion of Si_3N_4 , the sintering process is usually accelerated by additives, typically MgO, Al_2O_3 and Y_2O_3. These react with the SiO_2 present on the surface of the initial α - Si_3N_4 powder [32] to form an intergranular liquid. The presence of this liquid phase promotes rapid transport paths during densification by a solution - reprecipitation mechanism [33 - 36], shown schematically in Fig.2.1. It also acts as a solvent for the necessary α to β - Si_3N_4 conversion to take place. Both processes occur simultaneously during the early stages of liquid phase sintering, with the α to β transformation aiding in particle rearrangement [37]. Usually additional pressure must be applied to achieve full densification, e.g. in hot pressing and hot isostatic pressing.

Dense Si_3N_4-based ceramics are characterised by a multiphase microstructure where β - Si_3N_4 forms the principal component and the amorphous and/ or crystalline intergranular region forms the minor phase. This intergranular phase largely controls the thermomechanical properties of the ceramic rather than the primary Si_3N_4 component [38,39]. Therefore, much research into high temperature components is geared to optimising the level of sintering additive and tailoring the glass composition for subsequent crystallisation.

Sintering and the resultant microstructure evolution is a multistage and complex process, dependent on many material and processing parameters such as precise composition, quantity of surface SiO_2, α - Si_3N_4 grain size and shape, presence of impurities, temperature and pressure. An overview of progress in microstructural development of a range of monolithic Si_3N_4 materials can be found in selected review papers [38,40,41].

2.1.2. The Si - Y - O - N System.

The key to high temperature performance is the ability to achieve theoretical densification in a completely crystalline microstructure [38,42-44]. Crystalline phases retain their properties much closer to the eutectic temperature than an amorphous phase, which softens and enables rapid diffusion of ions. The recognition of a correlation between the loss of strength, loss of creep resistance and enhanced oxidation at high temperatures, and the softening of the intergranular silicate phases present in most Si_3N_4 based ceramics, has led to numerous attempts to control the viscosity and volume of these phases. This is reflected in the experimentation with different additive systems. The choice of the specific sintering additive is governed by :

a) the stability and viscosity of the liquid sintering medium;

b) the softening temperature of any residual glass;

c) the ease of crystallisation of the intergranular glass into an oxidation resistant phase.

Stable intergranular liquids result from the use of CaO, MgO, Al_2O_3, Nd_2O_3, La_2O_3 and Y_2O_3, and mixed combinations of these. Y_2O_3 has the advantage of a high eutectic liquid softening temperature, i.e. Y_2O_3 - SiO_2 at 1660°C, and thus has better potential than other systems for high temperaure applications [45]. However, higher sintering temperatures and pressures are required to achieve full densification.

The microstructural development and material properties of Y_2O_3 - containing Si_3N_4 based ceramics are sensitive to both the presence of amorphous residues and the type of crystalline phases present. Careful compositional selection is required when preparing materials in the Y - Si - O - N system, Fig.2.2, so that a minor phase is found which creates suitable densification kinetics during sintering and is readily recrystallised to a structure retaining oxidative stability up to at least 1400°C. Compositions within the Si_3N_4 - Si_2N_2O - $Y_2Si_2O_7$ phase field are particularly suitable in terms of ease of crystallisation, stability in oxidising environments, and the absence of significant volume changes [46,47]. Optimisation of compositions within this phase field, intended to minimise the intergranular amorphous component and enhance mechanical properties , has proved promising [48].

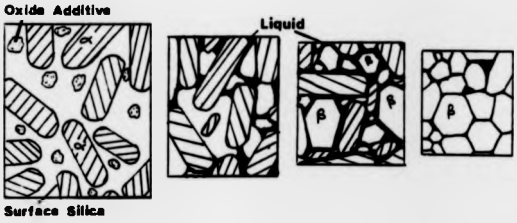

Fig.2.1. Schematic drawing of the solution - reprecipitation mechanism.

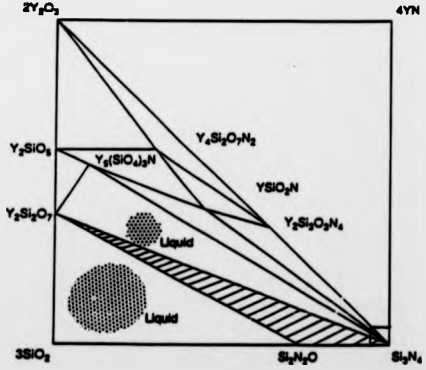

Fig.2.2. The Si_3N_4 - SiO_2 - Y_2O_3 -YN phase system at 1500°C [46,49,50].

2.1.3. Slip Casting.

Once the composition of the matrix has been decided the starting powders and dispersoids must be consolidated before densification. This can be done by a number of methods, but slip casting offers the possibility of preferred whisker orientation with little damage to the dispersoid. The slip casting process is strongly influenced by the properties of the Si_3N_4 powder and sintering additive suspension, and it is necessary to manipulate and control interparticle forces by an electrostatic method (pH control) [51-53]. This technique also helps to ensure heterogeneities are eliminated and are not reintroduced in subsequent processing steps.

When the ceramic powders are mixed in a polar liquid, counter - ions i.e. ions of opposite charge to the particle surface within the liquid, are attracted to the charged particle surface. Those counter - ions which are tightly adsorbed to the surface form the Stern's layer, which sets up an electrical potential due to the screening effect of the counter - ions. The remainder of the counter - ions form a diffuse layer around the particles (Gouy - Chapman's layer) the concentration of which decreases exponentially with distance [54]. When the particles migrate through the liquid, a layer of liquid molecules, called the lyosphere, remains bonded to the particle. The potential at the boundary between the lyosphere and the free liquid is called the zeta potential and this largely controls the rheological properties of the slip. Using a high solid loading usually produces a viscous, flocculated slip because attractive forces (largely Van der Waals forces) predominate. Adjusting the pH, influences the zeta potential, and repulsive forces can be made to predominate, so breaking up agglomerates and dispersing the constituents, i.e. deflocculation. Research is still taking place which can give a predictive understanding of the slurry rheology, as affected by the interparticle forces, particulate volume fraction, size and size distribution.

The electrostatic stability of multiphase aqueous Si_3N_4 slips, are strongly influenced by the electrolytic effects of the sintering additives, necessary to promote liquid phase sintering. Oxides like Y_2O_3 form positive counter ions by the dissociation of their hydroxide in water.

$$Y^{3+}(OH)_3 \text{ ----------> } Y^{3+} + 3(OH)^- \quad \ldots\ldots\ldots\ldots\ldots 2.1$$

Small concentrations of Y^{3+} ions i.e. 0.08mmol / l, have been found to be sufficient to cause rapid flocculation of Si_3N_4 powders at a pH of 8 [51]. This is shown in the Schulze - Hardy rule 2.2, which indicates that the critical flocculation concentration (cfc) depends strongly on the surface potential X, and the charge of the counterions Z.

$$cfc = B X^4 / A^2 Z^2 \quad \ldots\ldots\ldots\ldots\ldots 2.2 \quad [51]$$

where A = Hamaker constant

B = geometric constant

This shows that varying the concentration of the Y^{3+} or the Y containing sintering aid, has a significant effect on colloidal stability and consequently a pH > 8 has to be used for the electrostatic repulsive forces to break up agglomerates and disperse the constituents. The interparticle forces can then be made attractive to form a stable slip and then consolidated to form a powder compact by either tape casting, injection moulding or slip casting. Slip casting is a relatively simple technique in which the slip is poured into a mould and capillary action, due to the pores in the mould, withdraws the filtrate from the slip. A low density cake is formed on the mould surface which can be dried and densified using one of the fabrication routes mentioned later. Details of the mechanism of filtration and kinetics of cake deposition can be found in selected papers [55-57] .

2.1.4. Growth of SiC whiskers.

The main method of dispersoid reinforcement of the Si_3N_4 ceramic was the incorporation of SiC whiskers. These minute, high purity, single crystal fibres are produced commercially by a vapour - solid (VS) mechanism, more conventionally known as the rice - hull process [58,59]. Rice hulls are composed primarily of cellulose but also contain silica, and when they are heated in a coking furnace, the cellulose decomposes to yield carbon. When this coked product is heated in the 1200°C to 1800°C range, a carbothermal reaction occurs between the silica and carbon via the gas phase, and crystalline particles and whiskers of SiC are formed.

Recently, the VLS process has been developed and refined for the growth of SiC whiskers [60,61]. In this mechanism, V stands for Vapour feed gases, L for Liquid catalyst, and S for Solid crystalline growth. The distinguishing feature of this process is the presence of a liquid catalyst, such as a transition metal alloy. The catalyst solution is a preferred site for deposition of C and Si atoms in the vapour feed, and when it becomes supersaturated, SiC precipitates out. Whisker growth occurs at a rate determined by the speed at which the gases are fed into the system to cause supersaturation, and to a size proportional to the dimensions of the catalyst ball. It has been reported that whiskers measuring 3 - 5 μm in diameter, 16 mm in length and with an average tensile strength of 160 GPa can be grown [62].

2.1.5. Fabrication Techniques.

There are a variety of different fabrication routes which can be used in order to produce dense Si_3N_4-based components. The features of the main techniques are outlined below.

(a) Reaction Bonded Si_3N_4 Ceramics.

In this method silicon powder is consolidated by cold isostatic pressing (CIP), slip casting or injection moulding, followed by nitridation at 1400°C over several days. Only small dimensional changes occur during nitriding, so the process is suited to mass production of complex shaped components where little final machining is required. However, RBSN has a relatively high porosity which has a detrimental effect on strength and oxidation resistance. The density can be improved by following the nitriding stage with Hot Isostatic Pressing (HIP).

(b) Hot Pressed Si_3N_4 Ceramics.

In this technique, the Si_3N_4, sintering aid and dispersoids are uniaxially pressed in a graphite die using pressure, typically 20 - 40 MPa, at a temperature of 1650 - 1800°C [63]. The uniaxial nature of hot pressing promotes a certain degree of anisotropy in component properties, due to the preferred orientation of the β - Si_3N_4 grains and dispersoids perpendicular to the pressing direction [64,65]. The technique is limited in application because only simple shapes can be formed and diamond machining of hard densified material is very expensive.

(c) Pressureless Sintering of Si_3N_4 Ceramics.

The need to produce densified complex shaped Si_3N_4 components promoted the development of pressureless sintering. However, the presence of non-shrinking whiskers in the green body inhibits the bulk shrinkage of the sample, which is needed to accommodate densification by sintering. The resistance to such shrinkage caused by the stiff whiskers has thus frustrated the use of conventional pressureless sintering for the preparation of dense dispersoid-reinforced composites. Accordingly,

pressure-assisted techniques are required.

(d) Hot Isostatic Pressing of Si_3N_4 Ceramics.

Hot isostatic pressing (HIP) is a fabrication technique that involves the use of high isostatic pressures (100 - 300 MPa) and high temperatures (1650 - 1800°C), to assist densification by sintering and mechanical consolidation. It is essentially a combination of hot pressing and cold isostatic pressing but offers some potential advantages for Si_3N_4 based ceramics [66]. These are :

a) higher pressures are applied than in hot pressing, which means lower temperatures and shorter densification times are used;

b) theoretically dense composites can be obtained with less sintering aid;

c) fully isotropic properties can be obtained ;

d) complicated shapes can be made in a near net shape process.

The HIP process originated at the Battelle Memorial Institute, Ohio and was developed for diffusion bonding of clad nuclear fuel elements [67]. One of the first industries where HIP was introduced as a productive tool, was in the tungsten carbide industry, and applications such as the consolidation of high speed tool steel powders, nickel - based superalloys and healing of defects in castings were introduced [69]. As a result of increased temperatures and pressure capabilities of HIP equipment, the process was introduced in the ceramic industry for the densification of powders. There are two major routes for the HIP of Si_3N_4 based ceramics [69].

a) a green state ceramic article is formed and then encapsulated prior to HIP.

b) the green state material is sintered until the surface connecting porosity is closed, i.e. typically > 93% of theoretical density. The sintered part is then HIP without encapsulation to a higher density.The porous nature of green ceramic parts requires the

use of an impermeable barrier layer that totally envelops the ceramic during HIP. This encapsulant layer prevents penetration of the pressure transmitting gas into the ceramic article. If gas ingresses into the component, e.g. from encapsulant failure, the gas pressure acting within the interconnecting porosity of the ceramic will counteract the densification process.

HIP densification of Si_3N_4 was first achieved by researchers at ASEA [66,70 - 72] who placed a preformed body in an open-ended capsule of SiO_2 or borosilicate glass, i.e. tubular encapsulation [70]. It was then placed in a conventional furnace at 100°C and evacuated to 0.1 Pa for 8 hours using a vacuum pump attached to the open end of the capsule. The capsule was then backflushed with nitrogen to atmospheric pressure and sealed. Following sealing, the capsule was heated in a furnace to 1250°C, at which point the glass softens and becomes deformable. The temperature and pressure were then ramped up to their hold conditions, i.e. 1700 - 1800°C and 150 - 300 MPa, using either argon or helium as the pressurising gas. After HIP, the encapsulant glass was removed by sandblasting. A further development of this method, allowing slightly more complex shapes, involved packing the Si_3N_4 article in SiO_2 powder within a Pyrex glass capsule, Fig.2.3. The use of an inner glass powder that softens at a higher temperature than the capsule, allows the formation of an intermediate composition / viscosity region between the two glasses. This was found to be necessary because the Pyrex tends to run - off at temperatures in excess of 1000°C and the inner silica powder will not soften until 1250°C . The desire to fabricate more complex shaped parts, led to further investigations into methods of near net shape encapsulation via the use of a glass powder [73-80]. The article to be HIPed is placed in the glass powder within a graphite crucible, Fig.2.4. A barrier layer of boron nitride is used between the glass and the crucible to allow easy removal and prevent any

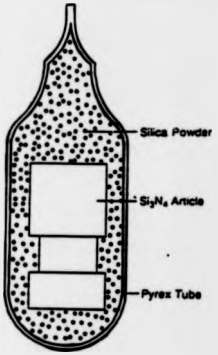

Fig.2.3. Schematic Representation of ASEA Tubular Encapsulation [72].

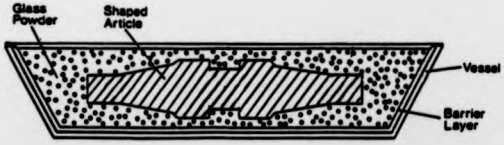

Fig.2.4. Schematic Diagram of ASEA Glass Powder Bed Encapsulation [73]

reaction occuring. The encapsulant melting is conducted under vacuum and full pressure is applied when the melted glass has a suitable viscosity, i.e. a maximum of 10^6 poise. Glass powder bed encapsulation has been shown to be suitable for the mass production of densified ceramics, with a maximum processing capacity of over 26,000 components in one HIP cycle [80].

The major disadvantage cited for the use of HIP of ceramics, is the relatively high cost. However, HIP is already an established fabrication route for the removal of porosity in WC - Co alloys [81,82], for the processing of Ti superalloys and electronic ceramics [83]. ABB Cerama AB are presently operating HIP units, ranging in volume from 5 to 600 litres, with the smaller units capable of 2000°C .

HIP development of ceramics is still in its infancy, but the technique will gain greater approval as costs are reduced and green state processing methods improve.

2.2. TOUGHENING MECHANISMS.

Engineering components fail at an applied stress below the calculated critical applied stress because of the presence of microscopic flaws, produced during the processing stage and/or during service. Inglis [84] considered such flaws as local stress concentrators which have the effect of magnifying the applied stress by 100 to 1000 times. To consider why some materials are more sensitive to flaws than others, a fracture mechanics approach was adopted. Griffith's work on crack stability [85], believed unstable fracture occurs when the energy loss when the crack propagates equals the energy created in forming two new surfaces.

$$\sigma_f = [(2E\gamma)/(\pi c)]^{1/2} \quad \ldots\ldots\ldots\ldots\ldots \quad 2.3$$

where σ_f = fracture stress
E = Young's Modulus
γ = surface energy
c = crack length

Other energy dissipative mechanisms, such as plasticity, exist during crack propagation. Irwin suggested that crack propagation will occur provided the energy release rate (G) exceeds the energy required to form the two new surfaces, i.e. when $G > 2\gamma$ [86]. Hence the modified Griffith equation of (2.3) becomes

$$\sigma_f = [(E G_c)/(\pi c)]^{1/2} \quad \ldots\ldots\ldots\ldots\ldots \quad 2.4$$

where G_c = the critical strain energy release rate or toughness.
The onset of fast fracture occurs when :

$$\sigma_f (\pi c)^{1/2} = (E G_c)^{1/2} \quad \ldots\ldots\ldots\ldots\ldots \quad 2.5$$

The right hand side of equation 2.5 depends on material properties only. Thus, the term $\sigma_f (\pi c)^{1/2}$, the critical stress intensity factor, K_c, is a material constant. This term is more usually called the fracture toughness.

Brittle fracture may be resolved into into three distinct modes, Fig.2.5, and thus G_c and K_c can be suffixed to describe the energy release in a specific mode of crack propagation. When a crack propagates in a direction perpendicular to the applied stress i.e. mode 1 K_c is denoted by K_{Ic} to indicate that this is the prevalent mode.

Si_3N_4 has a low K_{Ic} value and thus is very sensitive to flaws. This causes unreliability in fabricated parts because of variations in stress to failure of a

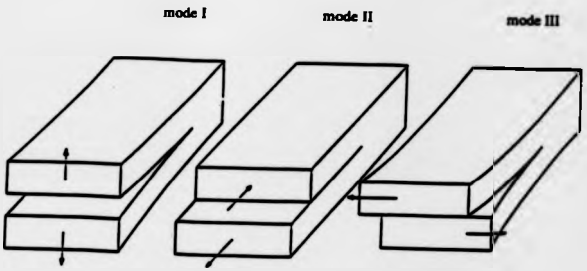

Fig.2.5. Brittle Fracture Modes.

sample of similar components. There are two different routes to achieve higher reliability :

a) the flaw control approach;

b) the toughening approach.

In the first route the various processing flaws are controlled by identifying and eliminating the dominant heterogeneity and the processing step responsible for it [87,88]. In the second approach microstructures are created which impart sufficient fracture resistance that the strength becomes insensitive to the size of the flaws [89].

There are a variety of mechanisms that contribute to toughening, such as process zone mechanisms, crack bridging mechanisms and crack deflection. Transformation toughening is a process zone mechanism [90,91] caused by the constraining effect of the residual strain field in particles around the crack tip undergoing phase transformation. As already mentioned, this temperature dependent process is prevalent in zirconia based materials but not in Si_3N_4.

2.2.1. Crack bridging mechanisms.

Reinforcing phases that bridge a crack surface, can be divided into those that are ductile and those that are brittle. Ductile toughened ceramics refers to metal toughened ceramics (cermets) and rely on high toughness and ductility to allow metal ligaments to exist and to contribute to toughness through plastic dissipation. Large local residual stresses caused by thermal expansion mismatch, are capable of suppressing local crack propagation and allow intact ligaments to exist behind the crack front [92,93].

Crack bridging with brittle materials with a toughness similar to that of the matrix is more subtle and requires residual stresses due to different elastic

constants, weak interfaces or both. The classical example of the formation of a bridging zone is seen in continuous fibre reinforced ceramics, where toughness is enhanced by the extensive pullout of the fibres in this zone [94-98] . Tough ceramics like this exhibit a typical stress / strain curve shown in Fig.2.6. In any analytical solution to these phenomena, the role of key matrix and dispersoid properties needs to be addressed.

If the elastic constants of the whisker are much larger than that of the matrix, the crack tip stresses can be altered so that a crack travelling normal to the whisker axis is deflected out of plane as it approaches the whisker [99]. However, in the case of SiC reinforced Si_3N_4 , the elastic properties of the two phases are similar i.e.Young's moduli are approximately 400 GPa and 300 GPa for SiC and Si_3N_4, respectively. Also, the fracture toughness values for Si_3N_4 are in the range 4 to 6 $MPa.m^{1/2}$ versus 3 to 4.5 $MPa.m^{1/2}$ for SiC. Thus deflection of the crack as it approaches the interface due to differences in elastic properties appear to be negligible in such systems.

The second process which avoids whisker fracture, involves debonding of the whisker / matrix interface as the crack approaches or just reaches the whisker, Fig.2.7. The magnitude of the toughening depends on the debond extent, the mode of reinforcement failure and residual stress effects. Theoretical models have been developed and compared to electron microscopy studies of the behaviour of dynamic and static cracks in whisker reinforced brittle matrices [100,101].

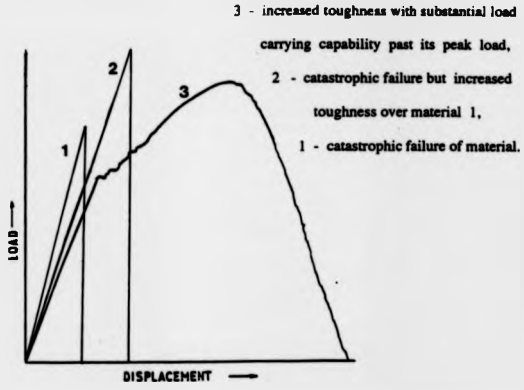

Fig. 2.6. Schematic illustration of typical load / displacement behaviour of different ceramics.

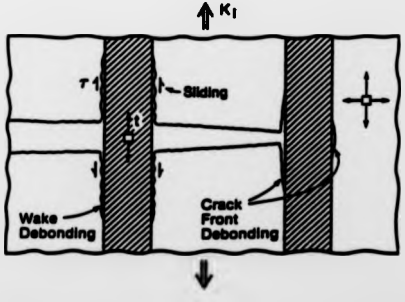

Fig.2.7. Schematic of a bridging zone in a reinforced composite [105]

2.2.1.a. Interface Debonding.

For a matrix crack subject to mode 1 loading, the occurrence of initial debonding rather than cracking into the whisker, is governed by the ratio of interface to whisker fracture energies T_i / T_f and the whisker orientation, Fig.2.8. For SiC / Si_3N_4 composites, T_i / T_f should be < 1/3 to debond whiskers normal to the crack plane. This prediction is independent of residual stress. Growth of the initial debond along the interface is influenced by the residual stress and whisker radius and it is most noticeable in the crack wake [103,104].

Analysis of wake debonding for interfaces under residual tension, as in SiC / Si_3N_4 composites, indicates that debond growth in the wake occurs when the stress, t on the whisker reaches a critical value t^*, given by :

$$t^* = 2.2\ E_f\ e_i \quad \ldots\ldots\ldots\ldots\ldots\ 2.6 \quad [103]$$

where E_f = Young's modulus for the whisker
e_i = misfit strain

When $t > t^*$, the debond propagates unstably up the interface.

2.2.1.b Toughening.

In reinforced ceramics which fracture by the growth of a single dominant flaw in Mode 1, there are four contributions which influence toughness, Fig.2.9. Debonding generates new surface and contributes positively to toughness. Frictional dissipation upon pullout results in local heating and again contributes positively. Residual stresses present in the material are partially relieved by matrix cracking and debonding, and thus detract from the toughness. When the whiskers fail, some of the elastic energy stored in the whisker is dissipated through acoustic waves and appears as a positive contribution to toughness. These effects are indicative of resistance curve behaviour, because each contribution is only fully realised when the whiskers fail and

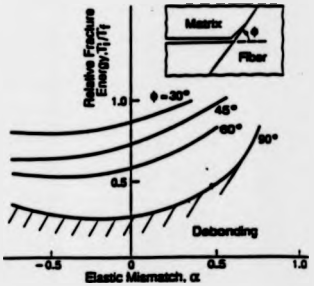

Fig.2.8. Debond diagram of the dependency of fracture energy on elastic mismatch and whisker orientation [101].

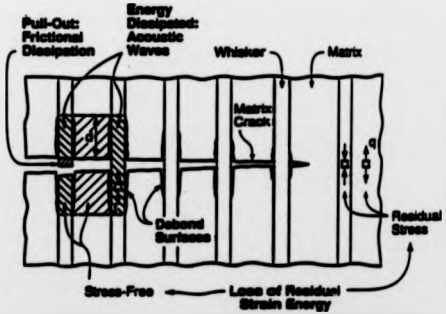

Fig.2.9. Schematic representation of the four mechanisms that contribute to toughening by whiskers [101].

pull-out [105]. The simplest possible result that is physically consistent with the mechanisms involved is given by :

$$\Delta G_c = f d [S^2/E - E \epsilon^2 + 4 (T_i / R)/(1 - f)] + 2 t f h_p^2 / R \quad ..... \; 2.7 \quad [101]$$

where :

ΔG_c = steady state toughening
f = volume fraction of whiskers
d = debond length
S = whisker strength
E = composite Young's Modulus
ϵ = misfit strain
T_i = fracture energy / unit area
R = whisker radius
t = sliding resistance
h_p = pullout length

The first term, S^2 / E is a bridging contribution and is simply the strain energy stored in the whisker over the debonded length on both sides of the matrix crack, before the whisker fails. The second term, $E \epsilon^2$ is the loss of residual strain energy in each composite element within the debond length, when the whisker fails. The third term is the energy needed to create the new surface caused by debonding. The fourth term is the pullout contribution, dissipated by frictional sliding of the interfaces.

The residual strain term is small in SiC / Si_3N_4 systems and can often be neglected [105]. The largest potential for toughness is in the pullout term, provided that h_p / R is large. Different pullout behaviour in ceramic composites produces a wide range of toughness values. The dominance of the pullout term for increased toughness, means optimising those whisker properties that optimise frictional dissipation. If whisker pullout does not contribute to toughness, the elastic energy and debonding energy terms tend to govern the fracture resistance, such that :

$$\Delta G_c = f d \; S^2 / E + 4 T_i \; f (d / R) / (1-f) \quad ..... \quad 2.8$$

All contributions scale with debond length, indicating that large d is desirable. The debond length d depends on the interface fracture energy, misfit strain and the frictional coefficient. The associated relationships are unknown, but dimensional analysis suggests that :

$$d/R = H(E R \varepsilon^2/T_i), S/E\varepsilon_i \quad \ldots\ldots\ldots\ldots \quad 2.9 \quad [103,104]$$

where H is a numerical function.

Thus, there is much scope for controlling toughness by manipulating the interface debonding, the sliding properties and by maximizing the dispersoid strength. The toughening contribution from the elastic strain energy stored in the whisker strength up to failure, is dominated by the whisker strength. Whiskers can, and must, have very high tensile strengths to sustain the applied stress within the wake of the crack tip, and in order to increase toughness. Since residual strain is generally detrimental, matched thermal expansions are desirable. Enhanced debonding is desirable, but the relative contributions to toughness from bridging and from the debonded surfaces, need elaboration.

From equation 2.9, the debond length should increase with increasing whisker radius, increasing whisker strength and decreasing T_i. d/ R and T_i are related in such a way that the contribution to ΔG_c from the energy of the debonded surfaces in equation 2.7, is expected to be weakly dependent on T_i and insensitive to whisker radius, but should increase as the whisker strength increases. For the bridging contribution, the direct dependence on debond length suggests that the contribution should increase as T_i decreases or the whisker radius increases and should become the dominant contribution to toughness for small T_i and large R, provided that the strength is also high.

Experimental work on SiC / Al_2O_3 [100], indicates a systematic

dependence of ΔG_c on R, confirming an important contribution of elastic bridging to toughening.

2.2.2 Crack deflection.

Second phase particles located in the near tip field of a propagating crack, perturb the front causing a reduction in the stress intensity. The reduced stress intensity depends on the character of the particles and the nature of the crack interaction. Quantitative crack deflection models have been proposed to predict the change in fracture toughness due to non-planar crack propagation using 3 dimensional [106] and 2 dimensional randomly arranged dispersoids [107]. The non-planar crack arises either from residual strains present in the material or from the existence of weakened interfaces.

2.2.2.a Crack deflection theory.

When the crack intercepts the dispersoid, the crack is forced to tilt out of the plane normal to the applied stress. Continued propagation around the dispersoid results in crack front twist, specifically when the orientation of adjacent dispersoids requires the crack to tilt in opposite directions. The increase in fracture toughness imparted by deflection of the crack, is evaluated from the local stress intensities at the tilted and twisted portions of the crack front. This is achieved by firstly assessing the local stress intensity factors K_I, K_{II} and K_{III} as a function of deflection angle. Crack advance is then assumed to be governed by the strain energy release rate, G, pertinent to each segment of the crack front along its deflected trajectory. The average $< G >$ across the crack front is then considered to represent the net crack driving force. This is compared with the strain energy release rate for an undeflected crack. The toughening

increment is computed by synthesising the tilt and twist components.

A summary of the analytical modeling of toughening from crack deflection for different dispersoids is shown in Fig.2.10. The spheres provide least effective toughening, discs an intermediate level and whiskers with large aspect ratio, the highest level of toughening. It is also noticeable that improved toughening is achieved by having a non- uniform distribution of sphere spacings, which would indicate that non-uniform spacing of whiskers and platelets may also be beneficial. Comparing whiskers randomly aligned in a 3 dimensional array [106] with those arranged in a 2 dimensional random distribution normal to the crack [107], show superior results for the latter, Fig.2.11. It is noticeable that the curves for a 2 dimensional random distribution of whiskers has a similar shape to that of a 3 dimensional random array. Also, the toughening increment becomes nearly independent of volume fraction above V_f = 0.20. For the 3 dimensional model, toughening arises mainly from the twist of the crack front; for the 2 dimensional model, both subsequent tilt and twist provide nearly the same contribution to the toughening. Fig.2.11 demonstrates that the toughness increase depends not only on the aspect ratio and volume fraction of whiskers, but also on the orientation of whiskers to the crack propagation plane.

2.2.2.b. Comparison of experimental work with crack deflection theory.

Experimental work on particle morphology effects in a barium silicate glass ceramic [108] and hot pressed SiC whisker glass matrix composites [109] showed the toughening trends agreed with those predicted from the crack deflection model. However, results show that dispersoid toughening is more effective in a glass matrix than in a polycrystalline ceramic matrix. This is because glasses show flat fracture surfaces which agree well with the model's assumption that the crack would propagate

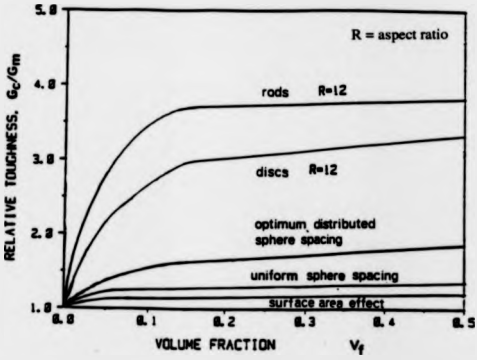

Fig.2.10. Summary of the relative toughness predictions from crack deflection model for 3 - dimensionally arranged dispersoids [106].

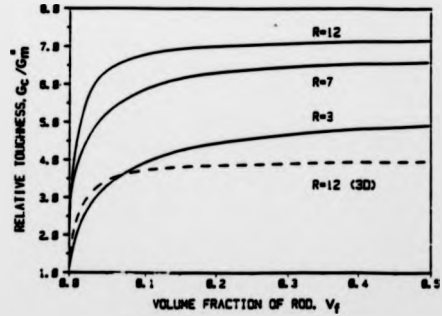

Fig.2.11. Relative toughness predictions of the crack deflection model for 2 - dimensional and 3 - dimensional arranged rods [107].

in a plane if no strong second phase particles exist. The addition of whiskers to glass matrix composites [109] changed the fracture morphology from a smooth to a rough surface. In this case, theoretical predictions and experimental results can be correlated.

Many polycrystalline ceramics, like Si_3N_4, exhibit intergranular fracture and the crack does not propagate in a plane, even in the absence of dispersoids. This means that there is already crack deflection in the ceramic, thus it is not reasonable to make a toughness prediction by using Fig.2.11 directly, because of the comparison with a plane fracture of the matrix. A toughening prediction should consider some kind of crack deflection due to intergranular fracture behaviour in the polycrystalline matrix. If the matrix grains are equiaxed, a relative crack deflection toughening value of $G_c / G_c^m = 1.56$ at a critical volume fraction, $V_f = 0.74$, was calculated [107]. This value,1.56, may be used as a good approximation to correct the crack deflection toughening curves for both 2 and 3 dimensional models and is illustrated in Fig.2.12. To compare with experimental data, the approximate relation between the critical stress intensity factor,K_c and the critical strain energy release rate, G_c has been used :

$$G_c = K_c^2 (1-\nu^2) / E \qquad \ldots\ldots\ldots\ldots\ldots \quad 2.10 \qquad [107]$$

where ν is the poisson's ratio.

The prediction of toughening in SiC whisker / Si_3N_4 composites, where matrix grains are elongated, is difficult. The anisotropy of toughness can be explained by the 2 dimensional model, but not by the 3 dimensional one. As there is already crack deflection by rod shaped β - Si_3N_4 grains in the matrix, the relative toughening due to crack deflection by the addition of SiC whiskers is lower than that in a matrix with equiaxed grains. Models which take account of grain size distribution have been suggested [110] but deviations from all crack deflection predictions occur because several toughening mechanisms are likely to operate simultaneously.

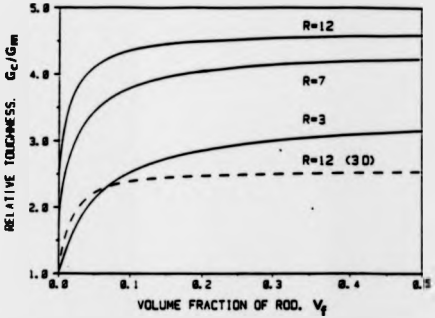

Fig.2.12. Relative toughness predictions for 2 - dimensional and 3 - dimensional randomly arranged rods compared with an intergranular fracture in the ceramic matrix with equiaxed grains [107].

2.2.3. Microcracking.

Microcracks can appear in the composite on cooling from the fabrication temperature because residual stresses arise due to thermal expansion or elastic modulus mismatch between different phases [111,112]. Greater contractive strains in the dispersoid can lead to a partial or complete peripheral crack. Lower contraction in the dispersoid can lead to cracks propagating out into the matrix. Microcracking not only depends on the magnitude of the thermomechanical stress field, but also on the size of the dispersoid phase. Evidence suggests that peripheral cracks form above a critical dispersoid diameter, D_c [113,114].

$$D_c = A Y_b / (E_c \varepsilon^2) \qquad \ldots\ldots\ldots\ldots\ldots\ldots \quad 2.11$$

where A = proportionality constant (= 9 for a particle and 6 for fibres),

Y_b = interfacial or grain boundary fracture energy,

E_c = Young's modulus of the composite,

ε = strain difference if neither the matrix nor the second phase were constraining the other.

Pre-existing microcracks, caused by property mismatches, are often large, giving weak materials. However, microcracks can be generated due to the superposition of the high tensile stresses concentrated near a crack tip and the mismatch stresses of the material [115]. As a result, a microcracked "process zone" is formed around the crack tip. The design of systems in which microcracking would only occur in the high stress region of a highly stressed crack, may be an important mechanism whereby the amount of strength limitation that microcracking may impose, can be kept small, allowing this to be a mechanism of toughening with good strengths. A number of substantive problems exist in the analysis of microcrack toughening, both experimental and theoretical. Among the problems are a poor fundamental understanding of the

degradation caused by the microcracks directly ahead of the crack front, as well as experimental microcrack detectability limitations [113].

An analysis of the toughening behaviour of microcracks formed around particles in a matrix, shows that it depends on the size of the microcracks and on the size and distribution of the dispersoid [116]. Useful toughening increases of 2 to 5 times that without microcracking are indicated for fairly narrow distributions of microcrack / dispersoid sizes.

2.2.4 Crack Branching.

Crack branching commonly occurs in combination with crack deflection and microcracking, Fig.2.13, [117]. If crack deflection or microcracking by themselves make a substantial improvement in fracture toughness, then having two cracks, both of which are also undergoing crack deflection or generating a broader zone of microcracking, should result in a higher level of fracture energy. Crack branching is a common occurrence in a wide variety of both particulate and fibre composites [118,119].

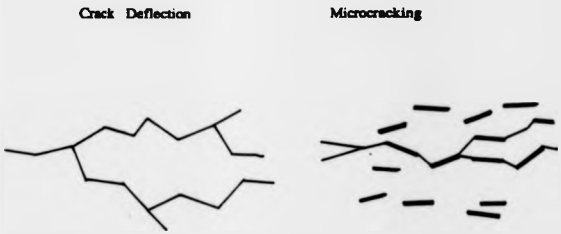

Fig.2.13. Schematic illustration of crack branching in combination with crack deflection and microcracking.

2.3. PROPERTIES OF SiC DISPERSOID REINFORCED Si_3N_4 CERAMICS.

Whisker reinforced ceramic matrix composites have received a great deal of attention in recent years now that commercial supplies of SiC whiskers are available. The sections below outline some of the results of previous research on some SiC dispersoid ceramic systems.

2.3.1. Room Temperature Mechanical Properties.

Initial work on hot - pressed SiC whisker reinforced alumina and mullite showed significant improvements in fracture toughness over the monolith [120,121]. These results stimulated work on hot pressed Si_3N_4 ceramics, but usually more modest increases in toughness were found [122-126]. However, there was evidence of much better reliability in the composites, i.e. values of 23 to 29 for Weibull's modulus of the composites compared with 10 to 15 for the monolith [122]. A large increase in fracture toughness with increasing whisker content, up to a value of 10.5 $MPa.m^{1/2}$ has been reported, using relatively large diameter, non - commercial VLS whiskers [127]. Results using various processing conditions and sintering additives in HIPed SiC whisker reinforced Si_3N_4 composites have shown varying success. Some researchers report modest gains [128,129], but often accompanied by reductions in fracture strength, while other reports have shown that whiskers are detrimental to both fracture strength and toughness [130,131]. The presence of impurities, processing problems and strong interfacial bonding have been cited as reasons for the decline in properties.

It has been shown that the orientation of whisker and elongated β - Si_3N_4 grains with respect to the crack plane has a significant effect on the fracture toughness [128]. Results indicate that the highest toughness is obtained when the axis of the acicular feature is 90° to the crack plane, indicating that crack bridging contributes to

the increased toughness of the system. There was also a linear relationship between fracture toughness and the quantity of elongated features perpendicular to the crack plane.

The oxidation and creep resistance of pure Si_3N_4 are known to be vastly superior to alloyed Si_3N_4 at very high temperatures. However, this is at the detriment of fracture toughness even though full densification can still take place [132]. This is because the fracture toughness of monolithic Si_3N_4 ceramics is dependent largely on the grain shape which develops during processing, and the amount of intergranular fracture [133,134]. In non - doped samples, equiaxed grains are formed because there is insufficient volume of liquid phase at consolidation temperature, which consequently does not allow the desirable formation of elongated β - Si_3N_4 grains. Introducing whiskers into a non-doped Si_3N_4 produced greater than 95.5% density, but it was found the fracture toughness was slightly below that of the doped composite [129,135], indicating that the matrix grain shape has an influence on the mechanical properties of the composite.

A major drawback with the use of fine, large aspect ratio whiskers is the health problems associated with them [136]. Consequently, some work has been conducted on developing less hazardous reinforcing media such as SiC platelets. Theoretical models of toughening mechanisms, suggest that platelets could be an effective substitute for whiskers [106]. SiC platelets incorporated into Al_2O_3 have shown increases in fracture toughness compared to the monolith [137,138] and a slight improvement with respect to a similar loading of whiskers.

A comparative study of the properties of the materials investigated in this research programme and other ceramic composite systems, will be discussed in chapter 7.

2.3.2. High Temperature Deformation.

At high temperatures and under load, ceramic materials show time dependent plastic deformation or creep. The total creep deformation can be expressed as the sum of the elastic, primary and secondary creep rates, Fig.2.14. Some materials also display a tertiary creep stage that involves a rapidly increasing creep strain, but this is not pronounced for ceramics.

Upon application of the load, the initial elastic strain is followed by primary creep in which the creep rate decreases with increasing strain and time. Secondary or steady state creep behaviour is widely described by a Arrhenius type equation :

$$E_s = A \sigma^n \exp(-Q/RT) \quad \ldots\ldots\ldots\ldots\ldots\ldots \quad 2.12$$

where E_s = steady state creep rate
A = constant
σ = applied stress
n = stress exponent
Q = activation energy for diffusion process
T = temperature.

Characterisation of the steady state creep rates is one of the main aspects of deformation studies, as this stage is usually assumed to occupy most of the sample lifetime. Experimental determination of n and Q can give an insight into the mechanisms of creep operating, but their values depend on combinations of σ, E and T. In some instances it has been reported that steady state creep rates were not reached in Si_3N_4 based ceramics as the structure is constantly changing with increasing strain and never reaches equilibrium [139,140]. However, steady state creep has generally been reported [141,142], and a comparison of the steady state behaviour of selected ceramic systems is illustrated in Fig. 2.15.

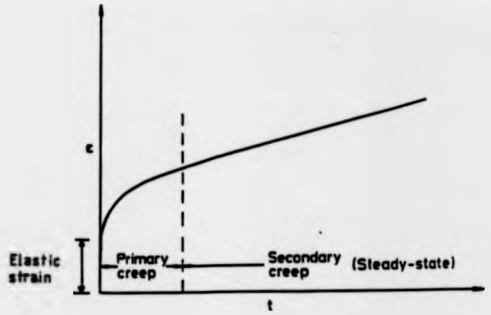

Fig.2.14. Schematic Diagram of Different Stages of Deformation During Creep at Constant Temperature and Stress.

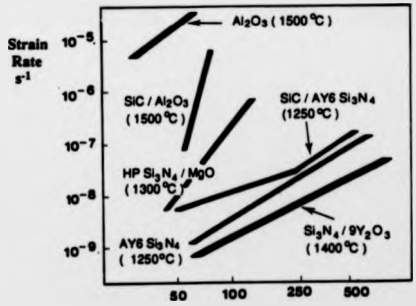

Fig.2.15. An Overview of the Steady - State Creep Behaviour of Selected Ceramics.

In practise the overall creep rates will be a superposition of different creep components. The creep component which dominates at any particular time depends on the microstructure as well as the experimental conditions. Viscoelastic effects usually account for the primary creep component [143]. In the long term, the predominant creep mechanisms in Si_3N_4 materials are grain boundary sliding accommodated by diffusion and cavitational controlled mechanisms [144-146]. Diffusional creep consists of two mechanisms i) Nabarro - Herring creep, which is a purely volume diffusion controlled process initiated by stress, which results in directed diffusional flow to relax the stress [147,148]; ii) Coble creep, where diffusion is assumed to occur through the grain boundaries only, and in ceramics involves the transport of the solid phase through the intergranular liquid, from regions of higher compression to regions of lower, and is driven by a gradient in chemical potential [149,150]. An important feature of these two diffusional creep mechanisms is the proportionality of the strain rate to the applied stress, so that the stress exponent n equals 1. Cavitational creep is the result of stresses in the grain boundaries which cause holes to nucleate in the glassy phase, if the ceramic contains residual amorphous regions [151-153]. The cavities nucleate at inhomogenieties, such as impurities, vapour bubbles, dislocations and ledges. The amount of cavitation increases as the viscosity of the glassy intergranular phase decreases and its volume fraction increases [150]. The stress exponent for this creep behaviour is usually > 1.5.

At elevated temperatures, failure of ceramic samples usually becomes time dependent. In the high stress regime, fracture is dominated by sub- critical crack growth from pre-existing flaws, whereas at low stress levels, failure is predominantly by creep rupture, as the result of the formation of microcracks by the coalescence of cavities. Minimising the volume of glassy phase can prevent cavity formation and

hence this damaging form of fracture.

It has been shown that incorporating SiC whiskers into a polycrystalline Al_2O_3 matrix reduces the creep rate significantly, although the stress exponent n changes from 2 for the monolith to 5 for the composite. This indicates that different mechanisms for creep are operating in each material [141,154]. Additions of SiC whiskers to a Si_3N_4 ceramic has been shown to increase the creep rate compared to the monolith, although it was reported that the viscosity of the intergranular phase decreased on incorporating whiskers into the monolith [142,155]. This indicates the critical nature of the intergranular phase in determining the creep behaviour of the material.

2.3.3. Oxidation of Si_3N_4 Ceramics.

The oxidation behaviour of Si_3N_4 based ceramics is important as their potential applications will involve extended use at relatively high temperatures. There are essentially two oxidation mechanisms, active and passive oxidation. Active oxidation occurs in the presence of low oxygen pressures and is characterised by an overall specimen weight loss due to the evolution of gaseous SiO and proceeds via ;

$$Si_3N_4 + 3/2\,O_2 \quad \text{-------->} \quad 3\,SiO + 2\,N_2 \qquad \ldots\ldots\ldots\ldots \quad 2.13$$

or $$Si_3N_4 + 3\,SiO_2 \quad \text{-------->} \quad 6\,SiO + 2\,N_2 \qquad \ldots\ldots\ldots\ldots \quad 2.14$$

Equation 2.14 arises from the reaction with the silica scale formed during passive oxidation.

Passive oxidation is of most interest to researchers because it occurs in normal atmospheric conditions and it results in an overall weight gain. Nitrides and carbides are thermodynamically less stable than oxides and are thus expected to oxidise in oxygen containing atmospheres such as air and and water vapour. Therefore, their

oxidation resistance depends on the kinetics of the oxidation reactions, 2.15 and 2.16.

$$Si_3N_4 + 3O_2 \text{ ------->} 3SiO_2 + 2N_2 \quad \ldots\ldots\ldots \quad 2.15$$

$$SiC + 3/2\,O_2 \text{ ------->} SiO_2 + CO \quad \ldots\ldots\ldots \quad 2.16$$

There is a synergistic phase influence in these composites, unlike in SiC whisker reinforced Al_2O_3 where mullite is formed. In the former a protective silica layer is formed and the oxidation rate is expected to follow a parabolic relationship of the form :

$$(\Delta W/S)^2 = k\,t \quad \ldots\ldots\ldots \quad 2.17$$

where ΔW = weight gain,
S = the reactive area,
k = parabolic rate constant,
t = time

Such a parabolic law has been reported to describe passive oxidation of pure Si_3N_4 and SiC by oxidation [156,157]. Under such conditions, the limiting step will normally be the oxygen diffusion through the silica layer, the nature of which must be of importance to the kinetics of the reaction. The presence of an intergranular phase and microstructural features makes the kinetic behaviour more complex. Several mechanisms have been proposed as the rate controlling mechanism, including the in - diffusion of O^{2-} and the out - diffusion of cationic species which are present in the intergranular phase as either the sintering additive or impurities [158,159]. The rate of oxide scale formation has been shown to be dependent upon the type and amount of intergranular phase present, and altering the viscosity of this phase, changes the oxidation resistance of the material [160-162].

2.4. PROJECT PHILOSOPHY AND OBJECTIVES.

Given the points raised in the forgoing chapters, the research project described in the following chapters had the following interlinked aims and objectives :

. to explore whether fully - dense ceramics matrix composites containing various types of SiC dispersoid reinforcement in a well characterised Si_3N_4 matrix could be prepared and fabricated to full or near full densities by Hot Pressing and HIP.

. to examine whether the reinforcement acted to provide sizeable flaws, thus reducing fracture strength, or whether significant toughening could be induced.

. to explore the extent to which such materials might show a higher reproducibility of properties than the Si_3N_4 matrix alone.

. to examine the high temperature deformation properties to see if the matrix/ reinforcement interfaces acted as longer diffusion paths, thus reducing creep rates.

CHAPTER THREE

EXPERIMENTAL TECHNIQUES.

This chapter describes the experimental techniques used for the preparation, characterisation and mechanical testing of the materials investigated during this research programme.

3.1. COMPOSITE PROCESSING.

Billets of the ceramic composites were prepared using two main steps. Firstly, by powder consolidation to a green shape by slip casting and secondly by the densification and microstructural development to eliminate porosity by HIP.

3.1.1. Slip Casting.

Slip casting offers the possibility of preferential alignment of the dispersoids, which theoretical models and practical situations in other materials suggest should enhance toughness of the monolith and composites containing a similar volume fraction of randomly oriented dispersoids. The matrix composition was prepared initially, by ball milling the constituents with propan-2-ol in 1 litre high density polyethylene containers. The milling media were 9mm diameter HIPed Si_3N_4 cylindrical balls*, which minimizes any powder contamination. Milling lasted for at least 24 hours, which ensured both a fine particle size and a homogeneous dispersion of the sintering aid, before the slurry was dried, crushed and sieved.

* Kemanord Engineering Ceramics, Ljungaverk, Sweden.

Research work involving whiskers in the dry state is extremely hazardous, so all processing involving whiskers in non-liquid media was conducted in a glove box. The as-received dispersoids were added to distilled water to make a 25 wt.% solid loading, and stirred for about 10 minutes. This helped disentangle agglomerates which could otherwise form unwanted heterogeneities. The sieved matrix material was also dispersed in water to form a 60 wt.% solid loading, stirred for 5 minutes, then the two separate slurries were mixed together. As high a fraction of solids as possible was formed because this avoids excessive shrinkage during the slip casting. However, the initial composite slurries produced became flocculated and non-pourable because of considerable particle- particle attraction due to the electrostatic interactions, steric hindrances, or a combination of both. By adding a few drops of ammonia to increase the pH, the viscosity of the slip decreased as the zeta potential increased. Increasing the pH further increased deflocculation so that near a pH of 10 there was obvious mass segregation of the dispersoid phase.

Working at a pH of 8.6 there was no segregation but the slip was quite viscous due to a degree of flocculation. In a relatively flocculated slip, liquid was immobilised in the interparticulate void space of the flocs and floc networks. The suspension was redispersed by high shear rates using a shear mixer. This decreased the apparent viscosity as the flocs and floc networks broke down and released the entrapped liquid. As the mechanically dispersed mixture leaves the high shear rate field, it flocs to form a new mixed particle network so that after about 20 minutes there appeared to be complete and homogeneous dispersion of the SiC dispersoid phase within the matrix.

Before consolidation, the slip must be free of entrapped air or chemical reactions that would produce gas bubbles during casting, as these will be incorporated

into the casting and may become critical defects in the final densified part. Air bubbles were introduced during shear blending and were removed by placing the beaker containing the slip into a dessicator, connecting to a vacuum pump and de-airing until the slip level did not rise.

The colloidally treated slurry was consolidated to form a powder compact by slip casting. Several different moulds were made, but all consisted of a flat plaster of paris base with walls made of a non-porous material such as plastic or glass, so that the water was only filtered through the base. The mould base was prepared by mixing water with the plaster of paris, which was then poured into a rectangular box and left to set for 24 hours. On addition of water to plaster of paris (hemihydrate), very fine needle shaped crystals of gypsum are precipitated, eqn. 3.1, which intertwine to form the porous plaster mould.

$$CaSO_4.1/2\ H_2O + 3/2\ H_2O \longrightarrow CaSO_4.2H_2O \qquad \ldots\ldots\ 3.1$$

Altering the plaster/water ratio varies the size of the irregularly shaped microscopic continuous capillaries and hence the suction pressure. All the moulds in this study were made from 4 parts water to 5 parts plaster (by weight) to produce a mould about 4cm thick, which was dried in a oven at 60°C for 24 hours before use. Glass or plastic walls were placed on the plaster base to form 7cm diameter discs and 2.5cm x 13cm rectangular shaped moulds.

The de-aired slip was poured into the moulds, water was filtered out due to a pressure gradient, and a cake was formed on top of the plaster, Fig.3.1. As consolidation of the ceramic particles proceeded, the cake also behaved as an additional filtering medium and flow channels were created as the filtrate passed through the consolidated layer. The filtration process behaves parabolically, with a decrease in consolidation rate with increasing filtration time. This rate decrease always limits the

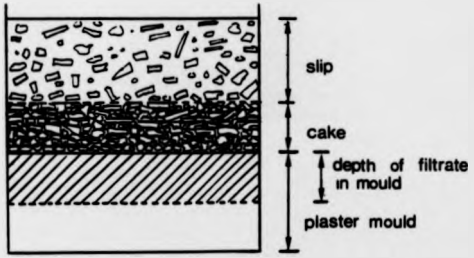

Fig.3.1. Cross-Section of Plaster of Paris Mould and Slip

usefulness of slip casting to a certain consolidation thickness. It was found that above a consolidation thickness of 2.5cm filtration through the cake and plaster was very difficult.

Once casting was completed, the cake began to dry and shrink away from the mould. This shrinkage was necessary otherwise the cake would be damaged during removal from the mould. Mould release was aided by coating the walls of the mould with a release agent such as silicone or olive oil. The cake was left in the mould for about 24 hours, which was sufficient to enable handling, and then it was dried in an oven at 60°C for a further 24 hours.

3.1.2. Densification.

The green state slip cast ceramics have only a density of between 40 and 50% that of the theoretical density and are consequently very brittle. To further densify them before HIP, they were vacuum packed in plastic bags, cold isostatically pressed (CIPed) at 150 MPa, removed from the plastic bags and fired at 1050°C for 4 hours in a N_2 atmosphere.

Samples containing 3- dimensionally randomly- arranged dispersoids were prepared in a similar way, except the slip casting stage was omitted. In these materials, all the constituents were ball milled together, then dried,crushed and sieved. The powder was then tightly packed into sealed rubber tubes, approximately 11cm long and 3cm in diameter, then CIPed.

All specimen compacts were then shipped to ABB Cerama in Sweden to be densified using their ASEA Quintus HIP system. The ceramic billets were encapsulated using the glass powder bed encapsulation process described on page 20. The encapsulant glass composition was not revealed by ABB Cerama, but it appears to

be similar to Pyrex [163]. HIPed sintering conditions were a temperature of 1725°C and a pressure of 160 MPa held for 1 hour, as shown in temperature / pressure profile in Fig.3.2. After HIP the encapsulant glass was removed by sand blasting and shipped back to the University of Warwick.

3.1.3. Hot Pressing.

The materials to be hot pressed were prepared in a similar way to the pre - slip casting stage outlined in 3.1.1. After shear blending the slurry mixture was filtered through a Buchner funnel and dried at 60°C for 24 hours. The thin sheet was cut to size and about 12g of this was stacked into a Boron Nitride (BN) coated graphite die, whilst in a glove box. This BN layer minimised reactions between the graphite and sample, and aided the removal of the hot pressed sample.

The die was placed concentrically inside a copper coil, through which cooling water passed, and thin BN coated graphite discs were placed in the bore of the die, at the bottom and the top of the sample. The graphite punch was inserted and the whole punch / die arrangement was carefully aligned with a hydraulically operated steel ram, as in Fig.3.3. A porous SiC disc , covered with saffil wool, was placed between the punch and the steel ram to provide thermal insulation, then the ram pressure was increased to about 10 MPa. The temperature was measured using a Pt-20% Rh/ Pt-40% Rh thermocouple placed in a closed end alumina sheath, which was inserted in a hole drilled into the body of the graphite die. To minimise heat loss, thermally insulating bubble alumina powder was poured into the chamber and Saffil board was placed over the enclosure.

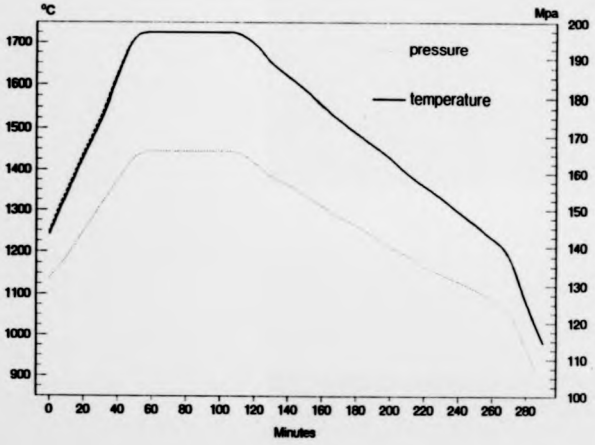

Fig.3.2. Temperature and Pressure Profile in HIP Furnace, Courtesy of ABB Cerama, Robertfors, Sweden.

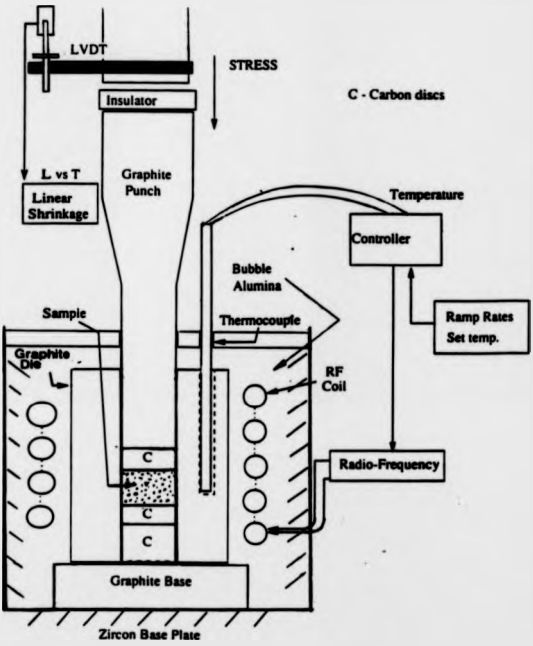

Fig.3.3. Schematic Diagram of the University of Warwick Hot Press.

The hot pressing furnace used radio frequency (R.F.) induction, coupled to the cooled copper coil, to heat the sample. R.F. power was increased slowly so that after 1/2 hour a power rating corresponding to a coil current of 0.9 Amps was maintained. Thereafter, the power and the applied pressure were increased in steady increments up to a operating power of 4 KW and a pressure of 22MPa. The temperature was controlled by an electronic PID controller and maintained at 1725 - 1750°C for at least 1 hour. Information on the linear displacement or shrinkage could be found from a LVDT attached to the moving ram and coupled to a dispacement / time chart recorder.

3.2. MICROSTRUCTURAL EVALUATION.

The following section describes the techniques used to characterise the densification of the ceramic materials, determine their constituents and to observe their microstructural features.

3.2.1. Density Measurement.

The densities of HIPed and hot pressed samples were measured using the Archimedes immersion method. Billets were cleaned in acetone then weighed on a micro-balance, first dry, M_a and then when immersed in methanol, M_m. The bulk density, ρ_s was calculated using equation 3.2.

$$\rho_s = \rho_m . M_a / (M_a - M_m) \quad \ldots\ldots\ldots\ldots\ldots \quad 3.2$$

where ρ_m = density of methanol.

The density of the green ceramic was measured by immersion in mercury using a Doulton densitometer. Mercury is a poor wetting agent and prevents penetration of the

liquid into the interconnecting porosity within the specimen.

3.2.2. X- Ray Diffraction (XRD)

XRD traces were obtained to gain information on the crystalline phases and polymorphic variations present in each specimen. Samples were ground and polished flat to a 1 μm finish, then analysed in a standard Philips horizontal scanning diffractometer. Spectra were taken using Cu $K_{\alpha 1}$ radiation of wavelength 1.5405 A, at a scanning rate of 1/2° $2\Theta min^{-1}$ for a 2Θ from 10° to 60°. With reference to the JCPDS files, the peaks obtained were converted to inter-planar d spacings using the Bragg equation.

3.2.3. Optical Microscopy.

Samples prepared for microscopy were first cut to size using an annular diamond bladed saw and then mounted in a conducting bakelite resin block. Surfaces were ground using successively finer wet SiC paper and polished with diamond lapping paste to a 1/4 μm polish. Optical micrographs were taken on a Carl Zeiss Ultraphot microscope.

3.2.4. Scanning Electron Microscopy.

Microstructural examination was performed using a Cambridge Instruments Stereoscan 250 Mk3 scanning electron microscope (SEM). Before observations, a thin conductive carbon or gold coating was evaporated onto the polished surface to prevent it charging in the electron beam. The facility was equipped with a K.E. Developments solid state back-scattered electron detector and a LINK AN 10,000 X-Ray micro-analysis system, fitted with a windowless detector.

3.2.5. Transmission Electron Microscopy.

Specimens prepared for the transmission electron microscope (TEM), were first cut to about 0.6mm thickness using the annular diamond saw, then ground to a thickness of approximately 150μm and polished on one side using 1/4 μm diamond paste. Discs of 3mm diameter were cut from the polished sections using a ultrasonic drill and a SiC suspension. The unpolished side of each disc was then dimpled using a South Bay Technology Inc. model 515 dimpling machine for a centre thickness of about 25μm using first 6μm and then a final 1/4 μm diamond paste. Discs were then thinned using an Ion Tech 5KV argon ion beam to produce electron transparent regions. These specimens were carbon coated and microscopy was performed on a JEOL 2000FX 200KV unit, fitted with a LINK systems 860 series X-Ray analyser. To examine the dispersoids at higher magnification in the TEM, a small amount was placed in a test tube and 5 drops of a plasticiser such as collodion amyl acetate were added. With the aid of a pipette, small droplets of the dispersoid suspension were allowed to dry on a 200 - mesh copper grid.

3.3. ROOM TEMPERATURE MECHANICAL TESTING.

Test bars from the densified billets were prepared both in-house using a Jones and Shipman surface grinder equipped with a diamond coated slitting wheel, and at P.S. Marsdens Ltd, Nottingham. In both cases, bars were machined to a 3.0 by 3.0mm cross-section, with the tensile face edges chamfered to 45°. All the test bars were machined from the bottom portion of the HIPed billets, with the tensile face being that surface parallel and closest to the bottom. The chamfers and tensile face were ground to a superfine polished finish (1/4 μm), whilst the remaining 3 faces were longitudinally ground to a 3μm polished finish. In all cases, the test bars were

machined to the maximum length possible and later cut to the length required by specific test fixtures.

3.3.1. Modulus of Rupture (M.O.R.)

The M.O.R. was measured in 4 point flexural mode using a jig with a outer span L, of 20mm and a inner span I, of 12mm. 4 point bending was preferred to 3 point because the applied moment and hence the outer fibre tensile stress, is constant over a portion of the beam and for thin beams the inner span is also characterised by an absence of shear stresses. The elastic outer fibre stress in 4 point bending was calculated from simple beam theory to give equation 3.3.

$$\sigma_f = 3 P_f (L - I) / 4 b h^2 \qquad \ldots\ldots\ldots\ldots\ldots\ldots \quad 3.3$$

where P_f = the fracture load
b = the specimen width
h = the specimen height

Mechanical testing was performed on a Instron 1122 machine with a 0 - 500 kg compression / tension load cell and using a cross-head speed of 0.5mm min^{-1}. Each end of the test bars was marked so that subsequent fracture surface investigations could be matched with the mechanical measurement. The test pieces and rollers were ultrasonically cleaned in acetone to remove grease and other contaminants. Care was taken to minimise load mislocation, beam twisting and unequal load application, as these would influence the calculated outer fibre stress.

There is normally a scatter of results found when measuring the fracture strength of ceramic materials the statistical nature of which depends on the probability that a flaw capable of initiating fracture at a specific applied stress is present. There are various statistical theories which have been developed, the best known of which uses the Weibull modulus as a measure of the reliability. The simplest form of Weibull's

approach is based on a weakest link model, the treatment of which is based partly on empirical reasoning, although there is increasing amount of theoretical justification for its use.

It has been deduced by statistical argument, that the most probable value of the survival probability for the j^{th} specimen in a total of n specimens is given by :

$$S_j = 1 - [(j - 0.3) / (n + 0.4)] \quad \ldots\ldots\ldots\ldots \quad 3.4$$

The Weibull Modulus m, is calculated from the gradient of a graph of $\ln \ln (1 / S_j)$ versus $\ln (x_j / x_o)$, where x_o is the value of x for which $S = 1/e = 0.37$ and x_j is the fracture strength of the j^{th} specimen.

$$\text{i.e. } \ln \ln (1/S) = m \ln (x / x_o) \quad \ldots\ldots\ldots\ldots \quad 3.5$$

A larger value for the Weibull modulus indicates a narrower strength distribution and hence greater reliability. Weibull statistics can be developed further by augmenting the Weibull equation with a stress area or stress volume integral term [164]. This allows comparison of results from different tests.

3.3.2. Vickers Hardness.

The Vickers indentation hardness is a method of measuring a material's resistance to penetration. A fixed load P, of 30 N was applied for 20 seconds via a Vickers diamond indenter and the dimensions of the residual impression were measured on the optical microscope using a graticule attachment. The Vickers Hardness, H_v is defined by :

$$H_v = P / A \quad \ldots\ldots\ldots\ldots \quad 3.6$$

where A is the projected area of the impression, defined generally by :

$$H_v = P / \alpha d^2 \quad \ldots\ldots\ldots\ldots \quad 3.7$$

where d is half the length of the diagonal and α is a numerical constant = 2 [165].

3.3.3. Fracture Toughness (K_{Ic})

There are a variety of methods for determining the fracture toughness of a ceramic, as expressed by the critical stress intensity factor K_{Ic}. Two methods were used in this study as comparative exercise; the single - edge notched beam (SENB) method, and the indentation fracture method.

The SENB method is well established [166,167] and consists of fracturing a beam specimen with a notch machined in the tensile face of the bar, Fig.3.4. The notch was cut by using a very thin annular diamond saw to a depth of 1mm, with the aid of an analogue clock gauge, and verified by using a travelling microscope. Fracture toughness was then measured using equation 3.8.

$$K_{Ic} = \frac{3 P_f (L - l) a^{1/2} [3.86 - 6.15 (a/h) + (a/h)^2]^{1/2}}{b h^2} \quad \ldots\ldots 3.8 \quad [168]$$

where a = the notch depth, and the other variables are as in equation 3.3.

The advantages of this technique are that it can be used for the determination of K_{Ic} at high temperature, test bars are easily prepared and it is a simple, well tried method. The only real disadvantages are the care needed when machining the notch and there is some doubt concerning the exact nature of the resulting microcracking at the tip of the notch. However, the expression assumes that the principles of linear elastic fracture mechanics can be applied. This means that the size of any plastic zone near the tip of the crack is sufficiently small to be negligible. The specimen dimensions should be large compared with the microstructural features of the material, which presents little problem in this case. Also, the notch should be atomically sharp at its tip. In many cases, the machining operation to produce the notch leaves sufficiently sharp cracks at the notch end for the data to be valid.

The indentation formed during the Vickers hardness test displays

complex crack systems which offer information regarding the fracture resistance of the ceramics. At the relatively high load used, two perpendicular half penny or median cracks, centred on the indentation are formed. These may be accompanied by extending cracks which initiate near the elastic-plastic boundary underneath the Vickers indenter. They form just prior to unloading and lie approximately parallel to the surface, propagating upon complete unloading. The extent of these fracture processes is used to give an estimation of the fracture toughness of the material using an equation :

$$K_c = 0.016 (E/H_v)^{1/2} (P/c^{3/2}) \quad \ldots\ldots\ldots \quad 3.9 \quad [165]$$

where E = Youngs Modulus

c = median crack length, Fig.3.5.

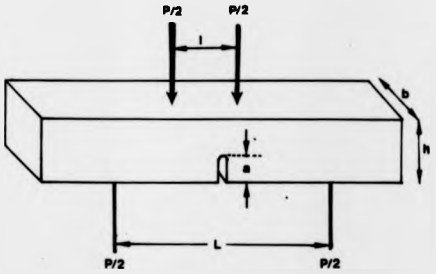

Fig.3.4. Schematic diagram of the SENB fracture toughness test piece.

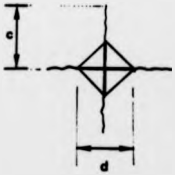

Fig.3.5. Schematic of indentation fracture toughness method showing planar view of cracks radiating from a Vickers indent.

3.4. HIGH TEMPERATURE PROPERTIES.

3.4.1. Creep.

High temperature deformation of selected compositions was performed using a 4 point bend creep rig, Fig. 3.6. The hot zone was created by using crusilite elements, powered by a Eurotherm controller via a R-type Pt - Pt/ Rh thermocouple, and was capable of operating at temperatures of over 1400°C. A slit furnace has been designed to allow ease of access to the specimen stage. Room temperature fluctuations were minimised using a thermostatically controlled air conditioning unit. The outer load supports consisted of a machined Refel SiC with the contact points set 23mm apart. The inner load points were SiC rollers held by a recrystallised alumina piece, the head of which had been ground into a domed shape to ensure proper axial loading. Creep deflection was measured using a capacitive LVDT, type 1071B, in conjunction with a model 22 AC- DC signal conditioner, and the output was connected to a multi-pen chart recorder. The LVDT and recorder were calibrated using feeler gauges of various known thicknesses, which were placed between the transducer and its platten.

The test bars, with a length of 30mm, were cleaned and inserted centrally between the rollers, then the furnace was closed and raised to the testing temperature at approximately 10°C / min. The apparatus was then allowed to stabilise for about 24 hours before a load P, corresponding to the calculated outer fibre stress σ in equation 3.10, was applied. Maximum strain ε_{max} is given by equation 3.11.

$$\sigma_{max} = \frac{P(L-I)}{2bh^2}\left(\frac{2n+1}{h}\right) \qquad \ldots\ldots\ldots\ldots\ldots 3.10$$

$$\varepsilon_{max} = \frac{6h}{(L-I)(L+2I)}\,Y \qquad \ldots\ldots\ldots\ldots\ldots 3.11 \quad [169]$$

where n = stress exponent (assumed =1 for diffusional creep)

Y = deflection at load points

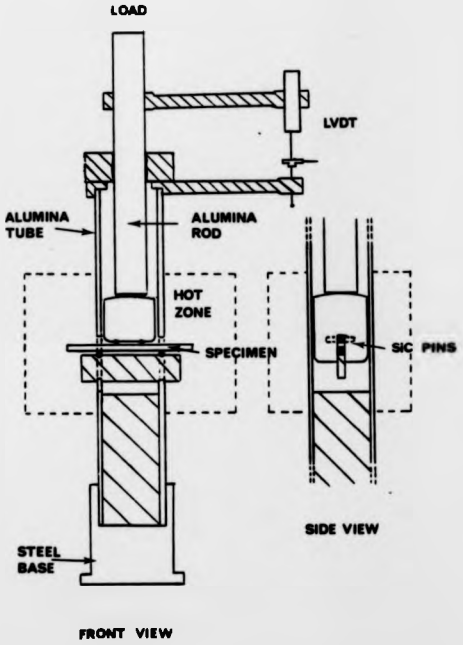

Fig.3.6. Schmatic diagram of 4 point bend creep apparatus.

Stress rupture was carried out in a similar manner to the creep deformation experiments at a constant temperature of 1400°C. The time to failure at a given load was indicated on the recording device.

3.4.2. Oxidation Resistance.

Passive oxidation tests were carried out in a high volume electric furnace using broken tests bars (3 x 3 cross-section) of selected compositions. Each specimen was placed on 2 SiC knife edge supports, which in turn were held in an inverted notched section of mullite tubing. The specimens were sectioned perpendicular to the major oxidation face and then polished to a 1 μm finish in order to observe the oxide scale development.

CHAPTER FOUR

MICROSTRUCTURAL EVALUATION.

4.1. INTRODUCTION.

One of the basic principles of materials science is that the properties of a material arise as a direct consequence of the material's microstructural features and correspondingly, the material's properties can be specifically engineered via microstructural modifications. To a large extent the type, size, shape, volume fraction, distribution and interfacial characteristics of the dispersoids, dictate the microstructual characteristics and properties of the ceramic composites investigated in this research programme. However, the matrix cannot be viewed merely as a cement that binds the dispersoids together because its microstructure and thermo - mechanical properties also play a very important and significant role.

In this chapter, the physical and chemical features of the dispersoids are surveyed, and the effect of processing and raw materials upon the bulk composite microstructure, phase evolution and the matrix / dispersoid interfacial characteristics are examined.

4.2. CHARACTERISATION OF DISPERSOIDS.

The main emphasis of the research programme was on SiC whisker reinforced composites, although subsequent work on platelet materials was performed when they became commercially available. Whiskers are needle - like high aspect ratio single crystals and are usually grown by the rice - hull process. Two different sources of these whiskers were used and both are illustrated in Fig.4.1 and Fig.4.2, to show

Fig.4.1. SEM micrograph of Tateho SiC whiskers.

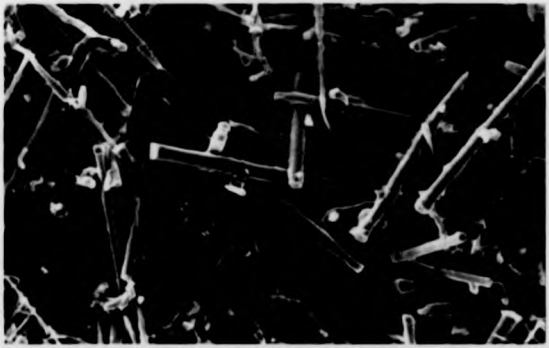

Fig.4.2. SEM micrograph of SNIA whiskers.

their general size and morphology. The initial source of whiskers from Tateho†, Fig.4.1, have relatively small diameters, ranging from 0.1 - 0.4 μm and lengths of between 5 and 40 μm, whereas whiskers from SNIA ‡ have larger diameters, averaging around 1.2μm, a narrower size distribution and have less of the irregularities and branches found in Tateho whiskers. It is presumed that both sources of whisker are manufactured from rice hulls because they are not as large as the non-commercial VLS whiskers which have diameters of at least 5 μm [62] . X-Ray Fluorescence (XRF) studies of the 2 types of whisker, Table 4.1 and 4.2, show there were a variety of chemical impurities, most possibly lying within the outer silica surface layer of these whiskers. Most important was the oxygen content which will be incorporated into the intergranular phase of the composite and influence its crystallisation behaviour.

Table 4.1. Chemical impurities in Tateho† SiC whiskers (wt.%)

Mg	Al	Ca	Fe	O
0.06	0.25	0.38	0.001	0.47

† SCW #1, Tateho Chemical Industries Co. Tokyo, Japan.

Table 4.2. Chemical impurities in SNIA‡ SiC whiskers (wt.%)

Ni	Fe	Al	O
0.11	< 0.05	< 0.08	0.16

‡ SNIA Fibre, Cesano Maderno, Italy.

SiC platelets have only recently been made available commercially and have received interest not just because of their toughening potential, but because they reportedly reduce the environmental problems associated with whiskers [170]. C-Axis § platelets are produced by a proprietary carbothermic reduction process in which SiO_2

and carbonaceous materials are reacted at 1950°C, with boron and aluminium as catalysts [171]. Regular shaped hexagonal platelets are formed, Fig.4.3, which have an average particle size of about 16 μm and an aspect ratio of between 8 and 10. Platelets supplied by American Matrix¥, Fig.4.4, are larger in size, more irregularly shaped and contain more debris. They have diameters ranging from 5 - 70 μm and an aspect ratio of between 2 and 14. XRF studies of the impurity contents of the two types of platelet are shown in table 4.3 and 4.4.

Table 4.3. Chemical impurities in C - Axis § SiC platelets (wt. %).

Al	Fe	Ca	Ti	Mg	O
0.60	0.01	0.01	0.003	0.002	0.22

§ C - Axis, Alcan International Ltd, Jonquiere, Quebec, Canada.

Table 4.4. Chemical impurities in American Matrix ¥ SiC platelets (wt.%).

Al	Fe	Ca	Mg	O
0.50	0.05	0.10	0.05	0.40

¥ - 325 mesh size, American Matrix platelets, supplied by Mandoval Ltd, Lightwater, Surrey.

When viewed in the TEM the whiskers show a high density of planar faults on close - packed planes, indicated by the dark contrast bands in the bright field image, Fig.4.5. A higher magnification image, Fig.4.6, shows the growth direction of the whisker along the <111> direction when viewed with a [110] incident beam. The streaking parallel to the whisker axis, seen in the electron diffraction pattern, results from the irregularly spaced stacking faults and thin lamellar twins which are perpendicular to the growth axis of the whisker. These stacking faults are created by

Fig.4.3. SEM micrograph of C- Axis SiC platelets.

Fig.4.4. SEM micrograph of American Matrix SiC platelets.

Fig.4.5. Low magnification TEM micrograph of Tateho whisker showing stacking faults.

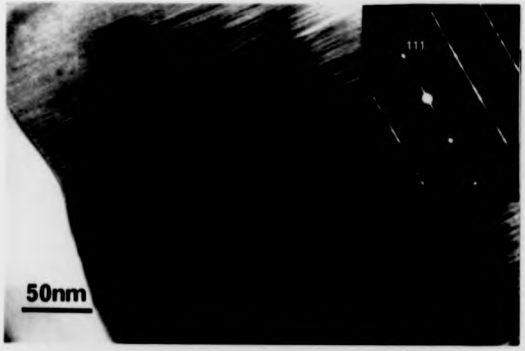

Fig.4.6. TEM micrograph and electron diffraction pattern showing <111> growth direction of whisker when viewed with an [110] incident beam.

adding or removing a layer of planes in the stacking sequence. The actual stacking order appears to be affected by the whisker growth conditions.

SiC exhibits a number of polytypes as a result of the different stacking sequences of the Si - C basal plane which leads to different repeat lengths in the c- axis of the unit cells. The structural types include a cubic (β) form and many hexagonal and rhombohedral (α) phases, but to describe all the polytypes effectively, the Ramsdell notation is used [172]. This notation consists of the number of double layers of Si and C atoms in the unit cell, followed by a letter denoting the Bravais lattice type (C for cubic, H for hexagonal and R for rhombohedral). Hundreds of polytypes have been identified, differing only by the sequences with which their fundamental layers are arranged. The longer period structures are based on a combination of the more commonly observed short period polytypes such as 3C, 4H, 6H and 15R. The electron diffraction pattern in Fig.4.6 gives a d - spacing of 2.52 Å, which corresponds to the (111) plane in the 3C β – SiC polytype.

A ^{29}Si MAS NMR spectra of the C - Axis platelets showed that there are a number of resolvable chemical shifts, Fig.4.7. These peaks arise as a consequence of the different stacking sequences in the SiC polytypes, and hence a number of different silicon atomic environments arise. These sites are distinguishable by the number and orientation of the neighbouring atoms and are generally labelled A,B,C,D [173]. The shifts from Fig.4.7 were compared with the chemical shift data obtained from pure SiC polytypes [173,174] and the individual peaks were assigned to polytype sites. The -25.14 ppm peak corresponds to a 6H polytype B site (- 25.4 ppm in the literature) and that at - 23.22 ppm can be assigned to the 4H polytype B site (-22.5 ppm in the literature). A combination of the signals from the C sites for the 4H and the 6H polytypes corresponds with the high intensity peak at -20.62 ppm because these

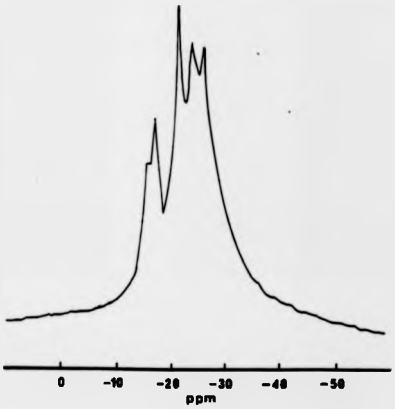

Fig.4.7. ^{29}Si MAS NMR trace of C-Axis Platelets.

two C sites have nearly coincident values (-19.7 and -20.9 in the literature respectively). The signal at -15.54 ppm corresponds to the 6H A site (-14.7 ppm in the literature) and the shoulder on this peak possibly comes from a small quantity of another polytype such as 2H. Differences in the chemical shift values of the observed spectra and for the pure polytypes could arise as a result of interaction between Si atoms and paramagnetic impurities in the sample. Confirmation that the 4H and the 6H polytypes were the major ones present was confirmed by XRD data shown later in this chapter.

4.3. MATERIAL COMPOSITIONS.

The composition of the matrix was specifically tailored so that the intergranular phase of the composite crystallised into Yttrium disilicate ($Y_2Si_2O_7$). Initially all compositions had a constant 5 wt.% Y_2O_3 additive level, but this was later modified with an additional 1 wt.% SiO_2 so that the resulting composition fell further into the Si_3N_4 - Si_2N_2O - $Y_2Si_2O_7$ phase field, Fig.4.8. The starting powder in every case was UBE α -Si_3N_4 ¶ which had an analysed oxygen content of 1.20 wt.% #, assumed to be present as SiO_2 on the powder surface, and a particle size ranging from 0.1 μm to 0.3 μm. Details of the chemical impurities are shown in Table 4.5. It was assumed there was no significant oxygen pickup during ball milling. The Y_2O_3 powder was supplied by Ventron Gmbh, Karlsruhe, Germany and had a purity of 99.99%.

Table 4.5. Chemical Analysis of UBE α - Si_3N_4¶ (ppm)

Cl	Fe	Ca	Al
< 100	< 100	< 50	< 50

¶ SN - E 10 , UBE Industries, Tokyo, Japan.

measured by LECO Analytical Instruments Ltd, Stockport, UK.

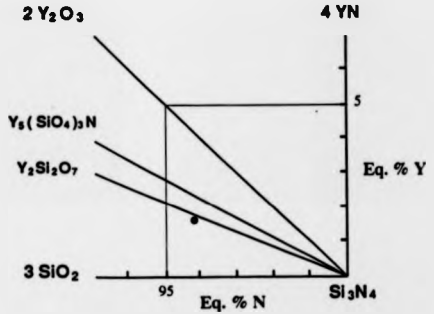

Fig.4.8. Enlarged Si_3N_4 corner of Y_2O_3 -YN - SiO_2 -Si_3N_4 phase diagram which was shown in Fig.2. 2. indicating the refined matrix composition.

A XRD trace of the UBE powder, Fig.4.9, confirms that it was predominantly α – Si_3N_4 , which is necessary for solution - reprecipitation and hence densification to take place.

The details of the compositions fabricated by HIP and hot pressing are listed on the next page in table 4.6., the matrix composition being the stated level of sintering aid (wt.%), with the residual being UBE Si_3N_4. It should be noted that the proportion of sintering aid to α – Si_3N_4 was constant, so that the relative proportion of sintering aid decreases with increasing SiC (wt.%) content. All compositions were slip cast and HIPed unless specified. Generally, at least 4 billets of each HIP composition were produced, because of the potential failure of the encapsulant during HIP and to obtain sufficient material for the mechanical testing.

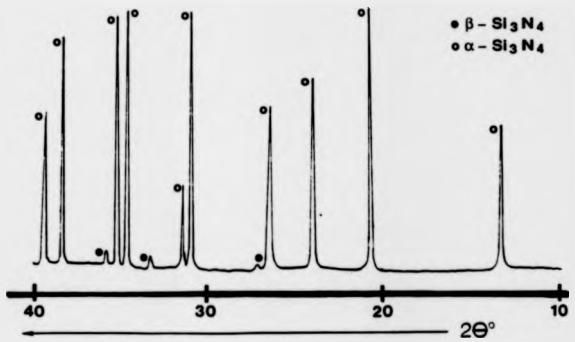

Fig.4.9. XRD trace of UBE Si_3N_4 powder (SN-E 10)

Table 4.6. Composition of Fabricated Composites.

Tateho Whiskers		SNLA Whiskers		C-Axis Platelets		Particles		Am. Mat. Platelets	
Matrix	% SiC	Matrix	% SiC	Matrix	%SiC	Matrix	% SiC	Matrix	% SiC
$5Y_2O_3$	0	$5Y_2O_3.1SiO_2$	0	$5Y_2O_3.1SiO_2$	0 #	$5Y_2O_3$	0		
"	10			"	10	"	5		
"	20	"	20	"	20	"	10		
"	30	"	30*	"	30 #*	"	25	$5Y_2O_3.1SiO_2$	30 #*
		"	40	"	40				

\# hot pressed as well as HIPed.

* also not slip cast (to obtain random distribution of dispersoids).

4.4. OPTICAL OBSERVATIONS

When the HIPed billets returned to Warwick it was noticeable that those containing whiskers and platelets, and which were slip cast, were distorted and showed a strong anisotropic shrinkage behaviour, Fig.4.10. This was more pronounced with the whisker containing billets and with increased dispersoid content. In contrast those samples that contained a high loading of whiskers but were simply CIPed and not slip cast, were reasonably uniform like the monolithic material. The distortion could be caused by inadequate dispersion of the whiskers in the slip, resulting in inhomogeneities within the densified composite. Non - uniform dispersion will result in uneven shrinkage of the HIPed billet because the non - sinterable whiskers restrict densification.

The distribution and orientation of the dispersoids were observed by first cutting the representative billets perpendicular and parallel to the face which was nearest to the plaster mould Fig.4.11. In an optical micrograph taken perpendicular to the billet base, the whiskers showed a preferred orientation in a plane parallel to the base, Fig.4.12a but are randomly oriented in this plane when viewed perpendicular to the ceramic base, Fig.4.12b. The anisotropy of the composite shrinkage can also be explained by the formation of a rigid whisker network as there will be shrinkage differences, due to this 2 - dimensional alignment of dispersoids and an anisotropic porosity distribution caused by closer particle packing parallel to the mould surface. In addition, the shrinkage of the matrix can be hindered by impinging whiskers, which could cause a preferential material flow out of the area between whisker planes. Therefore the billets would shrink much more in the direction perpendicular to the whisker planes, as has been observed. In the non - slip cast billets, there was little preferred dispersoid orientation and a more or less isotropic material was obtained,

Fig.4.12c, which would account for its uniform shrinkage behaviour.

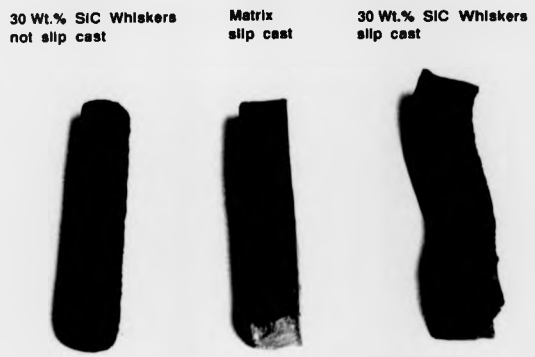

Fig.4.10. Photograph of HIPed billets.

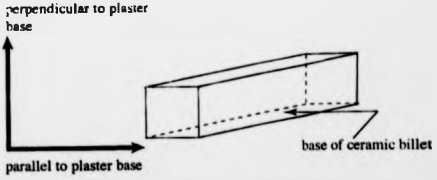

Fig.4.11. Schematic drawing of how billets were machined.

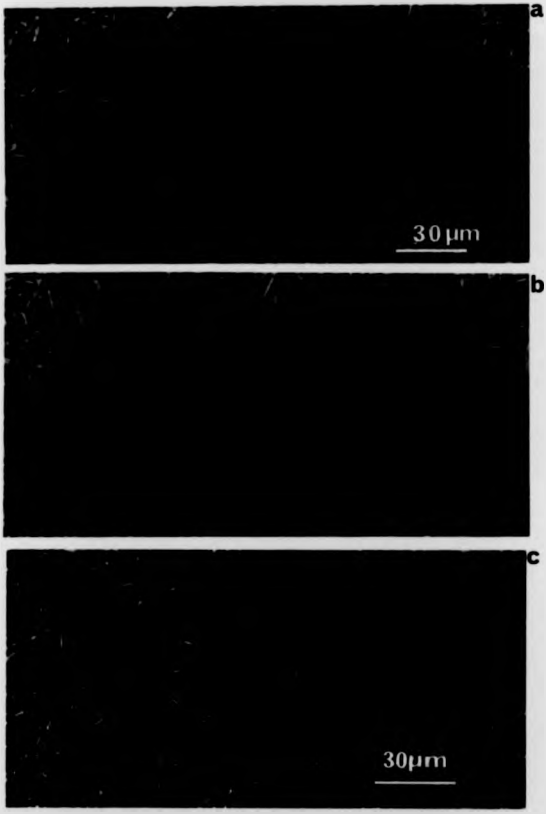

Fig.4.12. Optical Micrographs of HIPed composite containing 30wt.% SNIA whiskers taken a) perpendicular b) parallel to mould and c) from non - slip cast billet.

It is noticeable from the optical micrographs in Figs. 4.12, that there appears to be a reasonably homogeneous distribution of the whiskers throughout the composites with only occasional matrix agglomeration or the presence of large SiC particles.

There was also generally well dispersed and preferrential orientation of the platelets when viewed in the plane perpendicular to the billet base, as illustrated in the series of platelet loaded compostions shown in Fig.4.13. This was most apparent in the region closest to the base, but further up the billet, the platelet texture starts to randomise. This is illustrated in Fig.4.14, which shows 2 photographs taken parallel to the plaster mould; Fig.4.14b near the bottom of the billet, and 4.14a approximately 15mm above this. They show that the latter is quite randomised and there is less of the large [00C] face of the platelets visible. Confirmation of this is given in the accompanying XRD traces which showed a significant difference in the height of the [004] 4H SiC peak. This d value has the highest intensity of planes in the c direction, and its relative height will give a good indication of the orientation of the platelets.

After hot pressing, the dispersoids align themselves perpendicularly to the direction of applied pressure, but are randomly distributed in this perpendicular plane. Uniaxial shrinkage during the hot pressing causes the preferred orientation of the dispersoids, and microstructures similar to Figs. 4.12a and 4.13c were obtained.

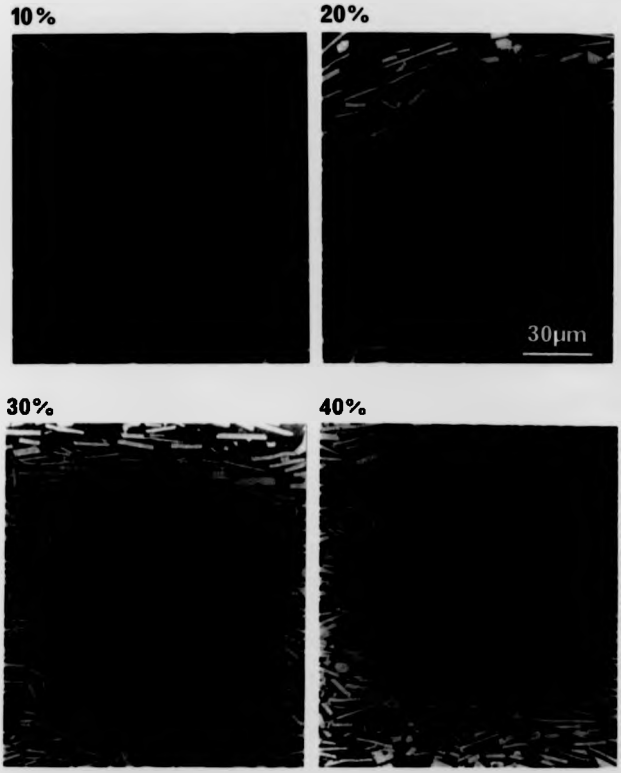

Fig.4.13. Optical Micrographs of the Series of Slip Cast Composites containing C - Axis Platelets.

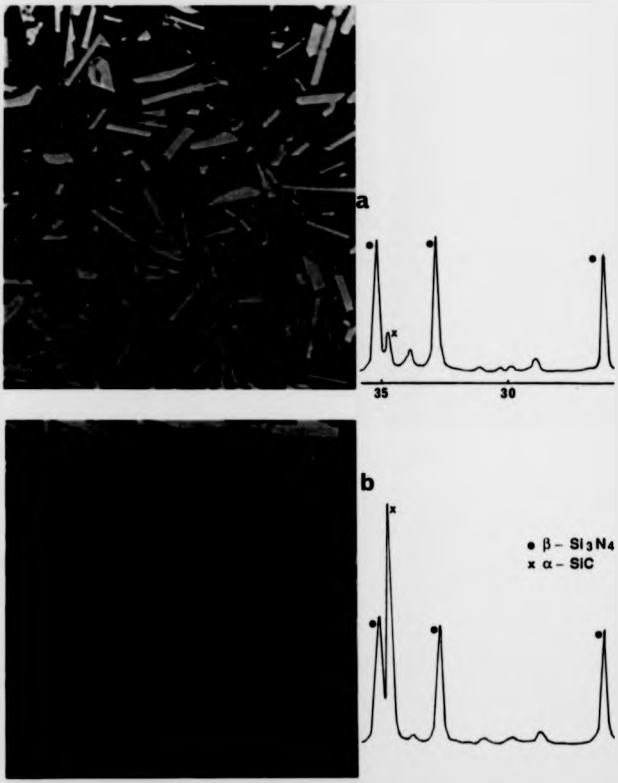

Fig. 4.14. Optical Micrographs with XRD traces of Composite containing 30 wt.% C- Axis Platelets, showing surface parallel to the bottom of billet.

4.5. DENSIFICATION.

It is very important when fabricating ceramic components that close to theoretical density is achieved because residual porosity will act as a source for failure under stress and thus it should be eliminated if good mechanical performance is to be achieved. The theoretical density was calculated from the weight proportion of the final constituents, taking changes induced by the sintering additives into account. For example, the theoretical density of the monolith with starting composition 5 wt.% Y_2O_3, 1 wt.% SiO_2 and 94 wt.% Si_3N_4 was calculated as below :

The oxygen content of the UBE Si_3N_4 was measured to be 1.20 wt.%, which if one assumes to be all in the form of a surface SiO_2 layer, is equivalent to 2.25 wt.% SiO_2. Therefore in a typical batch of 100g of material there was :

5g Y_2O_3, 91.89g Si_3N_4 and 3.11g SiO_2

If all the Y_2O_3 converts to $Y_2Si_2O_7$ then :

Y_2O_3 + 2 SiO_2 ----------> $Y_2Si_2O_7$

(5 / 225.8) moles 2 x (5 / 225.8) x 60 g (5 / 225.8) x 346 g

There is then 0.453 g of SiO_2 remaining which forms Si_2N_2O :

Si_3N_4 + SiO_2 ----------> 2 Si_2N_2O

(0.453 / 60) x 140 g (0.453 / 60) moles 2 x (0.453 / 60) x 100 g

Thus in the final composition there will be :

Si_3N_4 : 90.83 wt.% $Y_2Si_2O_7$: 7.66 wt.% Si_2N_2O : 1.51 wt.%

Similar calculations were made with compositions containing SiC additions and the theoretical densities of the composites were calculated, Table 4.6., using the weight proportion of each phase and its density. The densities (ρ) used for the individual phases were :

Si_3N_4 (3.19 gcm^{-3}), $Y_2Si_2O_7$ (3.98gcm^{-3}), Si_2N_2O (2.85 gcm^{-3}), SiC (3.20 gcm^{-3})

4.5. DENSIFICATION.

It is very important when fabricating ceramic components that close to theoretical density is achieved because residual porosity will act as a source for failure under stress and thus it should be eliminated if good mechanical performance is to be achieved. The theoretical density was calculated from the weight proportion of the final constituents, taking changes induced by the sintering additives into account. For example, the theoretical density of the monolith with starting composition 5 wt.% Y_2O_3, 1 wt.% SiO_2 and 94 wt.% Si_3N_4 was calculated as below :

The oxygen content of the UBE Si_3N_4 was measured to be 1.20 wt.%, which if one assumes to be all in the form of a surface SiO_2 layer, is equivalent to 2.25 wt.% SiO_2. Therefore in a typical batch of 100g of material there was :

$$5g\ Y_2O_3,\ 91.89g\ Si_3N_4\ \text{and}\ 3.11g\ SiO_2$$

If all the Y_2O_3 converts to $Y_2Si_2O_7$ then :

$$Y_2O_3 + 2\ SiO_2 \text{ ----------> } Y_2Si_2O_7$$

(5 / 225.8) moles 2 x (5 / 225.8) x 60 g (5 / 225.8) x 346 g

There is then 0.453 g of SiO_2 remaining which forms Si_2N_2O :

$$Si_3N_4 + SiO_2 \text{ ----------> } 2\ Si_2N_2O$$

(0.453 / 60) x 140 g (0.453 / 60) moles 2 x (0.453 / 60) x 100 g

Thus in the final composition there will be :

Si_3N_4 : 90.83 wt.% $Y_2Si_2O_7$: 7.66 wt.% Si_2N_2O : 1.51 wt.%

Similar calculations were made with compositions containing SiC additions and the theoretical densities of the composites were calculated, Table 4.6., using the weight proportion of each phase and its density. The densities (ρ) used for the individual phases were :

Si_3N_4 (3.19 gcm^{-3}), $Y_2Si_2O_7$ (3.98gcm^{-3}), Si_2N_2O (2.85 gcm^{-3}), SiC (3.20 gcm^{-3})

PAGINATION ERROR

Pg 85

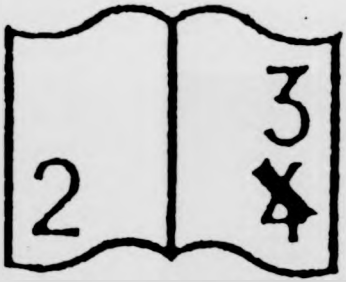

Table 4.7. Densities of Fabricated Composites.

Dispersoid	Wt.%	Density (exp.) g / cm ^{3}	Density (theo.) g / cm ^{3}	(exp. / theo.) %
Tateho whiskers	0	3.24	3.26	99.4
	20	3.23	3.25	99.4
	30	3.23	3.24	99.6
Particles	5	3.24	3.25	99.7
	10	3.24	3.25	99.7
	25	3.23	3.24	99.6
C- Axis Platelets	0	3.23	3.25	99.4
	10	3.23	3.25	99.4
	20	3.22	3.24	99.2
	30	3.21	3.24	99.1
	40	3.21	3.23	99.4
	30*	3.22	3.24	99.2
SNIA whiskers	20	3.23	3.24	99.6
	30	3.24	3.24	100.0
	40	2.37	3.23	73.4
	30*	3.23	3.24	100.0
Amer. Matrix Platelets	30	3.23	3.24	99.6
Monolith	0 #	3.17	3.25	97.5
SNIA (60 mins)	30 #	2.76	3.24	85.2
SNIA (87 mins)	30 #	3.09	3.24	95.3
C - Axis	30 #	3.13	3.24	96.6

exp. - experimental density. theo. - theoretical density.

hot pressed

* HIPed but not slip cast

The density measurements in table 4.6 indicate near full densification can be achieved using the HIP conditions of this programme, although the exact value of (exp. / theo.) was susceptible to minor variations. These included experimental errors caused by the resolution of the weighing process, and the calculation of the theoretical density of each composite assumes complete and stoichiometric reaction of all species. There was no obvious trend in the percentage of theoretical density with increasing SiC dispersoid content, largely because the high pressures exerted during HIP appears to achieve near theoretical density in all compositions . The only exception appears to be the composition containing 40wt.% SNIA whiskers for which there are two possible reasons. Firstly, the encapsulant glass possibly failed during the HIP cycle, which would result in gas ingress through the normally impermeable gas - barrier and hence preventing densification. Secondly, there may be a limit to the proportion of whiskers in the composite that would allow complete densification. This is important because the theoretical models, illustrated in chapter 2, suggest that increasing the dispersoid content will increase the fracture toughness of the composite. However, it was noticeable that the composite containing 40 wt.% C-Axis platelets was fully dense and the hot pressing results also indicate platelet containing composites densify easier than those containing whiskers.

It was clear from the density data for the hot pressed material that the densification in the monolith was much higher than that for a 30 wt.% whisker composite at the same temperature, pressure and time. This suggests that a longer hot pressing time was needed, but even after an extra 27 minutes, when the graphite punch broke, the whisker material was still not fully dense, which suggests the pressure used was not sufficient. The main problem when hot pressing was the frequent breaking of the punch during pressing which indicates a higher quality of graphite was needed in

order to increase the pressure and the percentage of successful runs.

Two main factors are believed to control the densification of the whisker containing materials. Firstly, the non - sintering SiC whiskers are constrained during shrinkage by the surrounding matrix material, so that tensile hoop and radial compressive stresses develop around the whiskers. These transient stresses will counteract the densification process and reduce the sintering rate. Secondly, the formation of a rigid network of whiskers will limit densification and inhibit further shrinkage of the matrix.

An attempt at pressureless sintering of a composite containing 30 wt.% whiskers was made by placing a small lump of the green compact in a BN coated graphite crucible, inserting in a vertical tube high temperature furnace, then sintering at 1725°C for 1 hour. However, there was little change in the density, from about 46 % to 47 %. This shows the use of HIP as a processing route, was very much a necessity with the range of compositions and materials studied in this programme rather than pressureless sintering and even hot pressing,.

4.6. PHASE EVOLUTION.

The crystallisation behaviour of the composites is important as this will largely control the high temperature mechanical properties of the material. XRD traces of the monolith and particle composites showed alpha Yttrium disilicate ($\alpha - Y_2Si_2O_7$) crystallised within the intergranular phase whereas there was no apparent trace of these peaks in the as-received Tateho whisker series Fig.4.15, indicating the intergranular phase was glassy. The latter was probably caused by the high oxygen content of these whiskers promoting vitrification of this phase. However, on heat treating these compositions at 1280°C for 24 hours in a N_2 atmosphere and allowing the sample to air

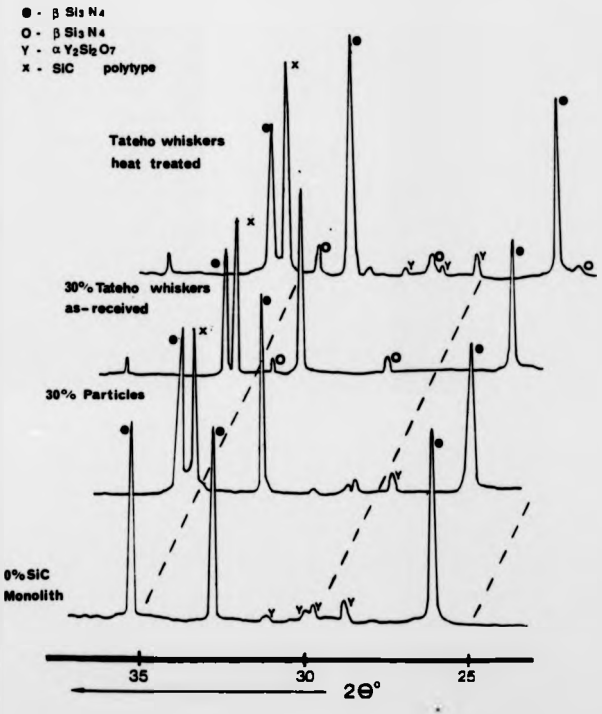

Fig.4.15. XRD Traces of Selected Compositions.

cool, the glassy intergranular phase crystallised to the disilicate. Indeed, all billets were heat treated under these conditions in order to establish the crystalline $\alpha - Y_2Si_2O_7$ within the intergranular region. There are a number of polymorphs of $Y_2Si_2O_7$, each having a different temperature stability region [175]. The XRD data of the pre- heat treated billets indicated that the cooling rates during the HIP runs generally favour the nucleation of the low temperature disilicate polymorph, i.e. $\alpha - Y_2Si_2O_7$.

There was usually complete transformation of the mainly $\alpha - Si_3N_4$ starting powder to $\beta - Si_3N_4$ after densification for all HIPed compositions, although there was some residual α phase in both the Tateho and SNIA whisker composites, Fig.4.16. In the 30wt.% SNIA whisker composite there was approximately 5 wt.% $\alpha - Si_3N_4$ remaining when calculated by the x-ray intensity comparison method [176], although the exact figure is affected by absorption coefficients, structure effects and preferential orientation. It is not fully understood how whiskers could restrict the α to β transformation, although this fact may have a small effect on the fracture toughness of these composites. This is because the $\alpha - Si_3N_4$ grains tend to be equiaxed whereas the $\beta - Si_3N_4$ tend to be more acicular, depending on the level of liquid phase, and it has been shown that increasing the aspect ratio of the Si_3N_4 grains, increases the fracture toughness of the material [48]. However, this small amount of residual α will probably not adversely effect the mechanical properties of the materials as the presence of high aspect ratio SiC whiskers should be more influential in terms of toughening potential.

Although it appeared that the intergranular phase of the SNIA whisker compositions had crystallised to the disilicate without heat treatment, all the compositions were heat treated to standardise the procedure. In this system, a Si_2N_2O peak appeared as the additional SiO_2 within the matrix brought the composition further

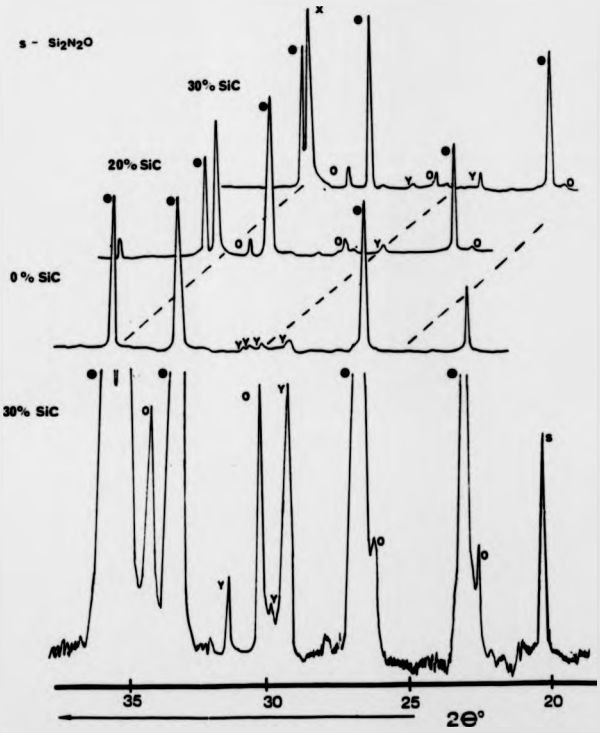

Fig.4.16. XRD Traces of SNIA Whisker Composite Series.

into the Si_3N_4 - $Y_2Si_2O_7$ - Si_2N_2O phase field, away from the tie-line, as seen in Fig.4.8.

In the C-Axis platelet composite series, Fig.4.17, the intergranular phase crystallised as the desirable yttrium disilicate phase and a minor volume of the oxynitride, except the 20 wt.% composition, which formed y - yttrium silicate. It has been shown elsewhere [175] that this silicate phase transforms to the α disilicate upon heating to 1200°C, so the 20wt.% platelet billets were post HIPed annealed at 1280°C for 24 hours and allowed to air cool. XRD confirmed that this heat treatment results in a conversion of the yttrium silicate phase to the α disilicate. It appears that the HIP conditions used by ABB Cerama generally favour the α disilicate, but if this low temperature disilicate polymorph does not have time to nucleate and grow, the y-yttrium silicate was formed. It can only be assumed that the thermal gradients occuring in the large volume furnace on cooling, were slightly different for the 20wt.% platelet composition. Therefore, in order to establish a standard intergranular phase, all the HIPed billets were annealed under the conditions outlined above.

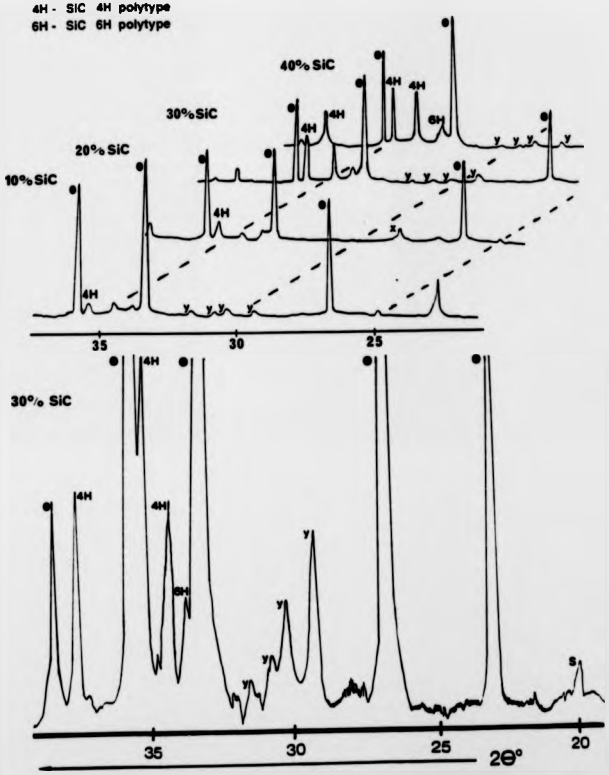

Fig.4.17. XRD traces of composites containing C-Axis platelets.

4.7. GENERAL MICROSTRUCTURE.

Polished specimens of the series of compositions, showed quite similar general microstrucures when viewed in the back scattered mode of the SEM. A relatively low magnification micrograph of the monolithic composition, Fig.4.18, shows it consists of relatively fine acicular Si_3N_4 grains (dark contrast) and a finely dispersed minor intergranular phase (light contrast). This phase contrast allows the yttrium disilicate to be easily distinguishable, because theYttria (Y) containing phase has a higher effective atomic number than Si_3N_4 and thus appears much lighter. However, it becomes more difficult when distinguishing between Si_3N_4 and SiC because they have similar backscattered electron intensities. C-Axis SiC platelets are considerably larger in size than the Si_3N_4 grains and are thus easily identifiable within the composite, Fig.4.19. Althougth the SiC whiskers have a higher aspect ratio (i.e. length : diameter) than the Si_3N_4 grains, their diameters are of the same order of magnitude, thus it was quite difficult to distingish between them, Fig.4.20. The backscattered electron density is essentially determined by the product of the effective atomic number, Z_{eff} and the density of atoms / unit volume of the material, ρ_{at} ,which is slighlty higher for SiC, and thus appears slighlty lighter than Si_3N_4.

The intergranular phase was relatively finely dispersed in all compositions and its volume fraction within the composite appeared to decrease gradually as the SiC level increased. It was difficult to quantify the proportion of the intergranular phase from the SEM micrographs because the imaging conditions necessary to view contrast between the different phases, produces a flaring effect in this matrix minor phase and thus exaggerates its volume. Calculations of the amount of this minor phase formed, assuming stoichiometric reactions, show that the weight percentage of the intergranular phase $Y_2Si_2O_7$, changes from approximately 7.6 % with

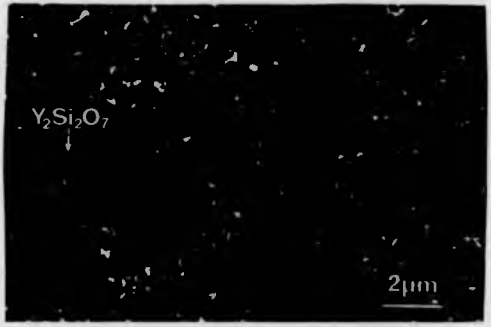

Fig.4.18. Typical back - scattered SEM image of the monolith material.

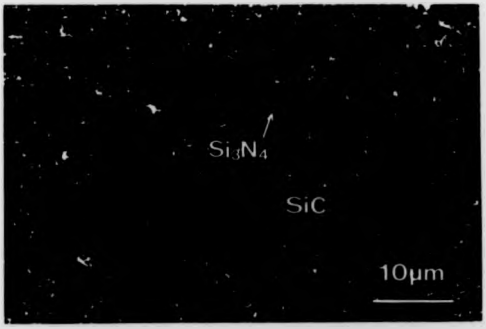

Fig.4.19. SEM backscattered image of composite containing 30 wt.% C - Axis platelets.

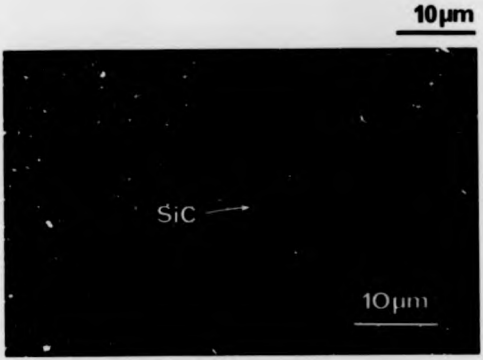

Fig.4.20. Typical SEM image of composite containing 30 wt.% SNIA whiskers.

0 % SiC to about 4.6 % in the composite containing 40 wt.% SiC. However, the ratio of disilicate to Si_3N_4 remains constant in the range of compositions, even though the SiC content changed.

In contrast to the relatively uniform and preferentially aligned C-Axis platelet composites, American Matrix platelets were irregular and show no apparent directionality, Fig.4.21. There were occasional small agglomerates of the minor phase around the periphery of the platelets, as in other compositions, probably due to not complete mixing. However, this does not have a detrimental effect on densification.

The dispersoids in the hot pressed specimens were relatively homogeneously aligned, approximately perpendicular to the hot pressing direction. Their general microstructure appeared quite similar to HIPed samples of equal volume fraction of dispersoid, Fig.4.22. It was difficult to speculate whether the microscopic black patches within the matrix were due to residual porosity, as indicated by the measured density data in table 4.6, or due to pullout produced during the grinding and polishing specimen preparation stage. These black patches were present in other apparently fully dense composites, suggesting pullout occurs.

No detailed quantitative study was made of the Si_3N_4 grain size and grain size distribution in the materials, but there did not appear to be any significant difference in matrix microstructure in HIPed composites of different type and volume fraction of dispersoid. Studies have shown that varying the minor phase volume and the processing parameters influences the aspect ratio and size of Si_3N_4 grains [48]. However, the matrix composition, relative volume of liquid phase and densification conditions were the same in all the HIPed composites used in this study, which suggests the matrices should be very similar, as briefly surveyed in Fig.4.26 in the next section.

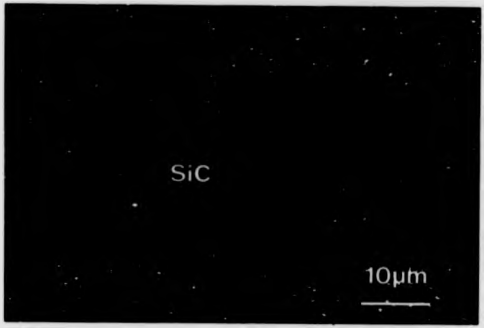

Fig.4.21. SEM backscattered image of HIPed composite containing 30 wt.% American Matrix platelets.

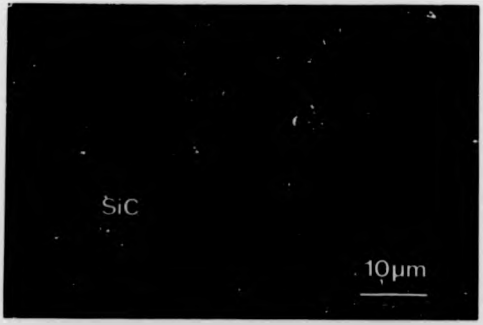

Fig.4.22. Typical SEM image of hot pressed composite containing 30 wt.% C - Axis Platelets.

4.8. HIGH RESOLUTION MICROSCOPY.

The higher spatial resolution possible with the TEM allows a more detailed characterisation of the materials' microstructure, particularly at interfaces, which play such a dominant role in their fracture behaviour.

After densification of the composites at elevated temperatures, SiC whiskers appeared very stable, and there was no obvious degradation of their structure or reaction with the matrix, Fig.4.23. This was primarily because they are single crystals, unlike microcrystalline SiC fibres such as Nicalon which degrade at temperatures > 1200°C. Fig.4.24 also shows the platelets were stable within the composite. A higher magnification view showed they have fewer stacking faults than the whiskers but contain what appeared to be dislocations through them, Fig.4.25. The micrograph in Fig.4.24 further emphasises that the platelets were considerably larger than the matrix grains. Images taken of the matrices of representative areas of different types of dispersoid reinforced composites show the general size and morphology of the Si_3N_4 grains, Fig.4.26. These Si_3N_4 grains consist of fine equiaxed grains, mostly in the lower part of the 0.1 - 0.5μm range, and larger acicular grains with lengths between 0.5 and 5 μm. There appeared to be little difference between the monolith microstructure and the matrix microstructure of the various composites although it was difficult to quantify the proportion and aspect ratio of the acicular grains because of their random orientation within the composite.The similarity in size and morphology of the Si_3N_4 grains tends to confirm the theory that similar proportions of sintering liquid to Si_3N_4 powder produces similar sized and shaped $\beta - Si_3N_4$ grains, even though there was a decreasing level of total additive volume with increasing SiC content.

A transverse view of the whiskers showed that some are hollow because the transient Y - Si - O liquid has flowed into the core during the composite consolidation, Fig.4.27. Longitudinal views showed this core region ran over a significant portion of the whisker length and will obviously have a detrimental effect on its fracture strength. This feature was occasionally seen in the Tateho whiskers but it

Fig.4.23. TEM image of HIPed Tateho SiC whisker in Si_3N_4 Matrix.

Fig.4.24. TEM image of C - Axis platelets in Si_3N_4 matrix

Fig.4.25. TEM image of C-Axis platelet showing dislocations.

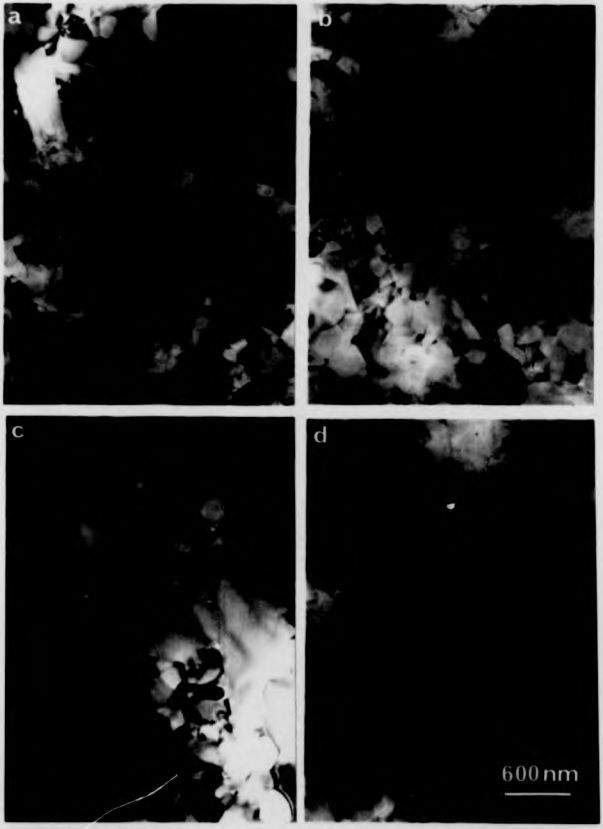

Fig.4.26. TEM images of HIPed matrix microstructure in a) the monolith, b) 30 wt.% C- Axis platelets, c) 30 wt.% SNIA whiskers and d) 30 wt.% American Matrix platelets.

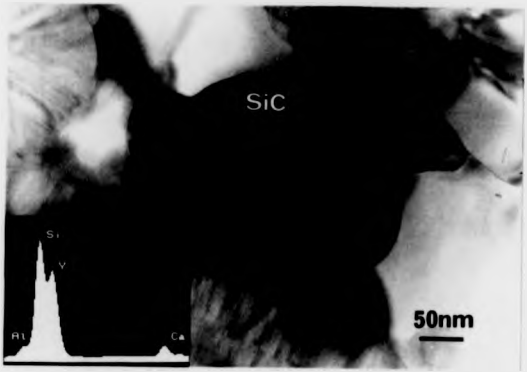

Fig.4.27. Transverse view of a hollow Tateho whiskers with EDX spectra.

was not apparent in the SNIA whiskers, Fig.4.28, which indicated the cavities occurred due to problems in the processing of the Tateho whiskers.

The intergranular phase was dispersed very finely throughout the microstructure, which makes electron diffraction or analysis very difficult. Larger regions were found in triple junctions and EDX analysis showed these contain a yttrium (Y), silicon (Si), oxygen (O) compound, and sometimes traces of metal impurities such as calcium (Ca) and aluminium (Al) were detected. These impurities probably originated from the dispersoids and were presumably incorporated into the intergranular phase when it was formed by the reaction of Y_2O_3 with the surface SiO_2. Reference to tables 4.1 to 4.3 show that calcium and aluminium were the major impurities in the dispersoids. However, the amount of impurities varied considerably between different types of dispersoids; analysis of a triple junction in a C - Axis platelet composite showed traces of Al, Fig. 4.29, whereas in a SNIA whisker composite impurity levels appeared too low for detection, Fig.4.30. The relatively small volume of the oxynitride phase in these composites, makes the detection of this phase very difficult.

Electron diffraction of the triple junction confirms they have crystallised during cooling, with a d - spacing of 1.225nm, indicating the presence of $\alpha - Y_2Si_2O_7$, Fig.4.31. Lattice imaging confirms the crystallinity of this region and this technique was also employed for the imaging of the detailed structure at a grain boundary. This is of particular importance to the high temperature time dependent properties of these ceramic materials. High resolution microscopy showed there was a very thin residual layer, typically 2nm thick, between the crystalline disilicate and the adjacent Si_3N_4 grain, Fig.4.32. It was difficult and probably unrealistic, to obtain exact dimensions of the residual layers in all compositions, as this requires all microscopy conditions to be satisfied simultaneously. However, observations indicated that the residual layer was present in the monolith and composites, and there did not appear to be a significant difference in the film thickness in these different materials. The exact nature of this phase was not discernible, but it was likely that the progressive crystallisation of the intergranular phase occurred until the disilicate composition was exhausted and the

Fig.4.28. Axial view of SNIA whisker with electron diffraction pattern showing growth direction.

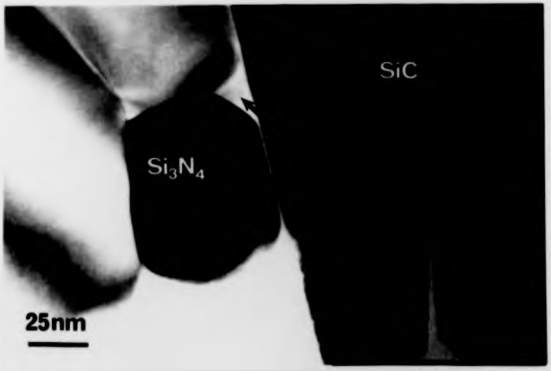

Fig.4.29. TEM micrograph with EDX spectra showing Al impurity within the triple junction of a C - Axis platelet composite.

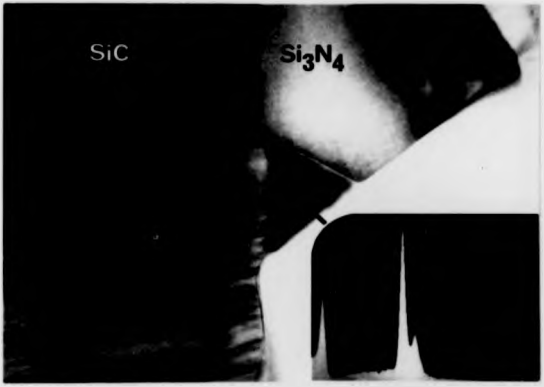

Fig.4.30. TEM image showing triple junction and EDX spectra in SNIA whisker composite

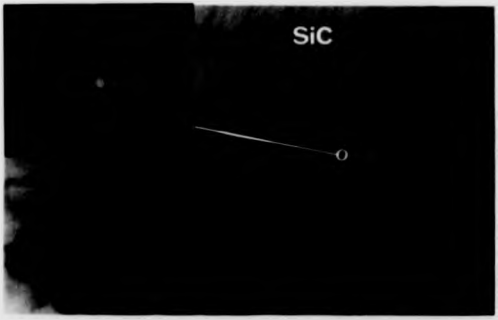

Fig.4.31. Electron Diffraction pattern and TEM image indicating α - $Y_2Si_2O_7$

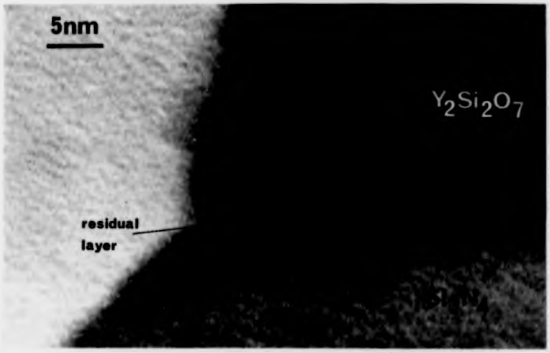

Fig.4.32 High resolution TEM image showing lattice fringes in a - $Y_2Si_2O_7$ triple junction and a residual interfacial film in a SNIA whisker composite.

Fig.4.33 TEM image showing a very thin interfacial film between two Si_3N_4 grains.

residual material remained as a thin layer of Y- Si - O containing glass at the boundary. It was diffficult to analyse these regions because they are below the resolution limit of the probe. Even under conditions which should be expected to favour complete crystallisation, it has been found that this residual film was retained. Similarly when two neighbouring Si_3N_4 grains have orientations that allow lattice fringe imaging in both simultaneously and the boundary was parallel with the incoming electron beam, it was possible to detect an intergranular film Fig.4.33. This enables an accurate estimation of the width of the layer as the lattice fringes result from known crystallographic dimensions. However, absence of lattice fringes within grain boundary phases is contentious proof of their existence [180].

The curved nature of the whiskers made it quite difficult to view the whisker / matrix interface parallel to the electon beam. Boundary layers are very thin so small tilts of the sample can render the layer effectively invisible. Although conditions were not perfect, there appeared to be a thin film between the whiskers and matrix, probably due to the siliceous nature of the as - received whiskers' surface, Fig.4.34. The intergranular films between the different materials adopt an equilibrium thickness as a result of two competing reactions; an attractive force between grains as a result of van der Waals forces, and a repulsive force attributed to a structural or steric interaction within the fluid intergranular film at temperature [177].

It has been reported elsewhere [178] that no glassy phase was observed at the interfaces between SiC whiskers and the surrounding Si_3N_4 matrix. However, the micrographs in that study suggested that the interfaces were inclined to the electron beam, where the interfacial layer would not be detected. It has been shown [101] that a thin layer can only be detected if the foil thickness t is such that $t < (a D/2)^{1/2}$, where a is the thickness of the interfacial layer and D is the diameter of the whisker, and importantly, if the interface is parallel to the electron beam. This indicates the need for good sample preparation and correct orientation in order to observe interfacial regions.

In the platelet composite debonding occurred, Fig.4.35. This was probably due to a thermal expansion mismatch between the platelet and the matrix on cooling from the densification temperature, resulting in interfacial tensile strain and

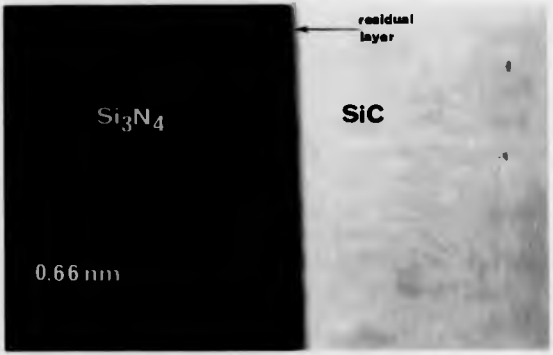

Fig.4.34. High resolution TEM image of interface between SNIA whisker and Si_3N_4 grain (courtesy of Dr G. Leng - Ward).

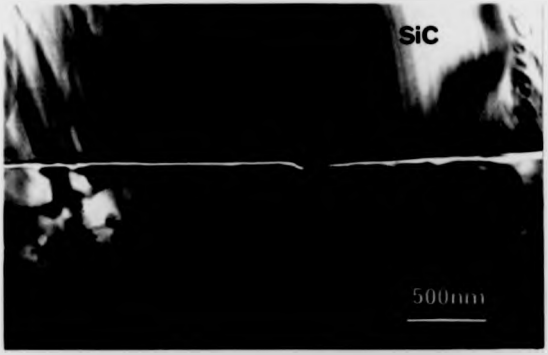

Fig.4.35. TEM image showing debonding at the interface between a C - Axis platelet and a Si_3N_4 grain.

debonding. The mismatch was amplified in the platelet composite because of their relatively large size compared to whiskers and helps to explain why pullout happened frequently when polishing these samples for optical and SEM investigation.

Detailed studies of the interfaces and debond regions in these materials have been quite difficult and further detailed study was limited by the time available to this aspect of the research programme. A more detailed microstructural study of the interfacial boundaries would have involved more dark field imaging, which uses the diffracted intensity from the interfacial layer, [179] and also the technique of Fresnel defocus imaging [180,181].

4.9. SUMMARY.

The main features which can concluded from this chapter on microstructural evaluation are :

1. near theoretical density can be achieved by HIP of Si_3N_4 based composites, containing at least 30 wt.% of SiC dispersoids. This was not possible by the hot pressing route because the maximum pressure available was not sufficient for complete densification. Any residual porosity would act as a nucleation site for subsequent failure under stress and should therefore be eliminated if the potential mechanical performance is to be achieved.

2. Optical micrographs have shown that the dispersoids can be relatively, homogeneously distributed and preferentially aligned by slip casting. This alignment was only 2 - dimensional, parallel to the base of the billets.

3. Close compositional control of the starting constituents produced the desired crystalline intergranular phase within the densified composites. Microscopy studies showed this intergranular phase was generally uniformly and finely dispersed throughout the matrices of the materials. Analysis confirmed these regions were crystalline, but also contained impurities originating from the dispersoids.

4. High resolution microscopy revealed a thin residual layer, typically 2nm thick, existed between the yttrium disilicate and the major phases for both the composite and monolithic materials. This film was probably amorphous in nature and

occurred as a result of the final residues having an incorrect stoichiometry for crystallisation. It may have a detrimental effect on the thermomechanical behaviour of these materials. However, both this and associated work suggests that it is difficult to produce completely dry grain boundaries in these materials.

5. The dispersoids were stable within the composites during elevated processing. However, the interfacial characteristics between the matrix/ whiskers and the matrix/ platelets were different. Platelet containing composites showed debonding at the interface whilst the whiskers appeared tightly bonded. This may prove a significant feature for the mechanical behaviour of these materials.

CHAPTER FIVE

ROOM TEMPERATURE MECHANICAL PROPERTIES.

5.1. INTRODUCTION.

Although monolithic Si_3N_4 and SiC have relatively high stiffness, hardness and strength, both exhibit brittle behaviour at room temperature. Thus the major rationale behind the development of ceramic composites is to overcome this problem by optimising microstructural features to produce both tougher and more reliable materials. This chapter describes the effects of the addition of various types and different volume fractions of SiC dispersoids upon the experimentally determined room temperature mechanical properties such as modulus of rupture (M.O.R.), fracture toughness and Vickers hardness of the resulting Si_3N_4 based composites. These properties are important in resisting mechanical chipping and bulk fracture of the ceramic material when used as engineering components such as turbine blades or cutting tools. The mechanical results are considered with fracture surface and crack interaction observations, from which some conclusions can be drawn regarding the toughening mechanisms operating in these materials.

5.2. MODULUS OF RUPTURE (M.O.R.)

Room temperature modulus of rupture measurements were performed on at least 7 test bars of each composition, as outlined in section 3.3.1, and with 15 specimens on some selected compositions. A comparison was made between the results obtained from a series of composites containing SNIA whiskers, C-Axis platelets,

American Matrix platelets and the unreinforced Si_3N_4. A plot of the Modulus of Rupture as a function of the SiC dispersoid content in Fig.5.1, shows the monolith has a relatively high average fracture strength and this value was more or less maintained at approximately 700 MPa with the addition of SiC whiskers. However, on addition of 10 wt.% C- Axis platelets there was a significant drop in strength, which was maintained up to the 30 wt.% loading, then there was a further decrease again with 40 wt.% platelets, to a value just over half that of the monolith. Composites containing the other type of platelet also showed a similar substantial decrease in fracture strength; its value being slightly less than a similar volume fraction of C - Axis platelets. The load - displacement graph for all the compositions exhibited elastic deformation up to the maximum load point, where catastrophic failure occured. There was no evidence of any controlled inelastic deformation normally associated with ideal fibre -reinforced composites as illustrated in Fig.2.6.

The M.O.R. of the monolith has a relatively high value, which is typical for Si_3N_4 materials which are theoretically dense, have a small grain size and have good homogeneity. This value was maintained with whisker additions, however the significant feature of Fig.5.1 was the behaviour of the platelet composites which indicated strength reducing flaws were introduced into these composites on addition of this type of dispersoid. The SEM micrographs in the previous chapter showed that the platelets are considerably larger than the matrix grain size but were still somewhat lower than the critical flaw size for the material, which from equation 2.5 is approximately 150μm. However, the relatively large platelet size will amplify the effect of thermal expansion mismatch between the dispersoid and matrix, as the mean

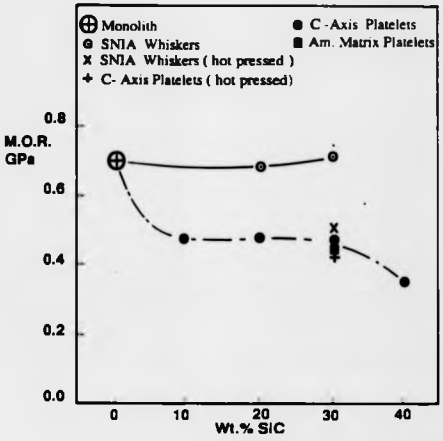

Fig.5.1. Graph of the Room Temperature Modulus of Rupture (M.O.R.) versus Dispersoid content for a series of different Composites. Samples were slip cast and HIPed unless stated otherwise.

coefficient of thermal expansion for Si_3N_4 and SiC are approximately 3.1 and 4.4 x 10^{-6} / °C, respectively. This probably introduced microcracks due to the stresses set up around the dispersoid as the billet cooled down from the fabrication temperature. Interlinkage of these microcracks will result in a reduction in fracture strength, especially when there were high concentrations of dispersoids, as seen in a 40 wt.% platelet composition. The American Matrix platelets have a greater variable size distribution, including some platelets up to 70μm in size, and debris which will magnify the effect of microcracking and introduce inhomogeneities, which will thus lower the average fracture strength.

A decrease in M.O.R. for the hot pressed samples was probably caused by the presence of pores in both materials as the results from table 4.7 showed the hot pressed samples were not fully dense. Pores obviously decrease the cross - sectional area on which the load was applied, but more importantly in this case, where the densities were still relatively high, the pores will also act as stress concentrators. This will result in the initiation of fast fracture at a lower load than for a fully dense specimen. These results from the hot pressed samples showed the same trend as those which were HIPed, i.e. the whisker containing composite had a higher strength than a similar volume fraction of a platelet containing composite.

Besides the mean fracture strength of the materials, information on the variation in the measured values is needed in order to assess the materials' reliability and potential as engineering components. Error bars were omitted from Fig.5.1 in order to avoid overlaps and confusion because of the number of data points. However, the reliability of representative compositions was deduced by Weibull statistical analysis of the spread of measurements, as outlined in section 3.3.1. For some compositions very few test specimens were available so meaningful interpretation on reliability would be

difficult. However, for three compositions, the HIPed monolith, the HIPed 30 wt.% SNIA whisker composite and the HIPed 30 wt.% C-Axis platelet composite, 15 M.O.R. measurements were made and a graph of the survival probability of these three compositions over the spread of M.O.R. results was plotted as Fig.5.2. This graph not only illustates the substantial reduction in strength of the platelet composite again, but also shows the survival probability fell more sharply for a narrower range of fracture strength values in the monolith and whisker containing material, than in the platelet containing material. This indicates a higher reliability for the former materials and can be quantified by using the results in Fig.5.2. and equation 3.6, to plot Fig.5.3. The best straight line was drawn for each set of data by linear regression, from which the gradient and hence the Weibull modulus could be obtained. Results obtained for the monolith and whisker material are similar but although values of around 15 are reasonable for ceramics they are still less than what is required for engine components, where values nearer to 30 are desirable. The low value of the platelet material indicates a wider distribution for strength reducing flaws, possibly due to the range of platelet sizes and clusters of platelets of variable size, which will influence the degree of microcracking and the range of potential critical flaws. It was noticeable from Fig.5.3 that there were one or two points at the outermost end of the graph, for both the whisker and platelet composites, which were distant from the general trend. One could argue that if these were discounted as aberations, the gradients for both these dispersoid compositions would increase and the Weibull modulus improve substantially to a more desirable value.

Although 15 specimens is generally sufficient for Weibull statistical analysis, evidently the larger the number of specimens (n) the sample contains, the smaller is the interval between adjacent values of S_j, the survival probability for the j^{th}

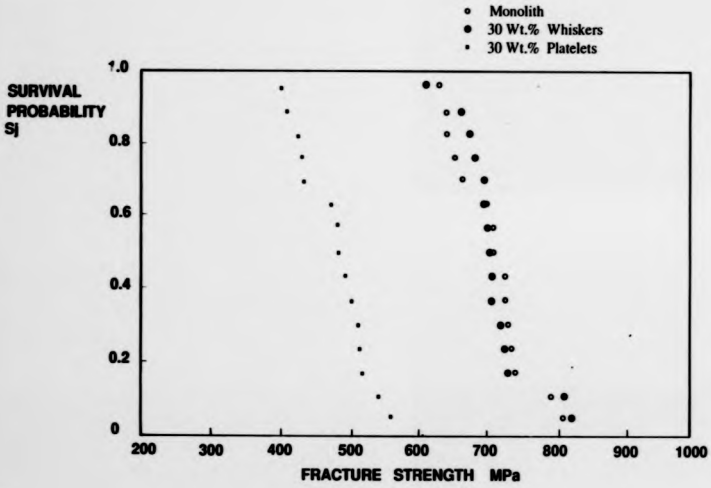

Fig.5.2. Graph Showing the Range of Fracture Strength Values of Representative Specimens against their Probability of Survival.

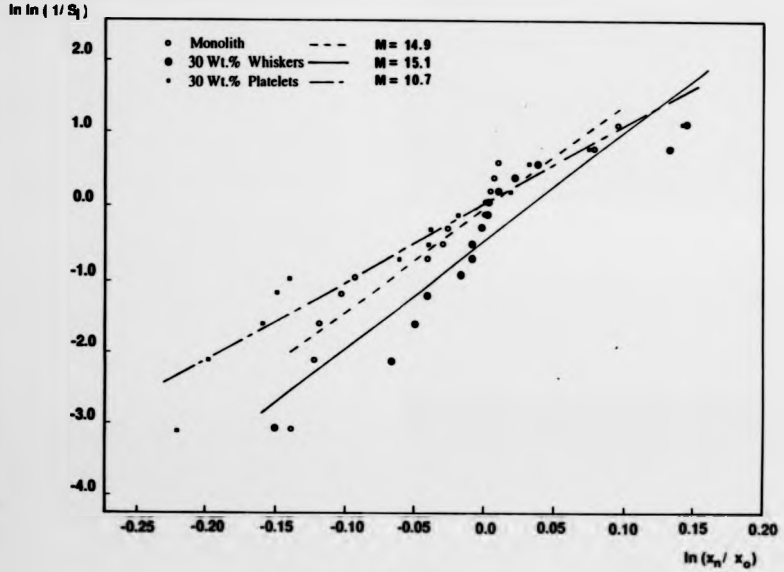

Fig.5.3. Graph Showing the Calculated Weibull Modulus Values of Representative Compositions.

specimen, and it will thus approach more closely to the value of Sj one would get for that specimen had an infinite number of test bars been used. Therefore confidence in the statistical results would increase if they were based on larger numbers of measurements.

Microstructural features associated with the fracture surface topography of the M.O.R. test bars help to identify the fracture origin. The area surrounding a fracture origin has a relatively smooth surface, indicating initial slow crack propagation whereas surrounding this area are radiating fissures in a rougher surface indicating faster fracture. Typical flaws which may be responsible for initiation of fracture include:

a) dispersoid agglomerates,

b) foreign inclusions,

c) porosity,

d) machining damage.

In most of the test bars, there were no obvious distinguishing features which could be identified as the point of fracture initiation Fig.5.4, although the vast majority of fractures probably originated at the tensile surface of the specimen because this was the region of maximum stress. The indications were that most test bars fractured by the interlinkage of surface microcracks caused by machining induced damage. Occasionally, fracture clearly originated from sub - surface particulate agglomeration, which can be seen in Fig.5.5a. This produced cracks which can be seen in Fig.5.5b, interlinkage of which ultimately led to failure at relatively low values. This occured in the composites of lowest fracture strength and was probably due to inadequate dispersion during the slip casting stage. However, this phenomenon was the exception rather than the rule.

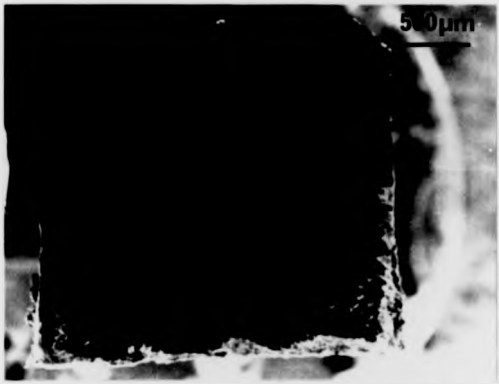

Fig.5.4. Typical fracture surface of a M.O.R. specimen bar showing no obvious source of fracture origin.

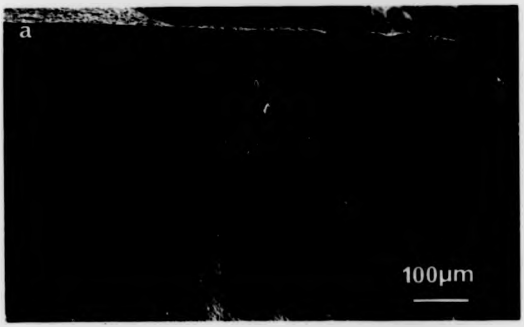

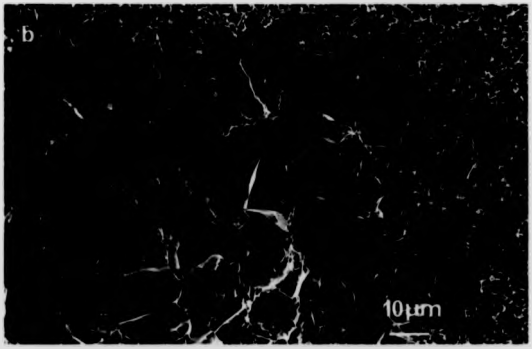

Fig.5.5a Low magnification image of 30 wt.% whisker composite M.O.R. bar showing specimen failure from region of particulate agglomeration; 5.5b higher magnification of Fig.5.5a, showing a crack within the agglomerate.

A side view of most test bars showed a lipping effect caused by a lateral deviation of the propagating crack as it approached the compressive face of the test bar. The progression of the crack was slowed by the compressive stress and forced to propagate along a path of least resistance, rather than the shortest distance route of the initial fast fracture. Quite often the test bars of the whisker and monolith samples fractured into at least three parts, two long pieces and a small central part, the start of crack deviation occurring near the compressive end.

5.3. VICKERS HARDNESS.

The Vickers hardness is not a constant parameter for a material as it shows load sensitivity in the low load regime. However, the applied load in this exercise was kept constant for all measurements, so although the readings were not absolute, a comparative study between different compositions could be made. Specimens were indented at least 20 times on the face perpendicular to the bottom of the billet and to account for anisotropy because of the dispersoid alignment, the two diagonals d_1 and d_2 were measured and the average diagonal dimension d was calculated from the harmonic mean $(d_1 \times d_2)^{1/2}$.

It can be seen from Fig.5.6. that increasing the SiC content of the composites gradually increased the Vickers hardness value, approximately according to a law of mixtures approach. However, for a similar volume fraction of dispersoids, whisker composites appear harder than those containing the platelets. It was not clear why this occurs but it was possibly due to the differing crystal orientation of the dispersoids with respect to the Vickers indent. Another reason may simply be experimental error. There was a wide spread of values obtained partly because of both the difficulty of keeping the load constant for the fixed time and obtaining an accurate

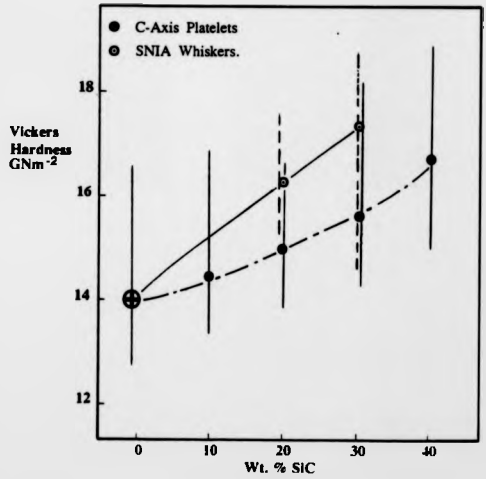

Fig.5.6. Plot of Vickers Hardness Values against Dispersoid Content.

measurement of the diagonal. However, it was clear that the general increase in average hardness of dispersoid composites over the monolith could prove beneficial in wear resistant applications.

5.4. FRACTURE TOUGHNESS.

The fracture toughness values of ceramic materials are probably their greatest disadvantage as potential engineering components and is the main reason for introducing the composite approach. Experimental results are now shown together with a fractography study which assists in explaining these observed results.

5.4.1. Experimental Results.

Fracture toughness measurements were obtained by two separate methods, as described in section 3.3.3, in order to compare the consistency of the results obtained. A minimum of 8 specimens for each HIPed composition and 4 for each hot pressed specimen were used in the SENB method and the results obtained from all the different compositions were plotted in Fig.5.7 . Error bars have been omitted to prevent them obscuring the mean calculated values for each composition, but generally errors were typically +/- 0.5 $MPa.m^{1/2}$.

For most types of composites there was a general increase in fracture toughness with increasing dispersoid content, the only exception was the addition of the small SiC particles which showed a gradual decrease instead. This can be explained by the fact that the interaction of the advancing crack front with the small equiaxed dispersoids, which replace generally similar sized but acicular Si_3N_4 grains, will result in diminished crack deflection and thus reduction of the K_{1c} , assuming there was no change in the general fracture mode. As more Si_3N_4 was replaced by the small

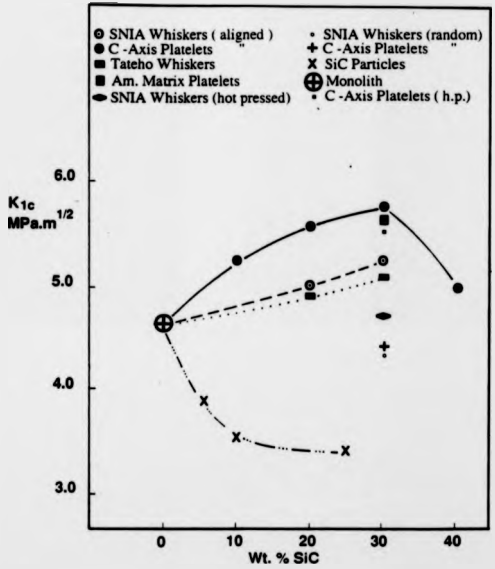

Fig.5.7 Fracture Toughness of Composites versus Dispersoid Content Measured Using the SENB Method.

particles, crack deflection will obviously reduce accordingly. It has been shown in another study [125] that increasing the size of SiC particles has a beneficial effect on the fracture toughness of a ceramic composite, but the results from Fig.5.7 indicated that the particles must meet a minimum size requirement with respect to the matrix grain size, in order to increase the toughness by crack deflection.

An interesting feature of Fig.5.7 was the small but nevertheless noticeably higher increase in fracture toughness values of the C-Axis platelet composites compared with composites containing a similar weight fraction of SNIA whiskers. This suggests there were differences in the mechanisms of toughening between the two types of dispersoid containing composite. However, the relative toughness increases over the monolith were relatively small in all cases and that enhanced toughening, as described in section 2.2, did not occur. This indicates that some of the toughening mechanisms outlined in that section, either do not operate or only operate to a limited extent in these composite systems.

Another significant feature of Fig.5.7 was the advantage of optimised alignment of the dispersoids relative to the crack plane, compared to a completely random distribution. Although the slip cast composites have been shown by optical microscopy to have 2 dimensionally randomly oriented dispersoids, the experimental results, for both whisker and platelet reinforced composites, showed that they had higher fracture toughness values than similar volume fractions of the 3 dimensionally randomly oriented dispersoid composites. Indeed, all the theoretical models concerning crack deflection and the wake toughening mechanisms, indicate that maximum toughness increases occur when the dispersoids are aligned perpendicular to the plane of crack propagation. So although the relative toughness increases are generally small, the results show there were preferential arrangements for the dispersoids in order to

enhance toughness. This suggests again that mechanisms for toughening were occurring in the preferentially aligned dispersoid composites, that did not occur, or occurred to a lesser degree, in the completely random arrangement. If this was the case, a completely aligned dispersoid arrangement should achieve even higher toughness values.

The hot pressed specimens showed a similar fracture toughness trend to those which were HIPed. However, it was more noticeable that the hot pressed C-Axis platelet composite had a much higher relative value than the whisker composite, which again suggests there was a difference in toughening behaviour between composites containing these different types of dispersoid. Both of the hot pressed composites had toughness values which were less than their respective HIPed compositions, probably due to their residual porosity in the former. However, it was noticeable that these hot pressed samples had higher values than the completely randomly oriented dispersoid HIPed composites. This indicates optimised alignment of the dispersoids was more important than complete theoretical density for toughness enhancement.

A slight difference in the values obtained for the HIPed composites containing the two types of whiskers was possibly due to the significant difference in the whisker diameters. Equation 2.9 suggests that increasing the diameter of the whiskers should have a beneficial effect on the bridging contribution for enhanced toughness. This has been confirmed experimentally elsewhere with the use of very large diameter VLS whiskers which showed substantial increases in toughness of the whisker reinforced composite over the monolith [127]. Figs. 4.1 and 4.2 showed that SNIA whiskers have average diameters 2 - 3 times that of the Tateho whiskers which may account for the slightly better fracture toughness values of the SNIA whisker composites. However, this improvement was very small and was well within

experimental error.

There was a major difference in the method of load application between the two fracture toughness techniques. In the bulk fracture toughness method (SENB) the applied load was increased progressively until the critical stress intensity factor was reached and the crack propagates until complete fracture of the specimen. In the indentation fracture toughness method the applied load was greater than that required to propagate a critical flaw. The crack therefore propagated until at some distance away from the applied load, the stress intensity fell below the critical value. Using equation 3.3, the Vickers hardness values from Fig.5.6, the Youngs Modulus values taken from a rule of mixtures approach, and the measured crack lengths, the indentation fracture toughness values were calculated. Fig.5.8 shows the plot of indentation fracture toughness for the SNIA whisker and C-Axis platelet composite series and a comparative plot of the values obtained by the SENB method. The Vickers indentation was positioned such that the surface radial cracks ran approximately parallel and perpendicular to the aligned dispersoids, therefore fracture toughness values in these two relative directions were obtained. This crack size/ indentation technique (perpendicular to dispersoids) produced lower fracture toughness values than the SENB method, but despite this discrepancy in absolute values obtained, there were distinct similarities in the trends across the series of compositions. Both techniques showed the advantage of using platelets over a similar volume fraction of whiskers and also both showed a small increase in fracture toughness with increasing dispersoid content. The results again show emphatically the advantage of aligning the dispersoid perpendicular to the crack so that the energy of propagation can be reduced because of microstructural crack interactions with the dispersoid. When cracks propagate parallel to the dispersoids little toughness increase was shown, even with increasing

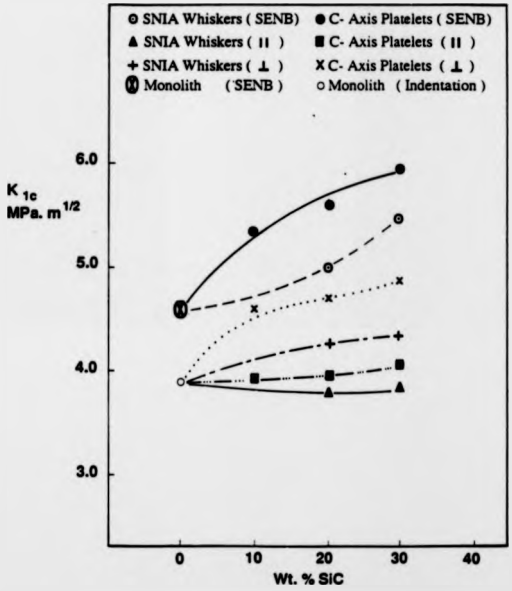

Fig.5.8. Fracture toughness of composites measured by indentation with comparative results obtained from the SENB method.

dispersoid content, presumably because of the small amount of crack / dispersoid interactions and hence the reduced ability of crack bridging to take place, compared to those propagating perpendicular to the dispersoid alignment.

The reasons for the differences in values between the SENB route and the indentation technique may be explained by the fundamental differences in their respective analyses. In the indentation technique there were difficulties associated with the measurement of the crack length, especially near the crack tip, which results in a systematic underestimate of the true crack length. The models for indentation fracture invariably consider the material to be completely isotropic and develop planar cracks under pure mode 1 loading. However, when there are crack / dispersoid interactions the cracks will not be developed under pure mode 1 loading conditions. Therefore it is necessary to specify the technique used when measuring K_{1c} if values are to be quoted as material property data. As a comparative exercise between different materials, either fracture toughness technique is useful. The indentation technique offers the advantages of being a relatively simple, non - destructive and quick method, requiring only small polished specimens. Testing is economical with material and it can be readily used as a quality control monitoring technique.

5.4.2. Fractography.

The fracture surfaces of the SENB test specimens are particular interest as they give information on the mode of fracture and evidence of any toughening mechanisms taking place in these materials. Micrographic examination of the specimens revealed that the fracture process was quite complex. The monolith showed a mixed mode of fracture, but it appeared to be predominantly intergranular as the faceted nature of the Si_3N_4 grains can be seen, Fig.5.9. Presumably it was energetically

more favourable to debond and follow an intergranular path rather than cleave through Si_3N_4 grains transgranularly. Consequently, the fracture surface was quite rough in appearance due to crack deflection around the grains.

Fracture surfaces of composites containing whiskers, aligned preferentially in a plane perpendicular to the crack front, showed little evidence of the whiskers protruding from the fracture plane, Fig.5.10. A few whiskers occasionally appeared to stand proud of the surface, but this pullout was limited to lengths of only one or two whisker diameters and hence contributed little to toughening. The vast majority of the whiskers failed transgranularly near to the fracture plane. However, it was still probable that the whiskers bridged the propagating crack for a short time because their high fracture stress makes them more resistant to crack propagation than the matrix. For pullout to occur, the bridging whisker must fracture in a position out of the principal crack plane and this will only happen if the whisker has some strength variation along its length. This does not appear to occur in these composites because the whiskers have failed in the crack plane, which was the region of highest tensile stress.

In contrast to the whisker composites, those containing preferentially aligned platelets showed platelets protruding out from the fracture surface, Fig.5.11, which indicated substantial debonding and pull out had occurred. Some of these platelets were unfractured and the presence of cavities showed that a large proportion of the platelets had been completely pulled out from one of the fracture faces. It is debateable whether these platelets have been "pulled out" in the classical sense, as described in section 2.2.1, because it has already been shown in Fig. 4.35, that there can be extensive debonding at the platelet / matrix interface before crack propagation occurs. This would suggest that as the crack faces separated, it would be relatively easy

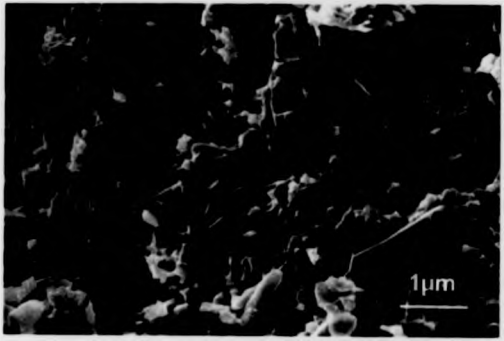

Fig.5.9 Fracture Surface of the Monolith.

Fig.5.10. Fracture Surface of 30 wt.% SNIA Whisker Composite.

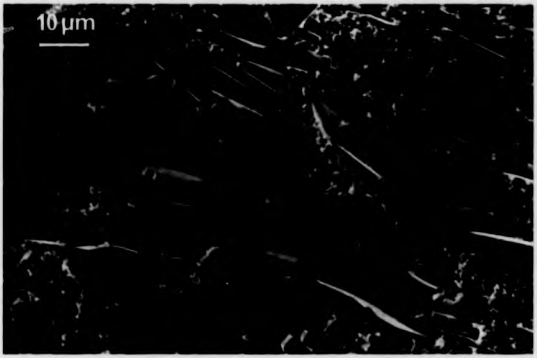

Fig.5.11. Fracture Surface of 30 wt.% C - Axis Platelet Composite.

for the platelets to detach from the fractured matrix. However, some of the protruding platelets have fractured, suggesting they bridged the crack, they were pulled out and then fractured, which would result in the increase in fracture toughness as shown in Fig.5.7. Platelet pullout lengths were relatively short, limited to an average of about 8μm. Hence, although there was an increase in fracture surface created, increments in fracture toughness were not substantial.

In randomly oriented dispersoid composites, the vast majority of whiskers and platelets are inclined to the advancing crack front as in Fig.5.12. They are subjected to flexural loading causing them to fail at lower applied stresses than for the solely axially loaded dispersoids. This meant the tendency for platelet fracture out of the principal crack plane was much reduced and any dispersoid failing out of this plane are unable to pullout due to their inclination. However, they are able to provide a interlocking of the crack face, thus restricting crack opening in a similar way to classical bridging. As the crack faces eventually part, the dispersoid fractures in the principal crack plane. The vast majority of dispersoids were not aligned for optimised toughening so significantly reducing any crack bridging contribution to the toughness of the material.

Observations of the cracks radiating from the indentations revealed the effects of direct interactions with the dispersoids. Cracks propagating in a direction nearly parallel to the alignment of the dispersoid were relatively unimpeded, with minimal crack deflection occurring. On striking a platelet edge - on, debonding occurred and the crack generally passed along the platelet / matrix interface, leaving the platelet unfractured, Fig.5.13a. As the dispersoid was not oriented for a significant crack bridging contribution, there was minimal toughening, as seen in Fig.5.8. When cracks interacted with whiskers aligned perpendicular to the direction of propagation,

interfacial debonding was not observed, Fig.5.14. Even when the whiskers were slightly inclined, transgranular fracture of the dispersoid occurred normal to the whisker axis, on the {111} type planes, presumably because the stacking fault planes were the low energy cleavage planes. It appears the development of a relatively strong bond between the whiskers and the matrix tended to inhibit crack deflection and growth of any debond along the interface. As the initiation of debonding is governed by the whisker orientation and the ratio of the interfacial fracture energy (T_i) to the whisker fracture energy (T_f), shown schematically in Fig.2.8, the observations indicate the interfacial shear strength was too high and the value of (T_i / T_f) lies outside the zone for debonding.

In platelet-containing composites, debonding along the dispersoid / matrix interface was quite often seen, especially if the platelet was slightly inclined to the crack propagation direction, Fig.5.13b. A TEM micrograph of an accidently damaged platelet-reinforced composite, Fig.5.15 shows a crack confined solely to the interfacial regions and preference for debonding along the platelet / matrix interface rather than transgranular fracture of the platelet.

It was clear from these observations that there were fundamental difference in the interfacial characteristics between the two main type of dispersoid composites, which indicates toughening mechanisms occurring in the platelet composites, occur to a lesser extent or not at all in the whisker reinforced composites.

The fracture path was generally limited to a single crack and only occasionally, usually in areas of high dispersoid density, was crack branching observed in the indented specimens. This division into two or more parallel cracks was usually short lived, which together with the scarcity of crack branching in general, indicates that any contribution of this mechanism to toughening of the material was minimal. No

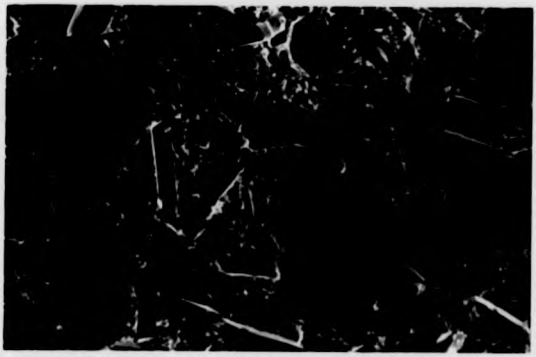

Fig.5.12. Fracture Surface of composite containing 30 wt.% of random oriented C- Axis platelets

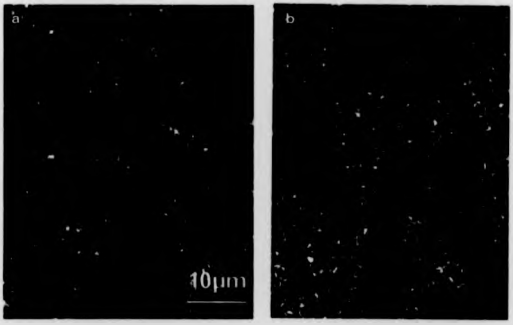

Fig.5.13. SEM micrograph of radiating cracks propagating a) parallel and b) perpendicular to aligned platelets

Fig.5.14. SEM image of crack propagating perpendicular to aligned whiskers.

Fig.5.15. TEM image of crack / platelet interaction.

evidence of microcracking was observed around the propagating cracks, although such microcracks might close after the indent load was removed.

5.4.3. Comparison of experimental results with theoretical predictions.

The experimental fracture toughness values for a series of dispersoid reinforced composites have been measured and a comparison with the toughness increments predicted from the toughening models illustrated in section 2.2, can be made. For crack deflection the toughening model for 2 dimensional randomly arranged rods compared with a matrix with equiaxed grains, Fig.2.12, comes closest to the situation here. If one takes the aspect ratio of SNIA whiskers as ranging from 8-10, and using a volume fraction of 30 wt.%, one would expect a relative toughness increment of at least 4 and a fracture toughness of approximately 2. However, the fracture surfaces revealed that the SiC whiskers were not frequently circumvented by propagating cracks when the whiskers were oriented normal or nearly normal to the crack front. Thus any toughening was due to crack bridging. Toughening increments due to crake wake toughening mechanisms were elaborated in section 2.2 and described using equation 2.7:

$$\Delta G_c = 2\,t\,f\,h_p^{\,2}/R - E\varepsilon^2 f d + 4\,T_i\,f\,(d/R)/(1-f) + f\,d\,S^2/E$$

It has been observed from fracture surface micrographs that the whisker pullout contribution, $2\,t\,f\,h_p^{\,2}/R$ can be neglected, and also the residual strain term $E\varepsilon^2 f d$, is negligible. For the debonding energy contribution, $4\,T_i\,f\,(d/R)/(1-f)$, it is difficult to determine explicitly the extent of debonding in these materials. This is because the debond and matrix crack opening displacement are small and difficult to detect. Usually the second whisker behind the crack tip is fractured indicating that the bridging zone is very small and debonds are limited to a range of R to 3R. If one

assumes a minimal value of d/R, equal to 1 and that T_i is the fracture energy of an amorphous silicate equal to approximately 8 Jm^{-2} [101], the debonding energy contribution equals approximately 17 $J.m^{-2}$.

The toughening contribution from the elastic strain energy stored in the whiskers up to failure is $f\,d\,S^2/E$. If the strength of the whiskers, S is assumed to be in the range of 4 to 8 GPa [186], the volume fraction, f equal to 0.3, the average whisker radius d, equal to 0.55μm, as observed in SEM micrographs, the Young's moduli of SiC and Si_3N_4 to be approximately 400 GPa and 300 GPa respectively and assuming a rule of mixtures approach to obtain the Young's modulus of the composite, a minimum toughening of approximately 8 $J.m^{-2}$ can be assigned to this toughening component. Hence a toughening contribution ΔG_c of approximately 25 $J.m^{-2}$ is achieved and if $K_c = (E G_c)^{1/2}$, then a fracture toughness increment of approximately 2.9 $MPa.m^{1/2}$ is possible. This is slightly more than observed experimentally, but it must be noted that the theoretical predictions are dependent on many assumptions. If the debond zone d is less than R, as is likely, ΔG_c would reduce correspondingly. The toughening contribution from the elastic strain energy stored in the dispersoids up to failure (or bridging contribution) $f\,d\,S^2/E$ is dominated by the choice of dispersoid strength. As platelets are crystallographically more perfect than whiskers, one would expect them to have a higher tensile strength and hence a greater bridging contribution.

5.5. SUMMARY

The results obtained throughout this chapter have shown the effects of different types of SiC dispersoid additions on the room temperature mechanical properties of the resulting composite. The observations have been presented in a comparative form and enable some general conclusions concerning the microstructural features which influence the materials' mechanical behaviour to be made. In summary;

1. The whisker composites maintain the relative high strength of the monolithic Si_3N_4 material, both of which have a reasonable Weibull modulus. Introducing platelets into the Si_3N_4 had a detrimental effect on the strength and reliability, probably because of the interlinkage of microcracks, formed as a result of a thermal expansion mismatch between the two major phases on cooling.

2. The addition of an increasing volume fraction of SiC dispersoids resulted in a general linear increase in the Vickers hardness values.

3. Both the SENB and the indentation method of fracture toughness measurement, showed generally, increasing values of toughness as the dispersoid additions increased. However, the toughness increases were disappointingly small and not as substantial as hoped for.

4. Fracture surfaces of the platelet reinforced composites showed evidence of pullout unlike the whisker composites. This probably explains the slight improvement in toughness of the platelet composites compared to the whisker composites because the interfacial bonding was weaker, which allowed substantial debonding to occur.

5. The results showed that preferential alignment of the dispersoids gave rise to fracture toughness anisotropy. Dispersoids aligned perpendicular to the propagating crack resulted in an increased probability for crack / dispersoid interactions, and hence the ability to activate toughening mechanisms.

These observations illustrated that clearly the character of the interfacial boundary regions was of considerable importance to the fracture behaviour of the materials. There appears to be two main reasons for these observed differences. Firstly, initial debonding at the dispersoid/matrix interface, as observed in platelet containing composites, appeared to be sensitive to the size of the dispersoid. For the whisker reinforced composites, the interfacial chemistry was such that a strong bond was formed between whiskers and the matrix, which prevented debonding and pullout occurring.

CHAPTER SIX

HIGH TEMPERATURE PROPERTIES

6.1. INTRODUCTION.

The long term application of engineering ceramics as high temperature structural materials requires a knowledge of their thermo - mechanical properties and their oxidation resistance. The first part of this chapter describes the results obtained from a comparative study of the creep deformation of representative compositions. This is followed by a discussion of the creep and long term failure mechanisms taking place in these materials. The latter part of the chapter describes the general effects of passive oxidation on the composites, in comparison with the monolithic material, as determined by the thickness and microstructure of the oxide scale.

6.2. HIGH TEMPERATURE DEFORMATION

The creep deformation of three representative compositions, a HIPed 30 wt.% aligned SNIA whisker composite, a HIPed 30 wt.% aligned C -Axis platelet composite and the HIPed monolith, were measured using the 4 point bend apparatus described in section 3.4, and calculated using equations 3.11 and 3.12. A plot of the variation of the strain of the test specimens as the deformation time increased, for a fixed applied stress of 150 MPa and at two testing temperatures, is shown in Fig.6.1. This graph shows that time dependent deformation became increasingly important as the temperature level increased. At 1300°C there was minimal deformation for both the whisker containg sample and the unreinforced sample, which has been found for a

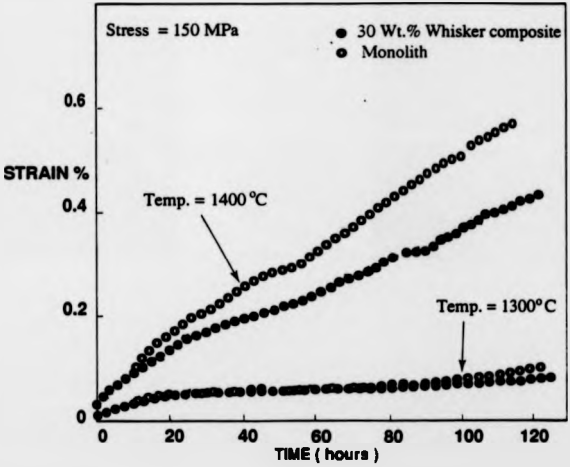

Fig.6.1. Plot of the creep strain against deformation time for a whisker composite and monolith specimens at two testing temperatures and a fixed load.

range of stress values at this temperature. At 1400°C there was an initial elastic strain in both these samples of about 0.02%, then there were relatively similar short primary creep stages. A number of the platelet composite specimens were tested under the same conditions outlined above, but all fractured relatively soon after the load was applied.

Examination of the data indicated there was a near constant creep rate for the specimens after approximately 0.2 % strain. It can be seen from Fig.6.1, that the whisker reinforced specimen had a slightly better creep resistance than the monolithic material. A region of an accelerating creep rate, often observed in metals, was not observed in these Si_3N_4 based ceramics within 120 hours of testing. Repeat experiments were performed on a number of the whisker containing specimen bars, cut out from the same billet of material, in order to eliminate variables such as thermal history, and stressed at 200 MPa under identical conditions. The reproducibility of test data was good at the indicated temperature and stress level, as shown in Fig.6.2, although there were inherent errors in the values obtained, as discussed later.

An indication of the deformation mechanisms exhibited by these materials is given by the value of the stress exponent (n), found using the relationship $\dot{\varepsilon} \propto \sigma^n$, where $\dot{\varepsilon}$ is the strain rate and σ is the applied stress. A graph of the steady state creep rates , over a range of applied loads, at a constant testing temperature, was plotted as Fig.6.3, and the gradient of the best straight line, determined by linear regression, gave a value which was equivalent to the stress exponent. The steady state creep rates were calculated after a minimum deformation time of 80 hours. The results from fig.6.3 confirmed that the whisker reinforced specimens had a better creep resistance, over a range of stress values, than the unreinforced material, but since these reduced creep rates did not result in a significant change in the value of the stress exponent, it appears that similar mechanisms controlled the deformation properties of

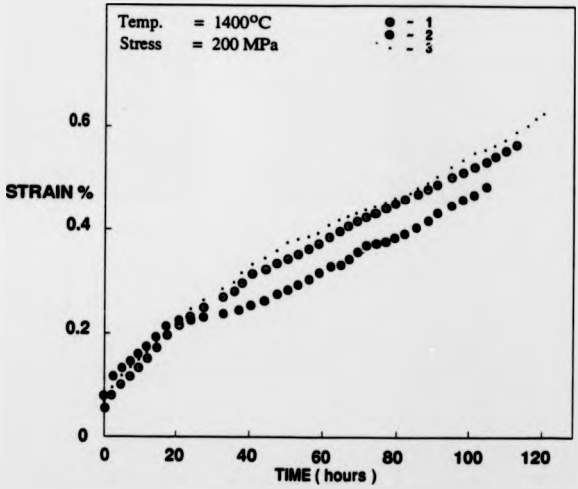

Fig.6.2. Plot of the variation of creep strain as a function of the deformation time for 3 specimens of the 30 wt.% SNIA whisker composite.

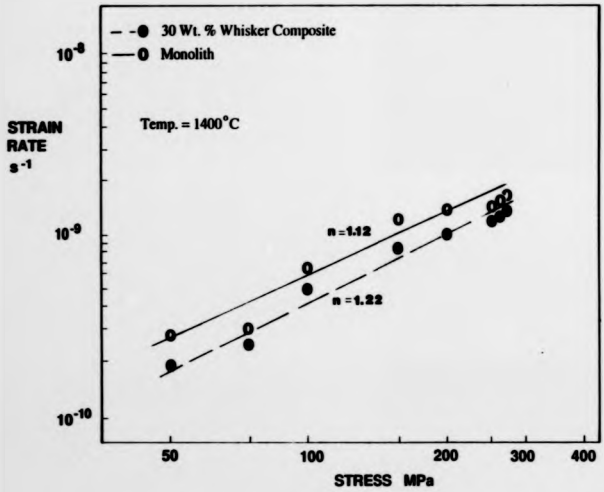

Fig.6.3. Graph showing the range of secondary creep rates as a function of the applied stress for the monolith and whisker composite at a constant temperature.

both materials.

There were a number of inherent errors involved when measuring the creep rates, which make absolute values difficult to obtain. These limitations were mainly concerned with the assumption that the neutral axis was the centre of the specimen, which implies that the creep properties in tension were similar to those in compression. If they were not, the neutral axis will be displaced. As deflection of the specimen became relatively large, the small beam assumptions used to derive equations 3.11 and 3.12 break down. During these conditions, the loading and support force are not exactly vertical as deformation increases, and thus the slippage at the load and support points becomes more serious. Although these problems will affect absolute values, the experimental results obtained still allow a comparative study of these materials to be investigated.

In view of the values of the observed stress exponents seen in Fig.6.3, high temperature deformation of these materials was believed to occur by diffusional creep. In this mechanism values of $n = 1$ are expected. The grain boundary diffusion coefficient D_b is very likely to be greater than the volume diffusion coefficient D_v, i.e. it is easier to transport matter along the amorphous layer than by volume diffusion. Hence Coble creep should predominate over Nabarro - Herring creep and is thought to be the main rate determining creep mechanism. The calculated values of $n = 1.12$ and $n = 1.22$, for the monolith and whisker containing composite respectively, were slightly above this figure, which indicated that the diffusional flow of matter from regions in compression to those in tension was hindered by the presence of the non -deforming whiskers. As diffusional processes dominate creep deformation, it was the volume of the residual amorphous layer present at the grain boundaries, that was the major factor determining the creep resistance of these materials. The fact that the results from Fig.6.3 showed both of these materials have relatively good high temperature deformation properties, was a consequence of the low value of D_b and the small effective cross - section of the amorphous grain boundaries in both materials.

The strain rate during Coble creep is inversely proportional to the

(effective grain size)^3 which suggests the reason for the slight improvement in creep resistance of the whisker reinforced composite probably lies in the increased mean diffusion lengths in this material during Coble creep. Obviously introducing relatively large acicular SiC whiskers at the expense of lower aspect ratio Si_3N_4 grains, and if all other physio - chemical features were similar, will increase the diffusional flow distances. This occurred in a composite material which electron microscopy and XRD has shown to have essentially similar matrix properties to the monolithic material.

One might have expected any additional silica content from the whiskers to alter the oxygen to nitrogen ratio and hence have a marked influence on the crystallisation behaviour of the intergranular phase and on the viscosity of the residual amorphous phase. Metal impurities will reduce the eutectic melting point of the grain boundary phase which will reduce creep resistance. Fortunately, these did not have a detrimental effect on the measured deformation properties of these materials. The results obtained illustrate the importance of tailoring the composition of the material to form desirable crystalline products with a relatively high eutectic melting point and to obtain a minimization of any residual amorphous phase.

6.3. STRESS RUPTURE.

One of the major problems concerning the high temperature engineering application of ceramics is that of delayed fracture. This is characterised by the sub - critical crack growth of pre- existing flaws in the high stress regime, at stresses lower than that for instantaneous crack propagation, and damage accumulation due to coalesence of cavities in the low stress regime. Experimental data on stress rupture was plotted as the time to failure of the specimen as a function of the applied stress, Fig.6.4. All tests were carried out at a constant temperature of 1400°C which is the target temperature for Si_3N_4 based components in heat engines. The stresses used in this study were rather high for potential engineering components, which are more likely to be designed to experience stresses around 100 MPa. However results from Fig.6.4 give an indication of the limitation of these materials.

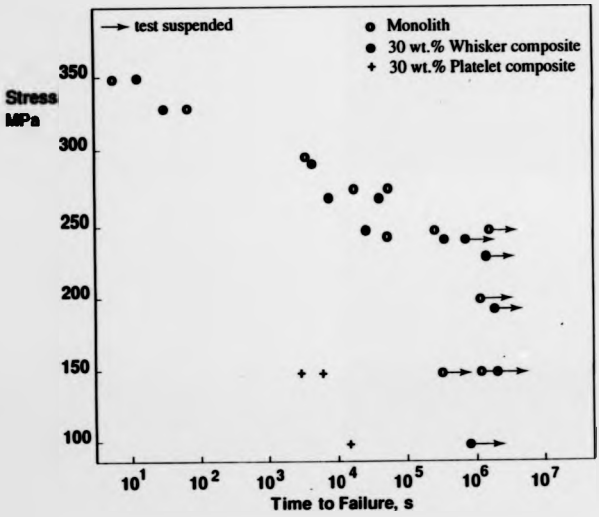

Fig.6.4. Stress rupture data for selective materials at 1400°C

At relatively high stresses, i.e. > 260 MPa, both the whisker and monolithic material specimens failed by fast fracture from within the inner span of the jig. The data were quite scattered, although consistently lower than that expected from M.O.R. results. It is not totally understood why these values were considerably lower than room temperature M.O.R. results, but grain boundary softening may be a factor. At stresses of 250 MPa and below, there were few short term failures with the whisker and monolithic samples, but the platelet composite specimens invariably failed at significantly lower stress levels than the other types of material. Unfortunately there were insufficient data to distinguish a discernable trend between the whisker reinforced composite and the unreinforced material, or to make definitive statements as to the failure mechanisms exhibited. However, some important features stand out from Fig.6.4. At 250 MPa there appeared to be a plateau in the stress rupture behaviour of the whisker and monolithic materials. This observation, that inherent defects do not propagate after prolonged deformation times at these stress levels, indicates that there was a threshold stress for crack growth, and this is believed to result from crack blunting by diffusional creep. The fact that both short term and long term failures can occur in the same material at the same stress level is attributed to the statistical distribution of inherent defect sizes, i.e. the larger defects were subjected to a stress intensity above the threshold value, the smaller defects below the theshold stress. Below 250 MPa all test pieces of the whisker reinforced and the unreinforced material survived at least 300 hours at 1400°C, indicating there was no low stress region where creep cavitation occurred.

Fracture surfaces of the stress rupture specimens were examined in the SEM, but detailed observations were largely obscured by post fracture oxidation of the fracture surface. In each case fracture appeared to be fast across the whole section.

Optical examination of the tensile faces of specimens that underwent substantial creep strain, did not reveal evidence of crack initiation or transverse cracks. A TEM specimen was prepared from the region just below the oxidation scale of the tensile face of a whisker reinforced composite test bar that had been subjected to a 200 MPa stress at 1400°C for 300 hours without failure, but had undergone substantial creep strain. A general TEM survey of the specimen showed a microstructure very similar to that observed in the untested condition. The Si_3N_4 grains retained their general morphology and faceted nature, and the intergranular phase dispersion appeared largely unchanged, Fig.6.5. This indicated the residual amorphous layer present between the Si_3N_4 grains and the disilicate phase can accommodate the diffusional transport of matter. A higher magnification image, Fig.6.6, showed no obvious debonding or microcracking at the whisker / matrix interface, which often occurs in other SiC whisker reinforced ceramic systems [179]. The grain boundary triple junction showed no voids or cavities which are normally associated with creep rupture. Creep rupture normally arises in materials containing a glassy phase and presumably arises due to cavity formation and subsequent diffusional interlinkage . The non - cavitational behaviour of this composite material is characteristic of a microstructure in which creep cavitation was suppressed because of a sub - critical residual glass volume for nucleation of cavities at the stress level used. This apparent absence of cavitational behaviour is totally consistent with a near fully crystalline microstructure of these materials.

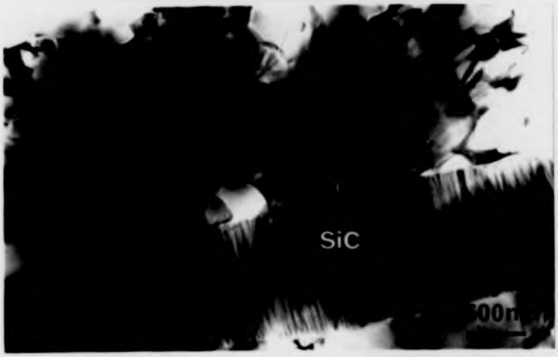

Fig.6.5. TEM micrograph showing the general microstructure of HIPed whisker reinforced composite which had undergone extensive creep deformation.

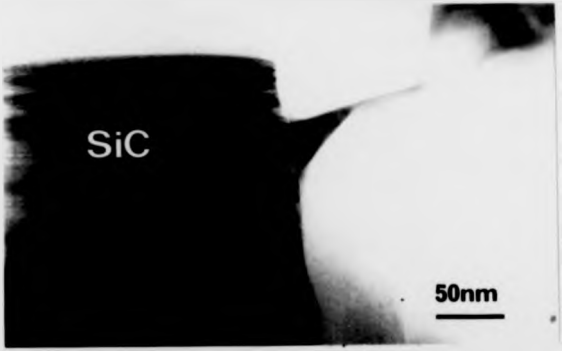

Fig.6.6. TEM micrograph showing no debonding at the whisker / matrix interface or cavity formation in the triple junction.

6.4. OXIDATION.

The oxidation behaviour of non - oxide ceramics is quite complex and the reproducibility of data is invariably poor, depending heavily on the testing furnace employed, as noted by other researchers [183]. Hence it is difficult to give a detailed evaluation of the thermochemical stability and kinetics of the composites, under passive oxidation conditions, in comparison with the Si_3N_4 monolithic material. Only a general comparison has been made, under notionally similar experimental conditions, by measuring the oxide scale thickness and microstructural features. No attempt was made at measuring the weight gain / unit area, so reliable determination of the oxidation kinetics was not possible.

Passive oxidation of all the materials produced no detectable oxide scale after 100 hours at 1200°C, but after a short term exposure of 12 hours at 1400°C, a thin oxide scale was formed in all materials tested, typically 1 - 2 μm in thickness. On looking at the top surface of a selection of representative specimens, oxidised at the target temperature of 1400°C for 100 hours, there a number of noticeable features. XRD of this top surface showed it comprised largely of cristobalite (the low temperature devitrified silica) which are the dark grey contrast regions in Fig.6.7. Since the analysis was performed at room temperature, the form of the silica scale at the oxidation temperature was not known. There were also needles and platelets of a $Y_2Si_2O_7$ phase (lightest contrast regions) which appeared to form in increasing amounts as the SiC content increased and were generally quite well dispersed throughout the surface. There was also an amorphous like silicate residue (light grey contrast) which EDAX has shown to contain yttrium. There was extensive cracking throughout all the samples, which was probably caused by a thermal expansion mismatch between the oxide film and the bulk material on cooling.

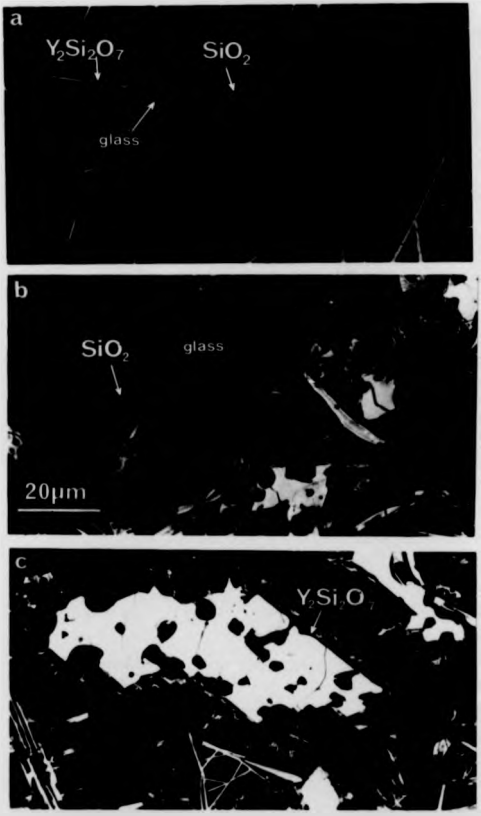

Fig.6.7. SEM micrographs of the top surface of a selection of representative samples, oxidised at 1400C for 100 hours, a) monolith, b) 30 wt.% whisker composite, c) 30 wt.% platelet composite.

Cross - sectional views of the oxidised samples showed that all the specimens had reasonably good oxidation resistance, with a slight increase in oxide thickness from the monolith to the whisker reinforced composite, then a further increase with the platelet reinforced material, Fig.6.8. The oxide layers were reasonably uniform and coherent along their lengths, varying between 4 - 8μm in thickness. The surface oxide usually contained fissures and bubbles in all compositions which were probably caused by N_2 and CO gas, formed as a by product of the oxidation of Si_3N_4 and SiC, respectively. When the gas pressure within the bubbles exceeds the ambient pressure, the bubbles will burst, causing cracking of the oxide layer and hence increase the rate of oxidation. Since the pores did not appear to be interconnected in the scale, a coherent layer generally remained over the substrate. Sometimes it was apparent that there was a layer between the oxide and the bulk material which differed from the established microstructure by a depletion of the light contrast intergranular phase. It is hard to identify from the micrographs, but it extended 4 - 6μm between the bulk material / oxide interface. There was also a distinct partial transformation of the α - $Y_2Si_2O_7$ to the β polymorph, detected by XRD. This can result in a volume increase of about 7% and consequently the possibility of cracking within the specimen.

It has been reported that the passive oxidation of Si_3N_4 based ceramics follows a near parabolic behaviour, which is controlled by a diffusional mechanism. The growth of the oxide layer is expected to occur by the inward diffusion of oxygen or molecules which react with Si_3N_4 and SiC. Initially the oxidation reaction takes place rapidly because of the direct contact of the Si_3N_4 and SiC phases with air. However, the silica formed acts as a protective layer and once this oxide layer covers the surface, the oxidation process is slowed down, resulting in excellent oxidation resistance for the material if the layer remains intact.

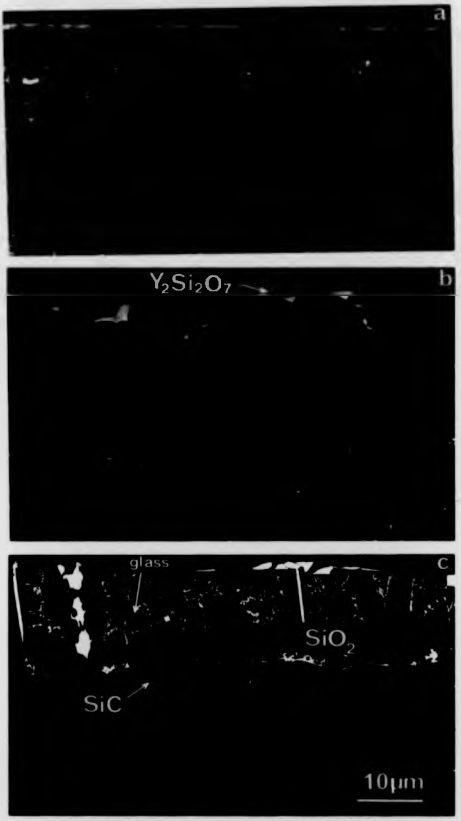

Fig.6.8. SEM micrographs of the cross section of the oxidised samples a) monolith, b) 30 wt.% whisker composite, c) 30 wt.% platelet composite.

The outer surface of the scale was formed first and was an indication of the scale composition during the intial or transient oxidation stage. The concentration of Y and impurities in this outer surface, indicates that there was rapid diffusion of these cations, which were present in the intergranular region, out of the substrate into the scale where the $Y_2Si_2O_7$ based crystals and the other silicate phase formed. It was probable that the formation of a SiO_2 layer created a chemical potential difference between the surface SiO_2 and the glassy grain boundary residue. A chemical diffusion couple occurred because of the relative instability of the two phases at the oxidation temperature, arising from the tendency to form a single equilibrium composition. As oxidation proceeded the out diffusing Y^{3+} cations reacted with Si^{4+} and O^{2-} ions to form crystalline $Y_2Si_2O_7$. The formation of this phase and the continued oxidation of Si_3N_4 and SiC by the indiffusion of O^{2-} anions, maintained a chemical imbalance between the grain boundary and the oxide scale during Y^{3+} out diffusion. As oxidation proceeds, the rate of Y^{3+} out diffusion will slow because of the relatively large cation size compared to the interstitial volume in the silica structure, and this was probably the rate controlling process in these materials. Thus the oxidation of the materials is determined by the ease of migration of the cations and hence the viscosity of the amorphous film. Lowering this viscosity will result in an increased transport of oxidant through the film, and therefore an increase in the oxidation rate of the material. Impurity elements such as Ca and Al will lower the devitrification temperature of silica, reduce the viscosity and hence the increase in oxide scale thickness .

As all these HIPed materials were close to theoretical density, there were no open porosity channels, such as in RBSN based materials, which would enhance oxidation. However, there is the possibility of oxidation causing a reduction in strength of the materials, and also dimensional changes caused by the scale formation. The

effect of oxidation on the overall failure process of these materials has not been studied in detail. There is the possibility that oxidation pits and pores beneath the oxide scale could behave as strength limiting defects when placed under stressed conditions for long exposure times. It has been reported that the oxidative degradation of oxynitride phases such as apatite [185] leads to time dependent failure in stress rupture. This was initiated by linkage of cavities formed in the near surface region, however there has been no evidence to suggest that this occurs in the disilicate containing matrix.

6.5. SUMMARY.

From the limited data collected on the high temperature properties of these materials the following comments can be made.

1. There was minimal deformation of the monolith and the whisker reinforced composite at 1300°C using a moderate stress level of 150 MPa.

2. Introduction of relatively large whiskers into the matrix increases diffusional flow distances and hence appears to improve the creep resistance slightly. The fine grained microstructure of the monolith produces short diffusion paths which is detrimental to the suppresssion of creep.

3. The thin residual film observed between the major phases by high resolution microscopy, probably provides a diffusional path for grain boundary creep. However, these materials have very good creep resistance which suggests the rapid diffusional transport paths provided by the interfacial residues have been kept to a minimum.

4. The lack of glassy residues eliminates the possibilities for nucleation of cavities, as found in many ceramics containing glassy triple junctions.

5. For the monolith and whisker reinforced composite, any time dependent growth of pre-existing flaws does not continue below the threshold stress value of approximately

250 MPa. However the platelet containing composite fractures at stress levels considerably below this level.

6. All the representative compositions showed good oxidation resistance, with only a small increase in oxide scale thickness with the introduction of the dispersoids into the matrix. There was evidence of cation out-diffusion to the surface of the oxidation samples.

CHAPTER SEVEN

CONCLUSIONS

7.1. INTRODUCTION.

Developments in the field of sintering additive chemistry have shown that compositions fabricated within the Si_3N_4 - SiO_2 - $Y_2Si_2O_7$ phase compatability triangle have promising high temperature properties [187]. These compositions probably represent the ultimate development of monolithic Si_3N_4 for high temperature use under long term loading. However, components manufactured from these materials suffer from the general ceramic characteristics of brittleness and unreliability. The main objective of this present work, was to introduce different types of dispersoids into a well characterised monolithic Si_3N_4, in order to improve the fracture toughness yet still maintain their high temperature properties. The principal aspects that were investigated were :

1. developing a method of fabricating a range of homogeneous and fully dense SiC - dispersoid reinforced Si_3N_4 composites.
2. conducting a microstructural assessment of the fabricated composites.
3. determining the room temperature mechanical properties of the range of materials formed and relating these findings to the observed microstructural features.
4. conducting a comparative investigation of the high temperature time dependent properties of representative compositions.

7.2. GENERAL CONCLUSIONS.

The general aims of the research programme have been achieved and the following main conclusions can be drawn .

The slip casting technique can be successfully used to form green state composite billets with a relatively uniform and preferentially aligned dispersoid arrangement. Conventional powder processing techniques were used to form randomly oriented dispersoid reinforced composites. Hot Isostatic Pressing (HIP), using the ABB Cerama facility, has been shown to completely densify composites containing at least 30 wt.% whiskers and 40 wt.% platelets. Both hot pressing and pressureless sintering of these materials, suffer from severe limitations as a production route. The pressures available with the in- house hot press were insufficient for complete densification, especially for whisker containing composites. Hot pressing also confines manufacture of materials to simple geometries such as discs. Pressureless sintering was found to be an unsuitable technique for densification of materials containing a relatively low sintering aid volume and non - compacting dispersoids. Hence, examination of HIPed SiC dispersoid reinforced Si_3N_4 composites formed the focal point of this research programme.

Both microstructural evaluation and XRD of the materials studied, has shown that close compositional control of the starting constituents results in the intergranular region of the densified composites largely crystallising to the desirable α– $Y_2Si_2O_7$ phase after heat treatment. High resolution microscopy does reveal a very thin residual film approximately 2nm in thickness, between the constituent phases. This film was probably amorphous in nature and was present in the monolith and composite materials. All types of SiC dispersoid appeared stable within the matrix after undergoing the HIPed processing. However, the matrix / dispersoid interfacial features were different, depending on what type of dispersoid was added. There are two main factors which determine whether a strong bond was formed between the dispersoid and the matrix, the relative size of the dispersoid and the interfacial chemistry. The platelets used were relatively large compared to the matrix grains, therefore the thermal

expansion mismatch, which develops on cooling from the HIP processing temperature, results in debonding at the matrix / platelet interface. The whiskers appeared to be below any threshold size at which thermal expansion mismatch causes debonding. High resolution microscopy in these materials suggests a thin glassy layer was present at the interface, which bonds the whiskers to the surrounding matrix.

The room temperature mechanical properties of these composites were related to the observed microstructural characteristics, specifically at the interface between the dispersoid and the matrix. Whiskers appeared to be tightly bonded to the matrix as there was little sign of interfacial debonding or whisker pullout as a result of crack propagation. However, with platelet containing composites, the platelets were seen protruding from the surface of the fracture face. These observations may help to explain why platelets appeared to be slightly better than whiskers as toughening aids. It was also concluded that the fracture toughness values were dependent upon the orientation of the dispersoids, being higher when they were aligned perpendicular to the plane of crack propagation than when parallel or randomly oriented. This anisotropy in properties arises because of the increased contribution of crack bridging and platelet pullout to the fracture toughness. Random orientation of dispersoids, to produce an isotropic material, results in no toughness increase. Although it was found that the fracture toughness value obtained was dependent on the experimental technique used, the toughness increment with a 30 wt.% dispersoid content was from 4.6 $MPa.m^{1/2}$ to 5.2 $MPa.m^{1/2}$ for the whisker composite, and to 5.8 $MPa.m^{1/2}$ for the platelet composite.

The room temperature fracture toughness values obtained during this research programme were of similar magnitude to the results obtained by other researchers working on SiC whisker reinforced Si_3N_4 composite systems. Values of

approximately 10.5 $MPa.m^{1/2}$ have been quoted for a 30 wt.% whisker loading. This was approximately 50% higher than the monolith value, however large diameter VLS whiskers where used in that study. It is difficult to compare values obtained because of the variety of techniques and testing conditions used by different researchers. However general trends can be compared and it has been found that increments in fracture toughness ranging up to a maximum of 40% have been achieved using whiskers derived from rice hulls. Even in the cases of maximum fracture toughness increments, fracture surface observations suggested there was only limited whisker pullout; it being the exception rather than the rule. This suggests dispersing as-received SiC whiskers into a Si_3N_4 matrix is not sufficient for maximum toughening increments to occur and that whisker pre-treatment is necessary.

The initial interest in whisker reinforced ceramic systems was sparked by the significant increments in fracture toughness which can been achieved both theoretically and experimentally in hot pressed SiC reinforced Al_2O_3 composite systems. Theoretical models predict increments 3 to 4 times that of the monolith [185] and experimental fracture toughness values which were more than double the value of the monolith have been quoted [120]. In this system, more evidence for whisker bridging and pullout has been observed. Electron microscopy has shown bridging zones, typically 4 to 6 times the whisker diameter and debond zones ranging between 2 and 6 times the whisker radius, were developed during crack propagation through the composite. Hence SiC / Al_2O_3 composite systems have a larger bridging and debonding contribution to the steady state toughening of the monolith than in the SiC / Si_3N_4 composite systems. This suggests there are differences in the interfacial chemistry between these two systems which results in the significant differences in toughening achieved.

A noticeable feature was the significant reduction in ambient fracture strength from approximately 710 MPa to 450 MPa on dispersing 10 wt.% of the platelets into the monolith. This was presumed to be caused by the interlinkage of microcracks, generated by the thermal expansion mismatch on cooling from the processing temperature. Although this type of dispersoid containg composite has promising toughening behaviour, the reduction in M.O.R. severely limits its usefulness. The whisker composites maintained the excellent high fracture strength of the monolith, which suggests there may be a theshold dispersoid size for microcracking to develop. However, both composite types show catastrophic failure after linear elastic behaviour rather than showing any controlled fracture.

There was a general rise in Vickers hardness values as the volume fraction of SiC dispersoid increased. This was not surprising as SiC is harder than Si_3N_4 and a general rule of mixtures approach was followed. Thus these materials may prove useful in wear resistance applications.

A representative whisker reinforced composite showed excellent creep resistant properties, with a strain rate of approximately 10^{-9} s^{-1} when subjected to a stress of 250 MPa at 1400°C. A stress exponent value of n just over 1 was shown, which was similar to the monolith and together with other evidence, suggests that grain boundary or Coble creep was the rate determining mechanism. Stress rupture data revealed an apparent stress theshold of approximately 250 MPa below which there was no long term failure of whisker composite and monolith specimens. Together with TEM observations, the absence of slow crack growth of pre-existing flaws suggests there was a non critical residual glass volume within these materials for the nucleation of cavities. This will prove beneficial under in-service conditions.

7.3. SPECIFIC CONCLUSIONS.

The specific conclusions to the main objectives of the research project listed in section 2.4. are :

. it has been shown that a well characterised Si_3N_4 matrix containing at least 30 wt.% of various types of SiC dispersoid reinforcement can be fabricated to full or near full density by HIP.

. mechanical testing has shown that introducing relatively large platelets into the matrix is detrimental to the fracture strength of the composite, unlike whiskers. However, there is a greater increase in the fracture toughness of a platelet composite compared with a whisker composite of similar volume fraction of dispersoid.

. Weibull analysis has shown that platelet composites are less reliable that the monolith although whisker composite show slightly greater reliability.

. high temperature deformation results indicate that introducing whiskers into the matrix and hence increasing diffusion paths, reduces creep rates.

7.4. SUGGESTIONS FOR FUTURE WORK.

This research programme has demonstrated that improvements in the fracture toughness of Si_3N_4 based ceramics can be achieved by introducing SiC whiskers into the matrix, and that the excellent high temperature properties of the monolith can be maintained. However, the improvements in fracture toughness were not substantial and therefore are specific areas in which further investigation would be beneficial.

It has been mentioned previously that whiskers manufactured using the VLS process have larger diameters and higher strengths than the whiskers derived from rice hulls, as used during this research programme, and hence would contribute more to

crack bridging. These VLS whiskers are not commercially available presently, but their introduction to the market could give beneficial toughness improvements. Platelet production is still in its infancy and the present sizes are relatively coarse. Consequently significant decreases in fracture strength are achieved. Thus finer grades may give similar fracture toughness values yet reduce their detrimental effect on the M.O.R. of the composite.

A major conclusion of this work is that the mechanical properties of the composite are dependent upon the interfacial characteristics. The obvious route in solving the problem of strong bond formation, is to reduce the interfacial fracture energy T_i. This can be done by pre - treating or coating the whisker with a material which would prevent a strong bond forming with the matrix. The optimum coating or interface structure and chemistry for SiC / Si_3N_4 is not presently known, although carbon coated whiskers is a possible candidate. However, some work conducted as part of this research programme, raised questions about the survival of a carbon layer on carbon coating whiskers when incorporated into a hot pressed composite. Given the importance of dispersoid / matrix debonding, more investigation into the interfacial behaviour is required.

The variability of fracture toughness values with different testing techniques suggests that there should be standardised methods of mechanical testing. This would enable more accurate comparison with the results obtained by other researchers.

These materials have a potential application temperature of 1400°C, so a more detailed survey of the high temperature toughness, creep and strength degradation behaviour is necessary. The effects of brine and aviation fuel environments on these material properties would assist in characterising their behaviour under in-service

conditions.

Dispersoid reinforced composites are cheaper and use more conventional powder processing techniques than continuous fibre reinforced composites. However, the limited increments in fracture toughness achieved by the former has meant that future developments in ceramic composite technology will probably be in the area of ceramic fibre reinforced ceramic composites. In these materials, non-catastrophic failure and substantial load carrying capability past the peak load is often observed. The fibres manufactured presently have high temperature limitations, but developments in both protective coatings and coatings to aid debonding are taking place.

As with any revolutionary development in materials design, potential improvements in properties must be weighed up with the additional financial costs involved in replacing existing materials and introducing new components. Thus it may be some time before the obvious advantages of ceramic composites will lead to substantial introduction of these materials and replacement of the current metal alloys.

REFERENCES.

[1] Moulson.A.J., J. Mat. Sci., Vol. 14, 1979, pp.1017.

[2] Katz.R.N., Science, Vol. 208, 1980, pp.84.

[3] Weaver.M.J., Mat.Sci. and Tech., Vol.3, 1987, pp.682.

[4] Ashby. M.F. and Jones, D.R., in Engineering Materials, An Introduction to their Properties and Applications, Pergamon Press, 1983.

[5] Garvie, R.C., Hannink. R.H.J. and Pascoe, R.T., Nature, Vol. 258, 1975, pp.703.

[6] Lange.F.F., J.Mat.Sci., Vol.17, 1982, pp.225.

[7] Lewis.M.H. Ceramics: Applications and Limitations, in Materials at their Limits, Inst. of Met. Publ., 1986, pp. 1 - 20.

[8] Katz.R.N., Mat.Sci. and Eng., Vol.71, 1985, pp.227.

[9] Morrell.R., Advanced Engineering with Ceramics, Brit. Ceram. Proc., No.46, April 1990, pp.1-11.

[10] Sorrell.C.C. and Mc Cartney.E.R., Materials Forum, Vol. 9, 1986, pp.149.

[11] Wachtman, J.B., in High Tech. Ceramics, ed. Vincenzini.P., Elsevier, 1987, pp.3069.

[12] Probst.H.B., Am. Ceram. Soc. Bull., Vol.59, 1980, pp.206.

[13] Anon., Fine Ceramics in Japan, Long Term Credit Bank of Japan (L.T.C.B.),Special Issue, Dec. 1984, cited in ref[5].

[14] Black.J.H., Bull. Amer. Ceram. Soc., Vol.64(1), 1985, pp 34 - 38.

[15] Butler. E.G., Int. J. High Tech. Ceramics, Vol.4, 1988, pp.93 - 102.

[16] Bennett.A., Advanced Engineering with Ceramics, Brit. Ceram. Proc., No.46, April 1990, pp.13-20.

[17] Seitz.E., in in High Tech. Ceramics, ed. Vincenzini.P., Elsevier, 1987, pp.3037.

[18] Mueller. J.L., Amer. Ceram. Soc. Bull., Vol.61, 1982, pp.588.

[19] Buljan.S-T. and Sarin. V.K., Composites, Vol.18, No.2, 1987, pp.99-105.

[20] Brennan.J.J., in Special Ceramics 6, ed. Popper.P, Brit. Ceram. Research Assoc., London, 1975, pp.123-129.

[21] Lindley.M.W. and Godfrey.D.J., Nature, Vol.229, Jan. 1971, pp.192-193.

[22] Guo.J., Mao. Z., Bao. C., Wang. R. and Yau. D., New Ceramic Material, Vol.4, No.4, 1975, pp.1-7.

[23] Yasima.S., J. Amer. Ceram. Soc., Vol.59, 1976, pp.324.

[24] Prewo. K. and Brennan, J.J., J. Mat. Sci., Vol.17, 1982, pp.1201.

[25] Rice. R.W., Ceram. Eng. Sci. Proc.1, Nos. 7-8, 1980, pp.424-443.

[26] Shetty. D.K. et.al., Ceram. Eng. Sci. Proc.6, Nos. 7-8, 1985, pp.632-645.

[27] Mack. J., Materials Edge, Nov. / Dec., 1988, pp. 26 -35.

[28] Tiegs. T.N. and Becher. P.F., Amer. Ceram. Soc. Bull., Vol. 66, 1987, pp.339-342.

[29] Klein. A., Adv. Mat. and Proc., No.9, 1986, pp. 26-33.

[30] Lewis. D., in Proc. of Conf. on Processing of Advanced Ceramics, Ed. Moya. J.S. and de Aza. S., Soc. Esp. Ceram. Vidr. Arganda del Rey, Madrid, 1986, pp.49-72.

[31] Suresh. S., J. Amer. Ceram. Soc., Vol.71, No.3, 1988, pp.C158 - C161.

[31b] Whitehead. A.J. , Page. T.F. and Higgins. I, Ceram. Eng. Sci. Proc., Vol. 10, 1989, pp. 986-997.

[32] Jack. K.H., in Processing of Crystalline Ceramics, Mat. Sci. Res., Vol.2, 111th Univ. Conf. on Ceram. Sci., North Carolina State Univ., eds. Partom et.al., 1978, pp.561.

[33] Kingery. W.D., J. Appl. Phys., Vol.30, 1959, pp.301.

[34] Drew. P. and Lewis. M.H., J. Mat. Sci., Vol.9, 1974, pp. 261.

[35] Lange. F.F., Int. Met. Rev., Vol. 1, 1980, pp.1

[36] Lewis. M.H., Leng-Ward. G., Winder. S.M. and Lumby. R.J., in Deformation of Ceramics II, eds. Tressler.R.E. and Brandt.R.C., Plenum Press, 1984, pp.605.

[37] Sarin. V.K., Mat. Sci. and Eng., Vol. A 105/106, 1988, pp.151-159.

[38] Lewis. M.H., in Micromechanisms of Plasticity and Fracture, eds. Taplin.R. and Lewis. M.H., Parsons Press, 1983, pp.181.

[39] Clarke. D.R., in Prog. in Nitrogen Ceramics, ed. Riley.F., Martinus Nijhoff, 1983, pp.341.

[40] Woetting. G. and Ziegler.G., Ceram. Int., Vol.10, 1984, pp.18

[41] Tuersley. I.P., Leng-Ward. G. and Lewis. M.H., in Proc. 3rd Int. Symp. on Ceram. Mat. and Comp. for Eng., Las Vegas, ed. Tennery. V.J., 1988, pp.856.

[42] Lange. F.F., in Prog. in Nitrogen Ceramics, ed. Riley.F., Martinus Nijhoff, 1983, pp.469.

[43] Lewis. M.H. and Lumby. R.J., Powder Met., Vol.26, 1983, pp.73.

[44] Lewis. M.H., Leng-Ward. G. and Mason. S., in Engineering with Ceramics II, ed. Freer. R, Brit. Ceram. Proc., No.39, Dec. 1987, pp.1.

[45] Gazza. G.E., Amer. Ceram. Soc. Bull. Vol.54, No.9, 1975, pp.778-781.

[46] Lange. F.F., J. Amer. Ceram. Soc., Vol. 60, No. 5-6, 1977, pp. 249-252.

[47] Singhal. S.C., in Prog. in Nitrogen Ceramics, ed. Riley.F., Martinus Nijhoff, 1977.

[48] Tuersley. I.P., Ph.D. Thesis, Univ. Warwick, 1990.

[49] Wills. R.R., J. Mat.Sci., Vol.11, 1976, pp.1305.

[50] Gaukler. L.J., Hohnke.H. and Tien. T.Y., J. Amer. Ceram. Soc., Vol.63, 1980, pp.35.

[51] Greil. P., Proc. 3rd Int. Symp. on Ceram. Mat. and Comp. for Eng., Las Vegas, ed. Tennery. V.J., 1988, pp.319-329.

[52] Qishey. F., ibid., pp.330-340.

[53] Hoffmann. M.J., Nagel. A. Greil. P and Petzow. G., J. Amer. Ceram. Soc., Vol.72, No.5, 1989, pp.765-769.

[54] Bratby. J., in Coagulation and Flocculation, Uplands Press Ltd, 1980, pp.28.

[55] Tiller. F. and Tsai. C-D., J. Amer. Ceram. Soc., Vol.69, No.12, 1986, pp.882-887.

[56] Akasy. I.A.and Schilling. C.H., in Ultrastructure Processing of Ceramics, Glasses and Composites, eds. Heich. L.L. and Ulrich. D.R., Wiley, N.Y., 1984, pp.483-491.

[57] Hampton. J., J. Amer. Ceram. Soc., Vol. 71, No.12, 1988, pp.1040-1045.

[58] Lee. J-G. and Cutler. I.B., Amer. Ceram. Bull., Vol.54, No.2, 1975, pp.195 -198.

[59] Nutt. S.R., J. Amer. Ceram. Soc., Vol. 71, No.3, 1988, pp. 149 - 156.

[60] Wagner. R.S. and Ellis. W.C., Appl. Phys. Lett., Vol.4, 1964, pp.39

[61] Milewski. J.V., Gac. F.D., Petrovic. J.J. and Skaggs. S.R., J. Mat.Sci., Vol.20, 1985, pp. 1160 - 1166.

[62] Shalek.P.D., Phillips. D.S., Christiansen. D.E., Katz. J.D., Parkinson. W.J. and Petrovic. J.J., in Whisker and Fiber - Toughened Ceramics, Proc. Int. Conf. Oak Ridge, Tennessee, USA, June 1988, pp.53 - 62.

[63] Yeh. H.C. and Sikora. P.F., Amer. Ceram. Soc. Bull., Vol.58, 1979, pp.444.

[64] Lange.F.F., J. Amer. Ceram. Soc. Vol.56, 1973, pp.518.

[65] Ziegler.G., Bentsen. L.D. and Hasselman. D.P.H., Comm. Amer. Ceram. Soc., Vol.64, 1981, pp. C-35.

[66] Larker. H.T., SAE Technical paper No. 770355, 1977.

[67] Saller. H.A., Canadian Patent 680160, 1964.

[68] Schwartz. N.B., Iron Age, Vol.206, 1970, pp.78.

[69] Larker. H.T., in Prog. in Nitrogen Ceramics, ed. Riley.F.L., Martinus Nijhoff, 1983.

[70] Adlerborn. J. and Larker. H.T., British Patent 1522705, 1978.

[71] Adlerborn. J., Larker. H.T. and Nilsson. J., British Patent 2024866A, 1979.

[72] Adlerborn. J., Larker. H.T., Mattsson. B. and Nilsson. J.,U.S. Patent 4081272, 1978.

[73] Adlerborn. J., Larker. H.T., Mattsson. B. and Nilsson. J., U.S. Patent 4446100, 1984.

[74] Adlerborn. J., Larker. H.T., Mattsson. B. and Nilsson. J., U.S. Patent 4478789, 1984.

[75] Adlerborn. J., Larker. H.T., Mattsson. B. and Nilsson. J., European Patent EP 0118702 A1, 1984.

[76] Adlerborn. J., Larker. H.T., Mattsson. B. and Nilsson. J., U.S. Patent 4568516, 1986.

[77] Larker. H.T., ASEA J., Vol.54, No.4, 1981, pp.85.

[78] Larker, H.T., in Emergent Process Methods for High Temperature Ceramics, Vol.17, eds. Davies.R.F .et.al., Plenum Publishing, 1984, pp.571.

[79] Larker. H.T., Mat. Sci. and Eng., Vol.71, 1985, pp.329.

[80] Adlerborn, J., Mat. and Design, Vol.8, No.4,1987, pp.229.

[81] Amberg. G. and Doxner. H., Powder Metall., Vol.20, 1977, pp.1

[82] Kolaska.H., Powder Metall. Int., Vol.21, No.1, 1989, pp.22.

[83] Sheppard. L.M., Adv. Mat. and Process., No.1, 1986, pp.24

[84] Inglis. C.E., Trans. Inst. Naval Archit., Vol.55, 1913, pp.219.

[85] Griffith. A.A., Phil.Trans. Royal Soc., London, Vol.211A, 1920, pp.163.

[86] Irwin. G.R., J. Weld., Vol.31, 1952, pp.450.

[87] Lange. F.F., J. Amer. Ceram. Soc., Vol. 72, No.1, 1989, pp.3-15.

[88] Evans. A.G., ibid., Vol.68, No.3, 1982, 127-137.

[89] Ruehle. M. and Evans. A.G., Prog. in Mat. Sci., Vol.33, 1989, pp.85-167.

[90] Evans. A.G. and Cannon. R.M., Acta Metall., Vol.34, No.5, 1986, pp.761-800.

[91] Mc Meeking, R.M. and Evans. A.G., J. Amer. Ceram. Soc., Vol.65, No.5, 1982, pp. 242-247.

[92] Sigl. L.S., Mataga. P., Dalgleish. B.J., Mc Meeking. R.M. and Evans. A.G., Acta Metall., Vol.36, No.3, 1988, pp.517-522.

[93] Erdogan. F. and Joseph. P.F., J. Amer. Ceram. Soc., Vol.72, No.2, 1989, pp.262-270.

[94] Kelly. A., in Strong Solids, Clarendon Press, Oxford, 1973.

[95] Marshall. D.B. and Evans. A.G., J. Amer. Ceram. Soc., Vol.68, No. 5, 1985, pp.225-231.

[96] Marshall. D.B., Acta Metall., Vol.32, No.11, 1985, pp.2013-2021.

[97] Evans.A.G. and Mc.Meeking.R.M., Acta Metall., Vol.34, No.12, 1986, pp.2435 - 2441.

[98] Prewo. K.M. and Brennan. J.J., J. Mat.Sci., Vol.15[2], 1980, pp.463 - 468.

[99] Erdogan. F., Eng. Fract. Mech., Vol. 4, No.4, 1972, pp.811 - 840.

[100] Becher.P.F., Hsueh. C-H., Angelini. P. and Tiegs. T.N., J. Amer. Ceram. Soc., Vol.71, No.12, 1988, pp.1050 - 1061.

[101] Campbell. G.H., Ruehle. M., Dalgleish. B.J. and Evans. A.G., ibid., Vol.73, No.3, 1990, pp.521 - 530.

[102] He. M.Y. and Hutchinson. J.W., J.Appl. Mech., Trans ASME, Vol.56, No.2, 1989, pp.746 - 753.

[103] Charalambides. P.G. and Evans. A.G., J. Amer. Ceram. Soc., Vol.72, No.5, 1989, pp.746 - 753.

[104] Sigl. L.S. and Evans.A.G., Mech Mater., 8, 1989, pp.1 - 12.

[105] Evans. A.G., J. Amer. Ceram. Soc., Vol.73, No.2, 1990, pp.187 - 206.

[106] Faber. K.T. and Evans. A.G., Acta Metall., Vol.31[4], 1983, pp.565 - 576.

[107] Liu. H., Weisskopf. K-L. and Petzow. G., J.Amer. Ceram. Soc., Vol.72, No.4, 1989, pp.559 - 563.

[108] Faber. F.T. and Evans. A.G., Acta Metall., Vol.31, No.4,, 1983, pp.577 - 584.

[109] Gadkaree, K.P. and Chyung.R., Amer. Ceram. Soc. Bull., Vol.65, No.2, 1986, pp.370 - 376.

[110] Buljan. S.T. and Zilberstein., in Mat. Res. Soc. Symp. Proc., Vol.78, Adv. Struc. Ceram., Ed. Becher.P.F. et.al., Mat. Res. Soc., Pittsburgh, 1986, pp.272-281.

[111] Rice.R.W. and Pohanka.R.C., J.Amer. Ceram. Soc., Vol.62, No. 11 - 12, 1979, pp.559 - 563.

[112] Evans. A.G., Acta. Metall., Vol.26, 1978, pp. 1845 - 1853.

[113] Lange. F.F., in Fract. Mech. of Ceram., Vol.4., Crack Growth and Microstructure, ed. Bradt, Hasselman and Lange, Plenum Press, N.Y., 1978, pp. 799 - 817.

[114] Rice. R.W., Cer. Eng. and Sci. Proc., Vol.2, No.78, 1981, pp.661 - 701.

[115] Rice. R.W. and Freiman. S.W., J. Amer. Ceram. Soc., Vol.64, No.6, 1981, pp.350 - 354.

[116] Evans. A.G. and Faber. K.T., ibid., Vol.64, 1981, pp.394.

[117] Rice. R.W., in Proc. 9th Ann. Conf. on Composites and Adv. Ceram. Mat., Florida, Jan. 1985, pp. 589 - 607.

[118] Wu. C., J. Mat. Sci., Vol.13, 1978, pp.2659 - 2670.

[119] Wu.C., ASTM, STP 745, 1982, pp.127 - 140.

[120] Wei. G.C. and Becher. P.F., Amer. Ceram. Soc. Bull., Vol.64, No.2, 1985, pp.298 - 304.

[121] Wei. G.C. and Becher. P.F., J. Amer. Ceram. Soc., Vol. 67, No.12, 1984, pp. C267 - C269.

[122] Hyami. R., Ueno. K., Kondou. I., Tamari. N. and Toibana. Y., in Tailoring Multiphase and Composite Ceramics, Mat. Sci. Res. Vol.20, Plenum Press, 1986, pp.663 - 674.

[123] Singh. J., Adv. Ceram. Mat., Vol.3, No.4, 1988, pp.357 - 360.

[124] Akimune. Y., Katano. Y. and Matoba. K., J. Amer. Ceram. Soc., Vol.72, No.5, 1989, pp.791 - 798.

[125] Buljan. S-T., Amer. Ceram.Soc. Bull., Vol.66, No.2, 1987, pp.347 - 352.

[126] Kodama. H. and Miyosh. T., in Ceram. Eng. Sci. Proc., Vol.10, No.9-10, 1989, pp.1072 - 1082.

[127] Shalek. P.D., Petrovic. J.J., Hurley. G.F., and Gac. F.D., Amer. Ceram. Soc. Bull., Vol.65, No.2, 1986, pp.351 - 356.

[128] Corbin. N.D., Willkens. C.R. Pujari. V.K., Mangaudis. M.J. and Yeckley. R.L., in Proc. Int. Conf. Whisker and Fiber - Toughened Ceramics. Oak Ridge, Tennessee, June 1988, pp. 131-138.

[129] Larker. H.T. and Adlerborn. J.E., in Proc. 3rd Int. Symp. Ceram. Mat. and Components for Engines, Las Vegas, Nov. 1988.

[130] Lundberg. R., Kahlman. L., Pompe. R. and Carlsson. R., Amer. Ceram. Soc. Bull., Vol.66, No.2, 1987, pp.330 -333.

[131] Peizhi. G., Weiru. Z., Yixian. X. and Qisheng. F., in Proc. 3rd Int. Symp. Ceram. Mat. and Components for Engines, Las Vegas, Nov.1988, pp.260 - 272.

[132] Miyamoto. Y., Tanaka. K., Shimada. M. and Koizumi. M., in Proc. 2nd. Int. Symp. Ceram. Mat. and Components for Engines, Luebeck, 1986, pp.271 - 278.

[133] Rice. R.W., J. Mat. Sci., Vol.20, 1985, pp.1392 - 1406.

[134] Wotting. G. and Ziegler. G., Science of Ceramics 12, ed. Vincenzini. P., 1983, pp. 361 - 370.

[135] Takemura. H., in Proc. Int. Conf. on Hot Isostatic Pressing, ed. Garvare, Centek Publ., Lulea, Sweden, 1988. pp.329 - 336.

[136] Bogoroch. R and Luck. S., in Proc. Int. Conf. Whisker and Fiber - Toughened Ceramics, Oak Ridge, Tennesaee, June 1988, pp.

[137] Baril. D. and Jain. M., Presented at the 2nd Int. Ceram. Sci. and Tech. Conf., Orlando, Florida, Nov., 1990. (in press) .

[138] Sakai. H., Matsuhiro. K. and Furuse. Y., ibid.

[139] Karunaratne. B. and Lewis. M.H., J. Mat. Sci., Vol.15, 1980, pp.449.

[140] Ernstberger. U., Int. J. High Tech. Ceram. No.3, 1990, pp.43.

[141] Chokshi. A.H. and Porter. J.R., J. Amer. Ceram. Soc., Vol.68, 1985, pp. C144.

[142] Porter. J.R., Lange. F.F. and Chokshi. A.H., Mat. Res. Soc. Symp. Proc. 78, 1987, pp.289 - 294.

[143] Lange. F.F., J. Mat. Sci., Vol.15, 1980, pp.611.

[144] Lange. F.F., ibid., Vol.15, 1980, pp.601 - 610.

[145] Raj. R., J. Eng. Mat. and Tech., April 1976, pp.132 - 139.

[146] Yeckley. R.L. and Siebein.K., in Proc. 3rd Int. Symp. Ceram. Mat. and Comp. for Engines, Las Vegas, Nov.1988, pp.751 - 765.

[147] Nabarro. F.R., in Report on a Conf. on the Strength of Solids, Physical Soc, London, 1948, pp.75 - 90.

[148] Herring. C., J. Appl. Phys., Vol.21, 1950, pp.437 - 445.

[149] Coble. R.L., ibid., Vol.34, 1963, pp.1679 - 1682.

[150] Pharr. G.M. and Ashby. M.F., J. Amer. Ceram. Soc., Vol.67, 1984, pp.129 - 138.

[151] Marion. J.E., Acta Metall., Vol.31, No.10, 1983, pp.1445 - 1457.

[152] Tsai. R.L. and Raj. R., Acta Metall., Vol.3, 1982, pp.1043 - 1058.

[153] Thouless. M.D. and Evans. A.G., J. Amer.Ceram. Soc., Vol.67, 1984, pp.721 - 731.

[154] Porter. J.R., Amer. Ceram. Soc. Bull., Vol.66, 1987, pp.343 - 347.

[155] Nixon. R.D., Mat. Res. Soc. Symp. Proc 78, 1987, pp.295 - 302.

[156] Wagner. C., Z. Phys. Chem., Vol.21B, 1933, pp.25.

[157] Horton. R.M. J.Amer. Ceram. Soc., Vol.52, 1969, pp.121.

[158] Cubbicciotti. D. and Lau. K.H., ibid., Vol. 61, 1978, pp.512

[159] Lewis. M.H. and Barnard.P., J. Mat. Sci., Vol.15, 1980, pp.443.

[160] Wu. C.C., ibid., Vol.16, 1981, pp.3099.

[161] Clarke. D.R. and Lange. F.F., J. Amer. Ceram. Soc., Vol.63, 1980, pp.586.

[162] Bibini. G.N., J. Mat. Sci., Vol.18, 1983, pp.231.

[163] Plucknett. K.P., PhD Thesis, Univ. of Warwick, 1990.

[164] Stanley. P., Proc. Inst. Mech. Eng. Vol. 190, 1979, pp.585.

[165] Antis. G.R., Lawn. B.R., Marshall. D.B. and Chantikul. P., J. Amer. Ceram. Soc., Vol. 64, 1981, pp.533 - 538.

[166] Lawn. B.R. and Marshall. D.B., ibid., Vol. 62, 1979, pp.342.

[167] Antis. G.R., Lawn. B.R., Marshall. D.B. and Chantikul. P. ibid., Vol.64, 1981, pp.539.

[168] Srawley. J.E. and Brown. B.F., ASTM Special Tech. Publ., No.410, pp.8 - 16.

[169] Hollenberg. G.W., Terwilliger. G.R. and Gordon. R.S., J. Amer. Ceram. Soc., Vol.54, No.4, 1971, pp.196 - 199.

[170] Malghan. S.G., Vaudin. M., Cline. J.P., Wang. P.S. and Lum. L.S., Presented at the 2nd Int. Ceram. Sci. and Tech. Conf., Orlando Florida, Nov. 1990, (in print).

[171] Jain. M., C-Axis Technology, Private Communication.

[172] Nutt. S.R., J. Amer. Ceram. Soc., Vol. 67, 1984, pp.428.

[173] Hartman. J.S., J. Amer. Chem. Soc., Vol.109, 1987, pp.6059 - 6067.

[174] Apperley. D.C., J.Amer. Ceram. Soc., Vol.74, 1991, pp.777 - 782.

[175] Liddell. K. and Thompson. D.P., in Brit. Ceram. Trans. J., Vol.85, 1986, pp.17 - 72.

[176] Gazzara. C.P. and Messier. D.R., Ceram. Bull., Vol.56, 1977, pp.777 - 780.

[177] Clarke. D.R., Ann. Rev. Mat.Sci., Vol.17, 1987, pp.57 - 74.

[178] Braue. W., in Proc. of the 46th Ann. Meeting of the Elect. Micro. Soc. of Amer., ed. Bailey, San Francisco Press, 1988, pp.734 - 735.

[179] Kim. M., Ruehle. M., Schmid. H. and Gauckler. L.J., Proc. 9th Int. Cong. E.M., Toronto, 1978, pp.302.

[180] Jepps. N.W., Stobbs. W.M. and Page. T.F., presented at EMAG, Cambridge, 7-10 September 1981, in Inst.Phys. Conf. Ser. No.61 : Chapter 10, pp.453-456.

[181] Barrett. R. and Page. T.F., Ceram. Eng. Sci. Proc., Vol.10, 1989, pp.897-910.

[182] Swan. H., in 4th Int. Symp. on Ceram. Mat. and Comp. for Engines, Gothenburg, June 1991, (in print).

[183] Maeda. M., J. Mat. Sci. Lett., Vol.8, 1989, pp.195-197.

[184] Van der Biest, O., Weber. C. and Garguet. L.A., in Proc. 3rd Int. Symp. on Ceram. Mat. and Comp. for Engines, ed. Tennery.V.J., Las Vegas, 1988, pp.729.

[185] Becher. P.F., Hsueh. C-H., Angelini. P. and Tiegs. T.N., in Whisker and Fiber-Toughened Ceramics, Proc. Int. Conf., Oak Ridge, Tennessee, June 1988, pp.109-112.

[186] Petrovic, J.J., J. Mat. Sci., Vol.20, 1985, pp.1167 - 1177.

[187] Thompson. D.P., Brit. Ceram. Trans., Vol.44, 1990, pp.1-14, Ed. Davidge. R.W. and Thompson. D.P., publ. Inst. Ceramics.